受入
91-11-83
高工研図書室

EUROPEAN ORGANIZATION FOR NUCLEAR RESEARCH

CERN-PPE/91-149
20 September 1991

Searches for New Particles in Z Decays Using the ALEPH Detector

The ALEPH Collaboration

Abstract

During 1989 and 1990 over 200,000 hadronic and leptonic events, corresponding to about 8.5 pb^{-1} of data, were collected in a scan of the Z peak using the ALEPH detector at the e^+e^- collider, LEP. These data, at the highest centre-of-mass energy available to date in e^+e^- collisions, have allowed a broad range of searches for new particles and new phenomena to be performed in a mass range significantly higher than previously attainable. The searches performed by ALEPH for Higgs bosons, supersymmetric particles and leptoquarks, and for evidence of compositeness are reviewed. No positive signals have been observed but a comprehensive set of mass and coupling limits is presented. Branching ratio limits are given for a number of "rare" Z decays.

(submitted to Physics Reports)

The ALEPH Collaboration

D. Decamp, B. Deschizeaux, C. Goy, J.-P. Lees, M.-N. Minard

Laboratoire de Physique des Particules (LAPP), IN^{2}P^3-CNRS, 74019 Annecy-le-Vieux Cedex, France

R. Alemany, J.M. Crespo, M. Delfino, E. Fernandez, V. Gaitan, Ll. Garrido, Ll.M. Mir, A. Pacheco

Laboratorio de Fisica de Altas Energias, Universidad Autonoma de Barcelona, 08193 Bellaterra (Barcelona), Spain[8]

M.G. Catanesi, D. Creanza, M. de Palma, A. Farilla, G. Iaselli, G. Maggi, M. Maggi, S. Natali, S. Nuzzo, M. Quattromini, A. Ranieri, G. Raso, F. Romano, F. Ruggieri, G. Selvaggi, L. Silvestris, P. Tempesta, G. Zito

INFN Sezione di Bari e Dipartimento di Fisica dell' Università, 70126 Bari, Italy

Y. Gao, H. Hu,[21] D. Huang, X. Huang, J. Lin, J. Lou, C. Qiao,[21] T. Ruan,[21] T. Wang, Y. Xie, D. Xu, R. Xu, J. Zhang, W. Zhao

Institute of High-Energy Physics, Academia Sinica, Beijing, The People's Republic of China[9]

W.B. Atwood,[2] L.A.T. Bauerdick, F. Bird,[4] E. Blucher, G. Bonvicini, F. Bossi, J. Boudreau, T.H. Burnett,[3] H. Drevermann, R.W. Forty, C. Grab,[23] R. Hagelberg, S. Haywood, J. Hilgart, B. Jost, M. Kasemann,[28] J. Knobloch, A. Lacourt, E. Lançon, I. Lehraus, T. Lohse, A. Lusiani, A. Marchioro, M. Martinez, P. Mato, S. Menary,[29] T. Meyer, A. Minten, A. Miotto, R. Miquel, H.-G. Moser, J. Nash, P. Palazzi, F. Ranjard, G. Redlinger, L. Rolandi,[30] A. Roth, J. Rothberg,[3] H. Rotscheidt, M. Saich, D. Schlatter, M. Schmelling, W. Tejessy, H. Wachsmuth, S. Wasserbaech, W. Wiedenmann, W. Witzeling, J. Wotschack

European Laboratory for Particle Physics (CERN), 1211 Geneva 23, Switzerland

Z. Ajaltouni, F. Badaud, M. Bardadin-Otwinowska, A.M. Bencheikh, R. El Fellous, A. Falvard, P. Gay, C. Guicheney, J. Harvey, P. Henrard, J. Jousset, B. Michel, J-C. Montret, D. Pallin, P. Perret, J. Proriol, F. Prulhière, G. Stimpfl

Laboratoire de Physique Corpusculaire, Université Blaise Pascal, IN^{2}P^3-CNRS, Clermont-Ferrand, 63177 Aubière, France

J.D. Hansen, J.R. Hansen, P.H. Hansen, R. Møllerud, B.S. Nilsson

Niels Bohr Institute, 2100 Copenhagen, Denmark[10]

I. Efthymiopoulos, E. Simopoulou, A. Vayaki

Nuclear Research Center Demokritos (NRCD), Athens, Greece

J. Badier, A. Blondel, G. Bonneaud, J. Bourotte, F. Braems, J.C. Brient, G. Fouque, A. Gamess, R. Guirlet, S. Orteu, A. Rosowsky, A. Rougé, M. Rumpf, R. Tanaka, H. Videau

Laboratoire de Physique Nucléaire et des Hautes Energies, Ecole Polytechnique, IN^{2}P^3-CNRS, 91128 Palaiseau Cedex, France

D.J. Candlin, E. Veitch

Department of Physics, University of Edinburgh, Edinburgh EH9 3JZ, United Kingdom[11]

L. Moneta, G. Parrini

Dipartimento di Fisica, Università di Firenze, INFN Sezione di Firenze, 50125 Firenze, Italy

M. Corden, C. Georgiopoulos, M. Ikeda, J. Lannutti, D. Levinthal,[16] M. Mermikides, L. Sawyer

Supercomputer Computations Research Institute and Dept. of Physics, Florida State University, Tallahassee, FL 32306, USA [13,14,15]

A. Antonelli, R. Baldini, G. Bencivenni, G. Bologna,[5] P. Campana, G. Capon, F. Cerutti, V. Chiarella, B. D'Ettorre-Piazzoli,[6] G. Felici, P. Laurelli, G. Mannocchi,[6] F. Murtas, G.P. Murtas, L. Passalacqua, M. Pepe-Altarelli, P. Picchi,[5] P. Zografou

Laboratori Nazionali dell'INFN (LNF-INFN), 00044 Frascati, Italy

B. Altoon, O. Boyle, A.W. Halley, I. ten Have, J.L. Hearns, J.G. Lynch, W.T. Morton, C. Raine, J.M. Scarr, K. Smith, A.S. Thompson, R.M. Turnbull

Department of Physics and Astronomy, University of Glasgow, Glasgow G12 8QQ, United Kingdom[11]

B. Brandl, O. Braun, R. Geiges, C. Geweniger, P. Hanke, V. Hepp, E.E. Kluge, Y. Maumary, A. Putzer, B. Rensch, A. Stahl, K. Tittel, M. Wunsch

Institut für Hochenergiephysik, Universität Heidelberg, 6900 Heidelberg, Fed. Rep. of Germany[17]

A.T. Belk, R. Beuselinck, D.M. Binnie, W. Cameron, M. Cattaneo, P.J. Dornan,[1] S. Dugeay, A.M. Greene, J.F. Hassard, N.M. Lieske, S.J. Patton, D.G. Payne, M.J. Phillips, J.K. Sedgbeer, G. Taylor, I.R. Tomalin, A.G. Wright

Department of Physics, Imperial College, London SW7 2BZ, United Kingdom[11]

P. Girtler, D. Kuhn, G. Rudolph

Institut für Experimentalphysik, Universität Innsbruck, 6020 Innsbruck, Austria[19]

C.K. Bowdery, T.J. Brodbeck, A.J. Finch, F. Foster, G. Hughes, N.R. Keemer, M. Nuttall, A. Patel, B.S. Rowlingson, T. Sloan, S.W. Snow, E.P. Whelan

Department of Physics, University of Lancaster, Lancaster LA1 4YB, United Kingdom[11]

T. Barczewski, K. Kleinknecht, J. Raab, B. Renk, S. Roehn, H.-G. Sander, H. Schmidt, F. Steeg, S.M. Walther, B. Wolf

Institut für Physik, Universität Mainz, 6500 Mainz, Fed. Rep. of Germany[17]

J-J. Aubert, C. Benchouk, V. Bernard, A. Bonissent, J. Carr, P. Coyle, J. Drinkard, F. Etienne, S. Papalexiou, P. Payre, B. Pietrzyk, Z. Qian, D. Rousseau, P. Schwemling, M. Talby

Centre de Physique des Particules, Faculté des Sciences de Luminy, IN^{2}P^3-CNRS, 13288 Marseille, France

S. Adlung, H. Becker, W. Blum, D. Brown, P. Cattaneo, G. Cowan, B. Dehning, H. Dietl, F. Dydak[26], M. Fernandez-Bosman, T. Hansl-Kozanecka,[2,22] A. Jahn, W. Kozanecki,[2] E. Lange, J. Lauber, G. Lütjens, G. Lutz, W. Männer, Y. Pan, R. Richter, J. Schröder, A.S. Schwarz, R. Settles, U. Stierlin, R. St. Denis, M. Takashima, J. Thomas, G. Wolf

Max-Planck-Institut für Physik und Astrophysik, Werner-Heisenberg-Institut für Physik, 8000 München, Fed. Rep. of Germany[17]

V. Bertin, J. Boucrot, O. Callot, X. Chen, A. Cordier, M. Davier, G. Ganis, J.-F. Grivaz, Ph. Heusse, P. Janot, D.W. Kim,[20] F. Le Diberder, J. Lefrançois,[1] A.-M. Lutz, J.-J. Veillet, I. Videau, Z. Zhang, F. Zomer

Laboratoire de l'Accélérateur Linéaire, Université de Paris-Sud, IN^{2}P^3-CNRS, 91405 Orsay Cedex, France

D. Abbaneo, S.R. Amendolia, G. Bagliesi, G. Batignani, L. Bosisio, U. Bottigli, C. Bradaschia, M. Carpinelli, M.A. Ciocci, R. Dell'Orso, I. Ferrante, F. Fidecaro,[1] L. Foà, E. Focardi, F. Forti, C. Gatto, A. Giassi, M.A. Giorgi, F. Ligabue, E.B. Mannelli, P.S. Marrocchesi, A. Messineo, F. Palla, G. Sanguinetti, J. Steinberger, R. Tenchini, G. Tonelli, G. Triggiani, C. Vannini, A. Venturi, P.G. Verdini, J. Walsh

Dipartimento di Fisica dell'Università, INFN Sezione di Pisa, e Scuola Normale Superiore, 56010 Pisa, Italy

J.M. Carter, M.G. Green,[1] P.V. March, T. Medcalf, I.S. Quazi, J.A. Strong, R.M. Thomas, L.R. West, T. Wildish

Department of Physics, Royal Holloway & Bedford New College, University of London, Surrey TW20 OEX, United Kingdom[11]

D.R. Botterill, R.W. Clifft, T.R. Edgecock, M. Edwards, S.M. Fisher, T.J. Jones, P.R. Norton, D.P. Salmon, J.C. Thompson

Particle Physics Dept., Rutherford Appleton Laboratory, Chilton, Didcot, Oxon OX11 OQX, United Kingdom[11]

B. Bloch-Devaux, P. Colas, E. Locci, S. Loucatos, E. Monnier, P. Perez, J.A. Perlas, F. Perrier, J. Rander, J.-F. Renardy, A. Roussarie, J.-P. Schuller, J. Schwindling, B. Vallage

Département de Physique des Particules Elémentaires, CEN-Saclay, 91191 Gif-sur-Yvette Cedex, France[18]

J.G. Ashman, C.N. Booth, C. Buttar, R. Carney, S. Cartwright, F. Combley, M. Dinsdale, M. Dogru, F. Hatfield, J. Martin, D. Parker, P. Reeves, L.F. Thompson

Department of Physics, University of Sheffield, Sheffield S3 7RH, United Kingdom[11]

E. Barberio, S. Brandt, C. Grupen, H. Meinhard, L. Mirabito, U. Schäfer, H. Seywerd

Fachbereich Physik, Universität Siegen, 5900 Siegen, Fed. Rep. of Germany[17]

G. Giannini, B. Gobbo, F. Ragusa,[25]U. Stiegler

Dipartimento di Fisica, Università di Trieste e INFN Sezione di Trieste, 34127 Trieste, Italy

L. Bellantoni, D. Cinabro, J.S. Conway, D.F. Cowen,[24]Z. Feng, D.P.S. Ferguson, Y.S. Gao, J. Grahl, J.L. Harton, R.C. Jared,[7] R.P. Johnson,[27] B.W. LeClaire, C. Lishka, Y.B. Pan, J.R. Pater, Y. Saadi, V. Sharma, Z.H. Shi, Y.H. Tang, A.M. Walsh, J.A. Wear,[27]F.V. Weber, M.H. Whitney, Sau Lan Wu, G. Zobernig

Department of Physics, University of Wisconsin, Madison, WI 53706, USA[12]

---

[1]Now at CERN.
[2]Permanent adddress: SLAC, Stanford, CA 94309, USA.
[3]Permanent address: University of Washington, Seattle, WA 98195, USA.
[4]Now at SSCL, Dallas, TX, U.S.A.
[5]Also Istituto di Fisica Generale, Università di Torino, Torino, Italy.
[6]Also Istituto di Cosmo-Geofisica del C.N.R., Torino, Italy.
[7]Permanent address: LBL, Berkeley, CA 94720, USA.
[8]Supported by CAICYT, Spain.
[9]Supported by the National Science Foundation of China.
[10]Supported by the Danish Natural Science Research Council.
[11]Supported by the UK Science and Engineering Research Council.
[12]Supported by the US Department of Energy, contract DE-AC02-76ER00881.
[13]Supported by the US Department of Energy, contract DE-FG05-87ER40319.
[14]Supported by the NSF, contract PHY-8451274.
[15]Supported by the US Department of Energy, contract DE-FC0S-85ER250000.
[16]Supported by SLOAN fellowship, contract BR 2703.
[17]Supported by the Bundesministerium für Forschung und Technologie, Fed. Rep. of Germany.
[18]Supported by the Institut de Recherche Fondamentale du C.E.A.
[19]Supported by Fonds zur Förderung der wissenschaftlichen Forschung, Austria.
[20]Supported by the Korean Science and Engineering Foundation and Ministry of Education.
[21]Supported by the World Laboratory.
[22]On leave of absence from MIT, Cambridge, MA 02139, USA.
[23]Now at ETH, Zürich, Switzerland.
[24]Now at California Institute of Technology, Pasadena, CA 91125, USA.
[25]Now at Dipartimento di Fisica, Università di Milano, Milano, Italy.
[26]Also at CERN, PPE Division, 1211 Geneva 23, Switzerland.
[27]Now at University of California, Santa Cruz, CA 95064, USA.
[28]Now at DESY, Hamburg, Germany.
[29]Now at Cornell University, Ithaca, NY 14853, USA.
[30]Also at Dipartimento di Fisica, Università di Trieste, Trieste, Italy.

Contents

1 Introduction

CERN's large electron-positron collider, LEP, was built to allow precision tests of the standard model of particle physics, initially through a high statistics study of the properties of the Z boson. The first results from data taken in 1989 and 1990 by the four LEP experiments have shown no deviations from this model. However the standard model has a number of unsatisfactory features, the principal ones being the large number of arbitrary parameters and the lack of direct evidence for the mass mechanism. It is therefore of great importance that with the advent of LEP a detailed search should be made for any evidence for new particles or phenomena.

LEP has three great advantages over earlier e^+e^- colliding beam machines such as PETRA, PEP and TRISTAN (a summary of limits from these machines can be found in refs [1] and [2]):

- it has a higher energy and therefore a higher mass reach in the search for new particles;
- the cross-section at the Z peak is two orders of magnitude higher than at the earlier machines where photon exchange dominates;
- there is a completely new mechanism available, s-channel Z exchange, which is expected to contribute to the production of particles coupling to mass, such as the Higgs boson.

An important consequence of the second of these is that within a relatively short running period it has been possible to exclude the existence of many postulated particles up to a mass of about $m_Z/2$ ($\sim 45\,\mathrm{GeV}/c^2$), the kinematic limit for pair production when running at the Z peak. It is therefore an appropriate time to review the procedures and results of the searches carried out at our LEP experiment, ALEPH. It is also appropriate to make the review in one place since, while searches for a single particle must frequently be made in several different event topologies, many unrelated physics channels have common selection procedures.

We begin the review with a brief summary of the major features of the ALEPH detector (section 2) and of the procedures by which particles are identified and measured in ALEPH (section 3). Then, assuming that the principal features of the Z boson are described by the standard model we show how a comparison of measured and predicted parameters of the Z can be used to set limits on the production of new particles which are already quite stringent. In later parts of the paper these width limits are used to set mass or coupling limits for specific types of new particle. However in many cases improved limits can be obtained by direct searches and the rest of the paper describes such searches.

In the standard model the Higgs mechanism of spontaneous symmetry breaking generates masses for the bosons and fermions. In the "minimal standard model" a single doublet of Higgs fields is introduced requiring the existence of one physical spin-0 Higgs boson. The mass of this boson is unspecified but must be less than about $1\,\mathrm{TeV}/c^2$ otherwise the quadratically divergent radiative corrections to its mass destroy the highly successful perturbative approach of the standard model. The search for such a minimal standard model Higgs is described in section 5 and such a particle is excluded for a mass below $48\,\mathrm{GeV}/c^2$. In non-minimal models additional doublets of Higgs fields are introduced leading to additional Higgs particles and the search for these is described in section 6. Recently it has been realized that radiative corrections due to the top quark may be large in this sector and we discuss in some detail the implications of such a large correction for the searches for these particles.

The minimal standard model has a number of theoretical problems including the requirement for ultrafine tuning of the Higgs parameters unless cancellation of the radiative corrections can be arranged. This can be achieved by the introduction of "supersymmetry" but at the expense of introducing a large number of supersymmetric particles differing in spin from the normal particles by half a unit. Again theoretical arguments require their mass to be less than about $1\,\mathrm{TeV}/c^2$. We describe the search for such particles in section 7.

A radically different approach to the mass problem is to postulate the existence of a further layer of structure in nature such that the quarks and leptons, and possibly the gauge bosons, are composite. There is no experimental evidence in support of this model and, indeed, there is a fundamental difficulty in reconciling the compositeness scale, which must be in the TeV range, with the mass scale of the quarks and leptons. Nevertheless, in the absence of evidence to the contrary, this idea should be seriously considered. The search for evidence of compositeness is described in section 8 where it is concluded that if excited particles exist they must have a mass greater than about $45\,\mathrm{GeV}/c^2$.

Leptoquarks, objects carrying both lepton and colour quantum numbers, appear in many theoretical schemes beyond the standard model. Searches and limits for these are presented in section 9. In section 10 we describe a more general search for a new weakly interacting particle with unknown coupling to the Z and set limits on the branching ratio of the Z to such a particle. Finally in section 11 we describe the search for certain rare decay modes of the Z which are either forbidden or have a very low branching ratio in the standard model.

One topic not reviewed here is the search for "new quarks and leptons", i.e. the top quark of the third generation and any particle of a postulated fourth generation, where the kinematic limit was essentially reached using the early LEP data. ALEPH published limits [3] on the top quark mass, $m_{\mathrm{t}} > 45.8\,\mathrm{GeV}/c^2$, and on a fourth generation down-type quark, $m_{\mathrm{b}'} > 46.0\,\mathrm{GeV}/c^2$. Heavy charged leptons, $\mathrm{L}^{\pm}$, and associated neutrinos ν_{L} were also excluded up to a mass of $42.7\,\mathrm{GeV}/c^2$ except for rather restrictive conditions, such as $m_{\nu} > m_{\mathrm{L}}$. The other LEP experiments published similar limits [4,5,6,7] at about the same time. Since then the CDF experiment at Fermilab has set a limit of $89\,\mathrm{GeV}/c^2$ for the t quark mass m_{t} [8] for decays *via* charged currents although this limit is invalidated if a charged Higgs exists with a mass more than a few GeV/c^2 below m_{t}. More recently, indirect determinations of the width of the $\mathrm{W}^{\pm}$ boson at $\overline{\mathrm{p}}\mathrm{p}$ colliders lead to a model independent limit of $51\,\mathrm{GeV}/c^2$ for m_{t} [9,10,11]. Thus the direct search for the top quark or for fourth generation particles has not been pursued further by ALEPH since 1989. However, a rather imprecise determination of m_{t} (assuming the validity of the standard model) can be made from its virtual effects on the Z and W bosons; in particular the Z and W mass and the Z leptonic width Γ_{ℓ} depend upon m_{t}. The quantities m_{Z} and Γ_{ℓ} have been determined precisely at LEP and m_{W} has been measured at $\overline{\mathrm{p}}\mathrm{p}$ colliders [12,13]. When these measurements are combined together with the ALEPH asymmetry measurements at the Z peak a value of m_{t} of $139^{+30}_{-35}\,\mathrm{GeV}/c^2$ is obtained [14] assuming a neutral Higgs mass of $200\,\mathrm{GeV}/c^2$, with an additional uncertainty of $^{+15}_{-22}\,\mathrm{GeV}/c^2$ when m_{H^0} is allowed to vary between $45\,\mathrm{GeV}/c^2$ and $1\,\mathrm{TeV}/c^2$.

Unless otherwise stated, all limits given in this report are at the 95% confidence level (c.l.). Each has been adjusted to include the systematic uncertainty.

2 The ALEPH Detector

The ALEPH detector is shown in fig 2.1. It is a large, multipurpose device with a cylindrical section (the "barrel") closed by two "endcaps" and covering almost 4π solid angle. Nearest to the beam pipe is a silicon strip microvertex detector, only partially installed during 1990 and not used for the analyses described in this paper. Surrounding this is a multilayer axial-wire drift chamber, the inner tracking chamber (ITC), which gives $r\phi$ coordinates for tracking and is also used for triggering. Next is the primary tracking device of ALEPH, a large time projection chamber (TPC) providing three dimensional track coordinates. A finely segmented electromagnetic calorimeter (ECAL), consisting of alternate layers of lead and proportional tubes, lies outside the TPC. The superconducting coil provides a uniform 1.5 T magnetic field which is returned in a large iron structure that both supports the experiment and is a fully instrumented hadron calorimeter (HCAL). Limited-streamer tubes fill hollow slots in the HCAL

and produce a digital pattern for tracking, as well as an analogue signal from projective towers for energy measurement. Finally, 92% of the solid angle is surrounded by muon chambers which measure a three dimensional coordinate for penetrating charged particles. The luminosity is measured by a luminosity calorimeter (LCAL) of similar construction to ECAL but located at a small angle to the beam direction. A small angle tracking device (SATR) with nine layers of drift chambers lies in front of LCAL. A detailed description of ALEPH can be found in ref. [15].

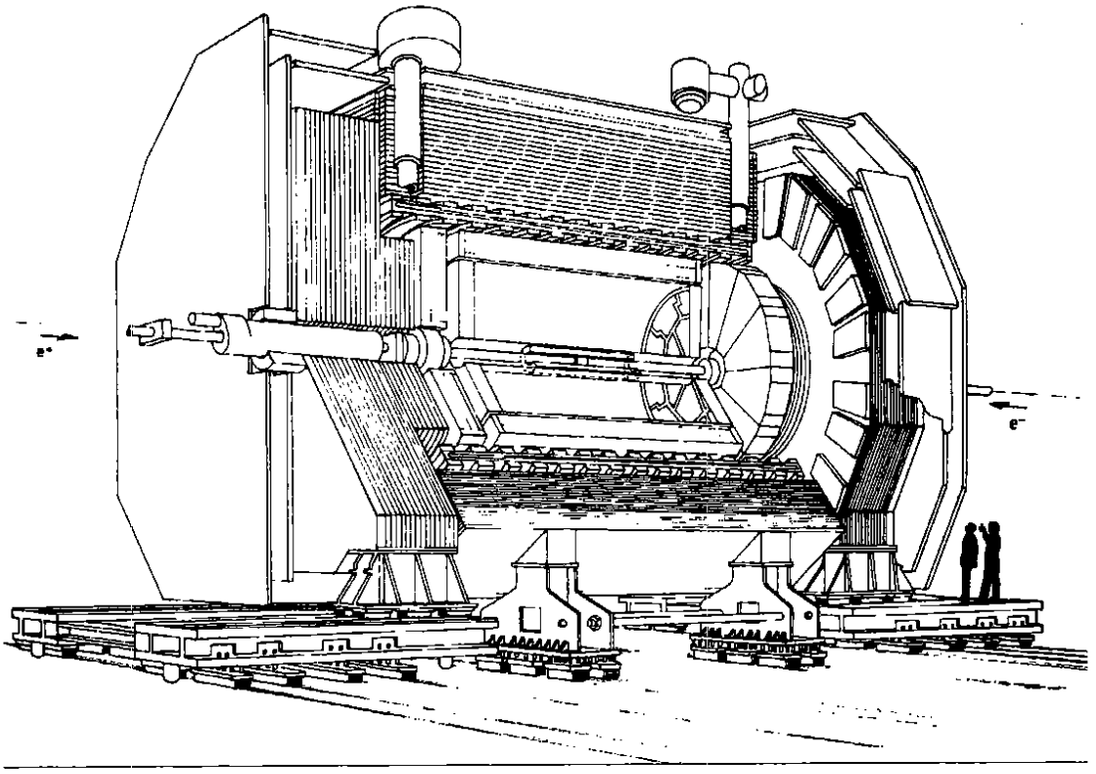

Figure 2.1: The ALEPH detector, approximately 11 m long and 11 m in diameter.

2.1 The Time Projection Chamber

The TPC has an inner radius of 0.3 m, an outer radius of 1.8 m and is 4.7 m long. Within this region it determines up to 21 space coordinates on a track and samples its ionization energy loss up to 360 times. Each end of the TPC is at ground potential while at the centre is a membrane of graphite coated mylar held at -26 kV. Together with inner and outer field cages these create a uniform field of approximately 115 V/cm. Ionization electrons drift from their production point to segmented proportional chambers on each end of the TPC where gas multiplication takes place. The magnetic field limits diffusion in the plane perpendicular to the magnetic field lines (the $r\phi$ plane). Cathode readout in the proportional chambers is *via* 21 concentric pad rows, each pad being 6.2 mm long in the azimuthal direction and 30 mm in the radial direction. The accurate position measurement of 160 μm in $r\phi$ is derived from the sharing of induced charge between a number of cathode pads. The z coordinate is derived from measurements of the drift time with a resolution of about 1 mm. Sense wires in the proportional chambers are also read out and their signals are used for dE/dx measurements; for lepton pair events with a full complement of wire measurements the resolution in dE/dx is 4.4% [16].

2.2 The Inner Tracking Chamber

The ITC is a conventional drift chamber 2 m long, positioned inside the TPC. It contains 960 sense wires strung between two aluminium end plates, each sense wire being surrounded by field wires in a hexagonal cell. The cells are organized into eight concentric layers; in the four inner layers there are 96 cells and in the four outer layers there are 144 cells. The cells in neighbouring layers are staggered by half a cell width. Thus the $r\phi$ coordinate is measured by the drift time with a precision of about 100 μm. The z coordinate is determined from the difference in arrival times of the pulses at the ends of each sense wire with a precision of 30 mm. The ITC provides the only tracking information in the first level trigger.

2.3 The Electromagnetic Calorimeter

The electromagnetic calorimeter (ECAL) is built in 36 modules, twelve in the barrel and twelve in each endcap, and covers 98% of the full solid angle. It lies inside the superconducting coil to minimize the amount of material in front of it. Each module contains 45 layers of lead interleaved with proportional wire chambers. Cathode pads in each layer of the wire chambers are connected internally to form "towers" oriented towards the interaction point. Each tower is read out in three sections in depth ("storeys") of four, nine and nine radiation lengths. There are 77,728 towers in all, each with an angular width of about $0.9° \times 0.9°$. The high granularity of the pads allows shower centroids to be located to ± 2 mm and provides excellent identification of electrons and photons within jets. Each wire plane is read out separately in every module. The wire signals have very low noise ($\sim$ 20 MeV) and are used in an energy trigger which can work at a threshold as low as 200 MeV. The longitudinal development of an electromagnetic shower may be observed on the 45 wire layers provided other showers are not present in the same module. The two measurements of energy in each module, from pads and wires, provides important protection from occasional malfunctioning of electronic channels in searches for rare events.

The gain of the ECAL gas is tracked by a number of small ionization chambers each containing an ^{55}Fe source. After correction the response of the modules is constant to better than 0.5%. The absolute energy calibration of each module is determined from Bhabha events. The energy resolution is $\Delta E/E = 0.017 + 0.19/\sqrt{E}$ with E in GeV.

2.4 The Hadron Calorimeter

The hadron calorimeter (HCAL) has 23 layers of iron absorber each 50 mm thick with limited streamer tubes $9 \times 9\,\mathrm{mm}^2$ in cross-section between each layer. It has a tower readout similar to the ECAL with pads of angular size about $3.7° \times 3.7°$. On the other side of the tubes are aluminium strips running the whole length of each tube, their digital readout providing a two dimensional view of the development of hadronic showers. The pad and strip readout again provides important redundancy in energy measurements. The wire signals are used for triggering. The energy resolution of the calorimeter is about $80\%/\sqrt{E}$ for hadronic showers. The whole of ECAL is rotated by about 2° relative to HCAL to avoid overlapping of the small gaps ("cracks") between modules.

Outside the iron are two double layers of streamer tubes, the muon chambers, used to provide two space coordinates for particles leaving the detector and hence improving the efficiency for muon identification. For the data described here only one of these layers was installed.

2.5 The Luminosity Calorimeter

The luminosity in ALEPH is determined by counting the rate of low angle Bhabha events in the luminosity calorimeter, LCAL [17]. In construction it is very similar to ECAL. It is built in two cylindrical halves, each half consisting of two semicircular modules. It is 24.6 radiation lengths in thickness. The angular acceptance is from 45 to 155 mrad. The energy resolution is $20\%/\sqrt{E}$. In many of the searches LCAL plays a crucial role in providing additional angular coverage, extending electromagnetic calorimetry down to smaller angles. However almost all cross-sections and limits are given relative to the Z cross-section and hence are determined from a count of the number of hadronic Z events rather than from the absolute value of the luminosity.

2.6 The Trigger

The trigger is organized into three levels. Level one decides whether or not to read out all detector elements. The level two trigger simply seeks to verify a level one charged track trigger by replacing the ITC tracking information with the more accurate TPC tracking information available 50 μs after the beam crossing. A level three software trigger is used to reject background such as beam-gas interactions and off-momentum particles hitting the vacuum chamber or collimators.

The principal level one triggers in ALEPH are:

- ECAL energy greater than 6.5 GeV in the barrel or 3.8 GeV in either endcap or greater than 1.6 GeV in both endcaps in coincidence;
- ECAL energy greater than 1.3 GeV in a module in the same azimuthal region as an ITC track;
- a particle penetrating HCAL in the same azimuthal region as an ITC track.

A number of subsidiary triggers provide high redundancy and allow trigger efficiencies to be precisely determined. These efficiencies are very close to 1.0 for most searches described in this report and are known to better than 1%.

3 Event Reconstruction and Monte Carlo Simulation

3.1 The Data Sample

The LEP data taking periods were from September to November 1989 and from April to August 1990. In both years an energy scan was made at 1 GeV intervals over a 7 GeV range centred at the Z peak. These energies and the amount of data taken at each are given in table 3.1.

Occasional defects in parts of the detector have led to the rejection of small samples of data for particular searches. As examples, about 5% of events taken are not used for searches which depend upon good knowledge of the muon trigger efficiency and about 1% are not used for searches involving identified photons.

3.2 Event Reconstruction

The principal components of event reconstruction in ALEPH are track finding in the TPC and ITC, cluster finding in the calorimeters, and matching of tracks and clusters to allow identification and energy measurement of charged and neutral particles.

Tracking in the TPC is done by finding space points consistent with a helix starting from the largest radius pad row and extrapolating inwards to find further points. A minimum of

Energy (GeV)	Hadronic Z events	Luminosity (nb^{-1})
88.2	2855	626
89.2	4904	579
90.2	12054	661
91.2	135839	4546
92.2	15632	740
93.2	8497	692
94.2	5837	733
95.0	95	16
Total	185713	8594

Table 3.1: Data taken with ALEPH during the scan of the Z peak (in this table some data sets differing by up to 200 MeV have been grouped together for convenience).

four points is required to define a track. Once found, multiple scattering errors are taken into account in determining its parameters. TPC track trajectories are projected back into the ITC and a search is made for ITC coordinates within a road in $r\phi$ and z. A final fit to a helix is made using all points from the two devices. Dimuon events with $|\cos\theta| < 0.8$ have been used to measure the momentum resolution of the combined tracking detectors; for high p_t tracks $\Delta p/p^2$ is $0.0008(\,\mathrm{GeV}/c)^{-1}$, corresponding to 3.6% for 45 GeV/c muons. In the rest of this paper only "good" tracks have been used in analyses, where a good track has at least four points in the TPC and originates from within a cylinder of length 140 mm and radius 25 mm coaxial with the beam and centred at the nominal collision point.

The reconstruction of calorimeter energy is based on "topological clusters", groups of storeys connected by at least one corner, including across the cracks between modules. Since projectivity of the calorimeter storeys is maintained in the overlap regions between the barrel and the endcaps, clusters are efficiently found in these regions although the energy measurement is somewhat degraded. Only storeys with energy above 30 MeV are included in a cluster and at least one storey in a cluster must have an energy above 90 MeV. Charged tracks are extrapolated to the calorimeters and associated to any cluster which contains a storey hit by the extrapolated track, thus defining a "charged cluster". A "neutral cluster" is any cluster not hit by an extrapolated track.

3.3 Particle Identification

An important feature of the ALEPH detector is its particle identification capability arising from the high segmentation of the calorimeters. Most searches described here do not rely heavily on this capability since the strongest selection criteria are topological. However, some of the channels require particle identification, particularly of leptons, and the principal features of the algorithms used are described here. More details can be found in refs [18,19].

3.3.1 Electrons and photons

Electron identification is performed using two independent measurements—the energy deposition in ECAL and the energy loss in the TPC. The former is most effective above 5 GeV, the latter is better at low energy.

Identification in ECAL is based on two variables which measure the degree to which an energy deposit near an extrapolated track conforms to that expected for an electron. The first,

R_T, compares the measured momentum, p, to the energy, E_0, deposited in the four towers closest to the extrapolated track. Test beam data have shown that the variable $X = E_0/p$ has a Gaussian distribution for electrons of a given energy with a mean $\overline{X}$ and variance $\sigma^2(X)$. Then

$$R_T = \frac{X - \overline{X}}{\sigma(X)}$$

is normally distributed with zero mean and unit variance. The variable R_L is similarly defined from the inverse of the mean position of the longitudinal energy deposition in the three stacks which also has a Gaussian distribution. Using these variables alone the electron efficiency is about 98% for isolated particles with energy above 2 GeV outside cracks and the overlap regions. The pion misidentification rate is less than 1%.

A similar procedure is used for photon identification with the requirement that no charged track points to the cluster. The transverse shape is measured by F_4, the fraction of the energy in the four highest energy towers of the cluster.

The energy loss measurement in the TPC, I_m, is based on the 60% truncated mean of the individual measurements of $\mathrm{d}E/\mathrm{d}x$ along a track. If I_e is the plateau ionization and $\sigma^2(I)$ is its variance, then for electrons

$$R_I = \frac{I_m - I_e}{\sigma(I)}$$

is again normally distributed with zero mean and unit variance. Use of R_I improves the electron efficiency and pion rejection between about 2 and 20 GeV.

3.3.2 Muons

When a charged particle crosses a plane of streamer tubes in HCAL typically between one and four adjacent tubes give signals. Muons are characterized by a track of such clusters penetrating all layers of the iron into the muon chambers. All charged tracks with momentum above 1 GeV/c are extrapolated through the detector. A cone three times larger than the rms displacement due to multiple scattering is defined along the extrapolated track and muons are selected according to the distribution of fired planes within this cone. Typically a track is considered to be a muon if more than nine planes fired in total, more than four of the last ten planes fired and the track extrapolates to within 4σ of a hit in the muon chambers. However, tighter or looser cuts may be used depending upon the requirements of a particular analysis. Typical muon finding efficiency in searches, where high efficiency is important, is 99% for energies above 5 GeV with a pion misidentification of 1.5%.

3.4 Energy Flow Reconstruction

In multihadronic events approximately 55% of the total energy is carried by the charged particles. Consequently, almost half of the event information is lost when the calorimetric information is ignored. This information may become particularly crucial in final states with a missing energy signature as frequently occurs in the search for new phenomena. Therefore, an energy flow reconstruction algorithm has been developed making use of most of the ALEPH subdetectors, taking advantage in particular of the redundancy of energy and momentum measurements, and of the photon, electron and muon identification capabilities.

3.4.1 Description of the method

For each event, the magnitude and direction of the energy flow is reconstructed using the following charged particle tracks and calorimeter clusters:

- good charged particle tracks (section 3.2) are counted as charged energy;
- V^0s (long-lived neutral particles decaying into two oppositely-charged particles) are kept if they point to the interaction vertex within the same tolerances as for good charged particle tracks;
- photons are counted as neutral electromagnetic energy;
- the remaining neutral hadronic energy is determined as follows from the calorimeter clusters. In a given cluster let E_e be the energy in the electromagnetic calorimeter not attributed to photons or electrons, E_h be the energy in the hadron calorimeter not attributed to muons, and E_c be the energy of the charged tracks, if any, topologically associated to the cluster and not positively identified as electrons or muons. Then the quantity E_n, defined as $E_h + rE_e - E_c$, is counted as neutral hadronic energy if significantly positive. Here r is the ratio of the responses for electrons and pions in the electromagnetic calorimeter ($r \sim 1.3$).

3.4.2 Performance of the reconstruction

The distribution of the energy reconstructed for hadronic Z events is shown in fig. 3.1, both for 190,000 real events and 265,000 fully simulated events. Data and simulation agree well over four orders of magnitude.

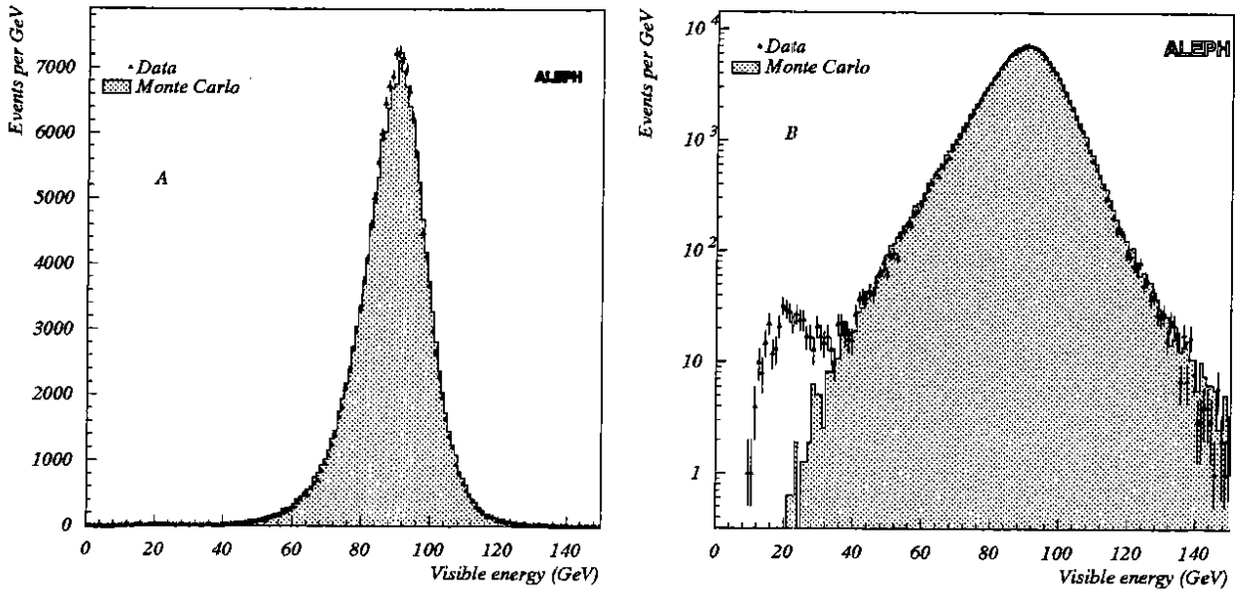

Figure 3.1: Distributions of the visible energy of hadronic events from the data (points with error bars) and from the simulation (filled area) on a linear scale (A) and on a logarithmic scale (B). The small excess of events in the low energy region is due to two-photon processes which have not been included in the Monte Carlo.

The mean value of this distribution is $\sim$ 89 GeV, and the charged, V^0, neutral electromagnetic and neutral hadronic energy fractions are 56%, 2%, 27% and 15% respectively. A Gaussian fit yields a resolution of 8 GeV on the visible energy (8 GeV/c^2 on the visible mass) for hadronic events well contained in the detector (i.e. such that the fraction of the total visible energy measured beyond 30° of the beam line exceeds 60%).

When applying this algorithm to the final state ($H^0 \rightarrow$ *hadrons*)$\nu\bar{\nu}$ with a 50 GeV/c^2 Higgs boson H^0, a reconstructed visible mass of 48 GeV/c^2 is achieved with a resolution of 5.5 GeV/c^2.

3.4.3 Control analysis and calibration

In order to check the resolutions and the absolute energy calibration, a control analysis has been performed on hard-radiative $q\bar{q}$ events, an example of which is shown in fig. 3.2. Ignoring the hard photon, this final state resembles a hadronic Higgs boson decay accompanied by a neutrino pair and gives the opportunity to check the energy reconstruction algorithm on real data over a wide domain of visible mass.

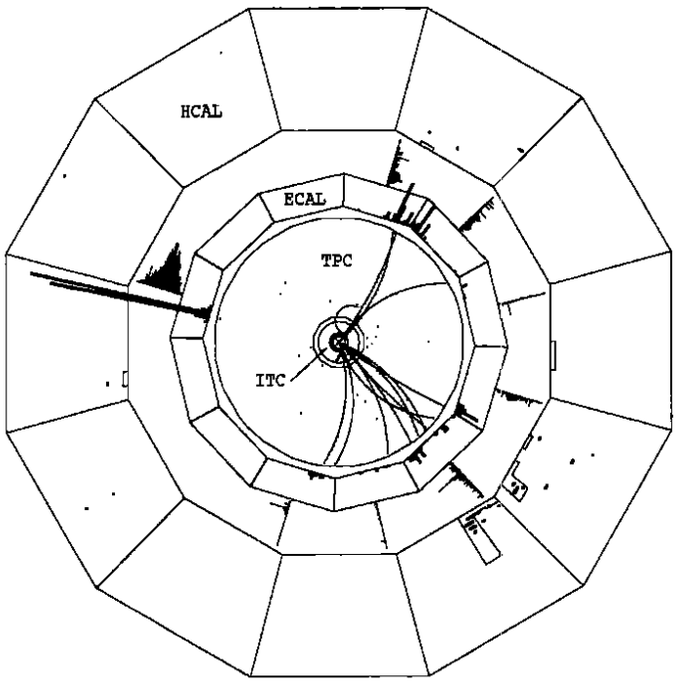

Figure 3.2: An event $e^+e^- \rightarrow Z \rightarrow q\bar{q}\gamma$ used for the energy flow algorithm calibration. The hard photon carries an energy of 36 GeV. The mass recoiling against it is 43 GeV/c^2, while the visible mass of the hadronic system is 39 GeV/c^2, consistent with the 4.5 GeV/c^2 mass resolution expected from a 40 GeV/c^2 Higgs Monte Carlo simulation. The total visible mass of the event is 89 GeV/c^2. Also indicated: the inner tracking chamber (ITC), the time projection chamber (TPC), the electromagnetic calorimeter (ECAL) and the hadron calorimeter (HCAL).

The selected events must have a photon with an energy in excess of 20 GeV. The photon is removed and the remaining hadronic system must satisfy the acoplanar jets selection criteria (section 5.3.5). In the data, 321 such events have been found. These events provide two methods for the determination of the mass of the hadronic system: the above direct determination of the visible mass M_{vis} from the charged particle momenta and the calorimeter cluster energies, and an indirect method, computing the recoil mass M_{rec} from the photon energy.

The distribution of the difference $\Delta M \equiv M_{rec} - M_{vis}$ between the two values of the hadronic mass is shown in fig. 3.3 for the data and for the Monte Carlo prediction. Both distributions are centred at 2 GeV/c^2 with a resolution of 6.2 GeV/c^2. The 2 GeV/c^2 shift is due to unavoidable losses in the direct determination of the visible mass such as dead zones of the detector, neutrinos from semi-leptonic decays of heavy quarks, or initial state radiation. The 6.2 GeV/c^2 resolution on ΔM comes from the convolution of the uncertainties on the photon energy (i.e. on M_{rec}) and on the visible mass M_{vis} of the hadronic system. In the selected events the mean photon energy is $\sim$ 30 GeV and therefore the mass of the recoiling system is centred at 50 GeV/c^2. In this configuration the uncertainty on the photon energy is 1.6 GeV and it directly translates into a 2.9 GeV/c^2 uncertainty on M_{rec}. The 5.5 GeV/c^2 resolution on M_{vis} thus inferred from this sample is in very close agreement with that expected for a 50 GeV/c^2 Higgs boson by a

Monte Carlo simulation of $(H^0 \rightarrow hadrons)(Z^* \rightarrow \nu\bar{\nu})$. This shows the reliability of the direct determination of the hadronic mass, both on data and on Monte Carlo, the only method usable for events with missing energy.

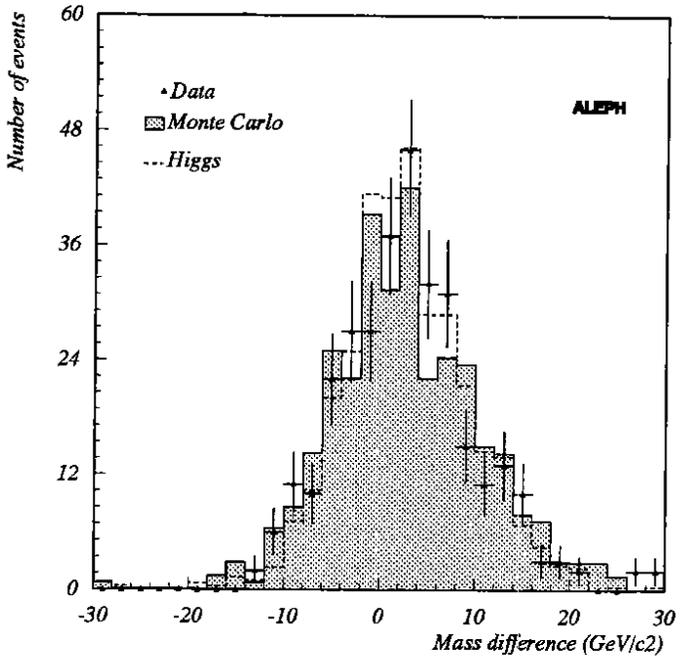

Figure 3.3: Distribution of the mass difference $\Delta M \equiv M_{rec} - M_{vis}$ in the $q\bar{q}\gamma$ events for the data (points with error bars) and the Monte Carlo (filled area). Same distribution (dashed line) for events of the type $(H^0 \rightarrow hadrons)\nu\bar{\nu}$ with $m_{H^0} = 50\,\mathrm{GeV}/c^2$ (here $M_{rec} \equiv m_{H^0}$).

3.5 Monte Carlo Simulation

The simulation of events in ALEPH has two principal elements: the use of physics generators to produce the four-momenta of particles according to the process under study, and the tracking of those particles through the simulated detector including interactions and decays.

Tracking is made in the GEANT/GHEISHA framework [20]. "Hits" are produced on tracks in the tracking detectors and are smeared by the appropriate spatial resolution and used to produce "raw data" containing the same information as real events. Showers in calorimeters are developed using the GEANT/GHEISHA tables and algorithms but, to speed up event generation, all electrons and positrons are parametrized in the calorimeters using parametrizations established from test beam data. The longitudinal energy distribution is parametrized $s^a e^{-bs}$, where s is the shower depth expressed in radiation lengths, and where $1/b$ and a/b are independent parameters. The transverse shape is parametrized according to the distance from the shower axis and the depth in the shower. Simulated analogue and digital signals are produced corresponding to those of real events; these are also used for a careful simulation of the trigger. Thus Monte Carlo events have the same data format as real events and are subsequently reconstructed in the same way to allow detection efficiencies to be determined and detailed comparisons of data and Monte Carlo distributions to be made.

4 Determination of Width Limits

4.1 Introduction

The parameters of the Z resonance obtained by fitting the lineshape of the decays into hadrons and charged leptons agree well with the standard model predictions [14]. However room is still left for a new hypothetical decay mode $Z \to X$ if its decay width is not too large. In this section we determine limits on the width Γ^X of a new channel from the lineshape parameters, assuming it contributes incoherently.

The analysis is based on the results of the combined fit to individual lepton and hadron cross-sections assuming lepton universality. It uses the fitted values of the total Z width, Γ_Z, the hadronic peak cross-section, σ_h^0, and hadron to lepton width ratio, R. Each value is compared to the prediction from the standard model plus a contribution from a new channel, and a maximum allowed value of Γ^X is determined at the 95% c.l. In general, the limit on Γ^X is expressed in terms of topological branching ratios

$$x_h = \Gamma_h^X/\Gamma^X, \quad x_\ell = \Gamma_\ell^X/\Gamma^X \quad \text{and} \quad x_{inv} = \Gamma_{inv}^X/\Gamma^X$$

(satisfying $x_h + x_\ell + x_{inv} = 1$) where the subscripts h, ℓ and inv refer to event topologies which would be classified as standard Z decays into hadrons, a pair of collinear leptons or neither respectively. The variables used in this analysis cover different regions of x_h and x_ℓ.

Standard model predictions depend on unknown or uncertain parameters, such as the top quark and Higgs boson masses, and the strong coupling constant. In this analysis these parameters were always chosen to give the most conservative limit. The limits obtained from width ratios are expected to be more robust since theoretical uncertainties partly cancel. Moreover, new phenomena may have virtual effects in addition to the real production being investigated which again may spoil total and partial widths more than width ratios.

4.2 Setting the Limits

Standard model predictions were calculated [21,22] allowing the top quark and Higgs boson masses, m_t and m_{H^0}, and the strong coupling constant, α_s, to vary within the limits $87 \le m_t \le 200\,\mathrm{GeV}/c^2$, $50 \le m_{H^0} \le 1000\,\mathrm{GeV}/c^2$ and $0.107 \le \alpha_s \le 0.125$, where the uncertainty in α_s is given by the one standard deviation error of the ALEPH measurement [23].

The allowed interval of a variable was determined assuming a Gaussian measurement error and imposing the standard model bound. In the case of the total width the model provides a lower bound (corresponding to $m_t = 87\,\mathrm{GeV}/c^2$, $m_{H^0} = 1000\,\mathrm{GeV}/c^2$ and $\alpha_s = 0.107$). The area above the bound is divided in proportion 95:5 and the dividing line gives the position of the upper bound. The width limit at 95% c.l. is $\Gamma^X < 46\,\mathrm{MeV}$ independent of topology. The details of the calculation are given in table 4.1.

The peak hadronic cross-section is related to the widths by the expression:

$$\sigma_h^0 = \frac{12\pi}{m_Z^2}\,\frac{\Gamma_\ell \Gamma_h}{\Gamma_Z^2}.$$

The existence of an extra channel, X, implies the following (negative) change of σ_h^0:

$$\Delta\sigma_h^0 = \sigma_h^0 \left[\left(\frac{\Gamma_Z}{\Gamma_Z + \Gamma^X} \right)^2 \frac{\Gamma_h + x_h \Gamma^X}{\Gamma_h} - 1 \right] \approx \sigma_h^0 \frac{\Gamma^X}{\Gamma_Z} \left[\frac{x_h}{B_h} - 2 \right],$$

where only first order terms in Γ^X/Γ_Z are kept and $B_h = \Gamma_h/\Gamma_Z$. The boundary of the allowed region in the plane (Γ^X, x_h) is given by the relation:

$$\Gamma^X = \Gamma_Z \frac{\Delta\sigma_h^0}{\sigma_h^0} \left(\frac{x_h}{B_h} - 2 \right)^{-1}.$$

Variable	Measured value	S.M. bound	Other-side bound	Allowed interval
Γ_Z (MeV)	2484 ± 17	> 2468	< 2514	46
σ_h^0 (nb)	41.44 ± 0.36	< 41.53	> 40.76	-0.77
R	21.00 ± 0.20	< 20.86	> 20.55	-0.31
R	21.00 ± 0.20	> 20.69	< 21.33	0.64

Table 4.1: Determination of the interval allowed by the standard model and consistent with the data at the 95% confidence level.

The value of $\Delta\sigma_h^0$ is determined from the measurement and from the standard model bound $\sigma_h^0 < 41.53\,\mathrm{nb}$ corresponding to $m_t = 200\,\mathrm{GeV}/c^2$, $m_{H^0} = 1000\,\mathrm{GeV}/c^2$ and $\alpha_s = 0.107$.

A similar analysis has been performed for the ratio R. The change in R due to a new channel depends both on x_ℓ and x_h and is given by the formula:

$$\Delta R = \frac{\Gamma_h + x_h\Gamma^X}{\Gamma_\ell + \frac{1}{3}x_\ell\Gamma^X} - \frac{\Gamma_h}{\Gamma_\ell} \approx R\frac{\Gamma^X}{\Gamma_Z}\left(\frac{x_h}{B_h} - \frac{x_\ell}{3B_\ell}\right)$$

where B_ℓ $(= \Gamma_\ell/\Gamma_Z)$ is the branching ratio for Z decay into one charged lepton family.

This leads to the limit

$$\Gamma^X = \Gamma_Z\frac{\Delta R}{R}\left(\frac{x_h}{B_h} - \frac{x_\ell}{3B_\ell}\right)^{-1}.$$

The value of ΔR is determined separately in two regions of x_ℓ/x_h in which ΔR has opposite sign leading to two entries in table 4.1.

The contour plot in fig. 4.1(a) summarizes the topology-dependent limits plotted as a function of leptonic and hadronic branching ratios of the new process. For small x_ℓ the limit is independent of x_ℓ and comes from σ_h^0 when x_h is less than 0.7 and from Γ_Z for larger values of x_h. In the remaining area R is the most effective. The limit for a given x_h independent of x_ℓ is plotted in fig. 4.1(b). The analogous plot for x_ℓ is shown in fig. 4.1(c).

In the case of a totally invisible decay mode the limit $\Gamma_{inv}^X = 22\,\mathrm{MeV} = 0.13\Gamma_\nu$ is obtained from the measurement of $\Gamma_{inv}/\Gamma_\ell = 5.91 \pm 0.15$ $(N_\nu = 2.97 \pm 0.07)$ and the conservative standard model prediction 5.97, with the same treatment of confidence intervals.

In conclusion, limits from width ratios are generally better than those derived from the total width. However they are useful only if the topological hadronic or leptonic branching ratio of the new process is known. The limits for some particular topologies are given in table 4.2. They are translated into mass limits in later sections of this report.

Topology	Origin	Width limit (MeV)	Br. limit (%)
any	Γ_Z	46	1.9
non-hadronic	σ_h^0	23	1.0
purely leptonic	R	3.7	0.15
invisible	N_ν	22	0.9

Table 4.2: Width limits from the ALEPH Z lineshape measurements.

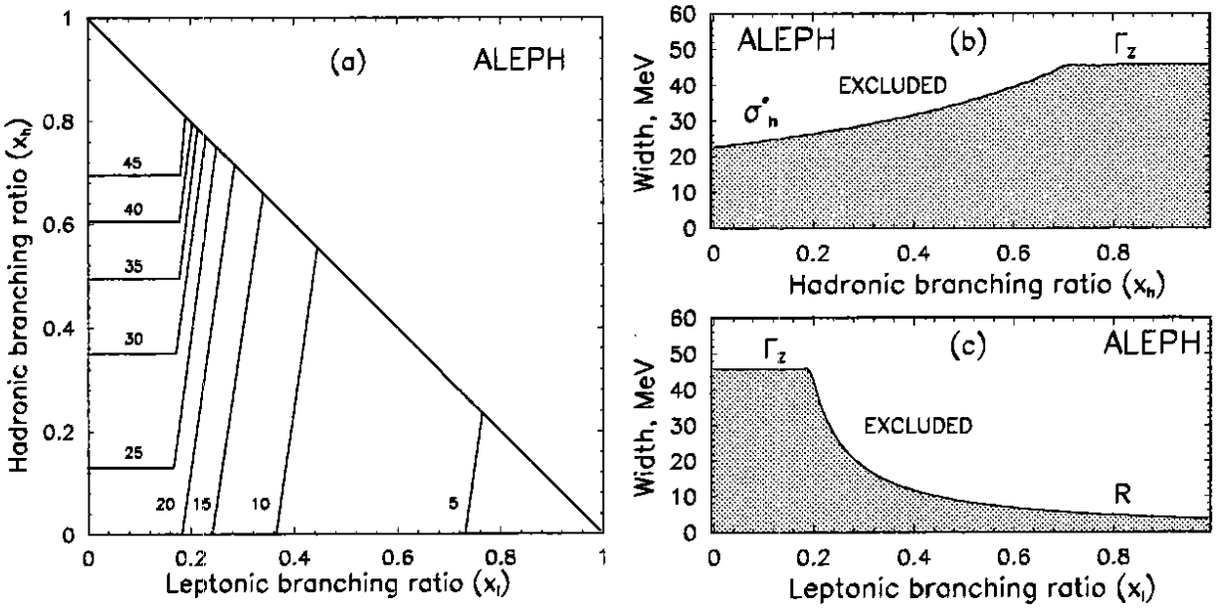

Figure 4.1: (a) width limit contours in MeV in the two dimensional plane of hadronic and leptonic branching ratio. In addition the excluded widths for a new process are shown for (b) decay into hadrons (c) decay into leptons, with the labels indicating the origin of each limit.

5 The Minimal Standard Model Higgs Boson

5.1 Introduction

In the minimal standard model, the spontaneous breaking of $SU(2)_L \times U(1)_Y$ is achieved at the expense of the introduction of a doublet of complex Higgs fields ϕ in self-interaction. As ϕ develops a vacuum expectation value v, the W and Z bosons acquire their masses while three of the four initial degrees of freedom are absorbed. A single Higgs scalar particle H^0 therefore results. This same mechanism can also induce masses for the matter fermions if Yukawa couplings of the type $\lambda f\bar{f}\phi$ are present. The standard Higgs boson therefore appears as a cornerstone of the minimal standard model of electroweak interactions.

The most direct experimental manifestation of this crucial aspect of the theory would be the observation of the production and the decay of the Higgs boson *via* the Bjorken process [24] $e^+e^- \rightarrow Z \rightarrow Z^*H^0$ (fig. 5.1) which should be achievable during the first phase of LEP if its mass is below $65 - 70\,\mathrm{GeV}/c^2$. This process has already been investigated by ALEPH [25,26,27,28,29] and the other LEP collaborations—DELPHI [30,31,32], L3 [33,34,35] and OPAL [36,37,38,39,40]. Searches for many different topologies have been carried out with the ALEPH detector in order to be sensitive to most of the possible final states induced by the process $e^+e^- \rightarrow H^0Z^*$. The purpose is twofold: *(i)* to achieve the highest efficiency for large Higgs masses, and *(ii)* to increase the exclusion level of significance at lower masses in order to exclude standard Higgs-like objects with weaker couplings to the Z, for example the neutral Higgs bosons of supersymmetry.

The relative Z^* decay branching ratios on the one hand (70% into hadrons, 20% into neutrinos and 10% into charged leptons) and the Higgs boson decay topologies as a function of its mass on the other have led to a search strategy briefly described below. The searches in the different topologies have been optimized to reject background and maximize efficiencies in the mass range where they are most useful. The efficiency of each search as a function of mass was calculated by Monte Carlo and used to derive limits in the whole mass domain. Although 66%

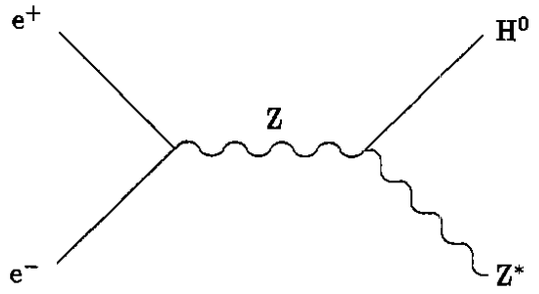

Figure 5.1: Feynman diagram for production of a Higgs boson via the Bjorken process.

of events at high Higgs mass produce a four-jet topology from $Z^* \to q\bar{q}$ and $H^0 \to q\bar{q}$, the high background from standard hadronic decays of the Z excludes their use in the search for the Higgs boson

5.1.1 Very low Higgs mass domain: $m_{H^0} < 2m_\mu$.

When the Higgs mass is less than twice the muon mass, the only available final states for its decay are e^+e^- through the direct H^0ee coupling and $\gamma\gamma$ *via* loop diagrams. Because of the weakness of the H^0ee coupling, the lifetime of such a light Higgs boson is non-negligible and has to be taken into account in the analysis; for $m_{H^0} = 40\,\mathrm{MeV}/c^2$, for instance, the lifetime is about 100 ps, which leads to a mean free path of $\sim$ 6 m for a Higgs produced in the decay $Z \to H^0Z^*$. This mean free path increases as $1/m^2_{H^0}$, rendering a very light Higgs practically "invisible" in Z decays. Such an invisible Higgs can be detected indirectly if the Z^* decays to an e^+e^- or $\mu^+\mu^-$ pair thanks to the missing energy-momentum in the event which produces an energetic acoplanar lepton pair. This search would also be applicable to the $\nu\bar{\nu}$ decays of the Higgs boson, were the neutrinos massive.

5.1.2 Intermediate Higgs mass domain: $2m_\mu < m_{H^0} < 15\,\mathrm{GeV}/c^2$.

For m_{H^0} smaller than twice the D mass, the main Higgs decay topology is into two charged particles. Therefore, a search for acoplanar charged particle pairs with substantial missing energy is relevant when $Z^* \to \nu\bar{\nu}$. This topology is also characteristic of the configuration $(H^0 \to \tau^+\tau^-)(Z^* \to \nu\bar{\nu})$ and has been extended to be made sensitive to the 3-prong decays of the τ. In the configuration $(H^0 \to \tau^+\tau^-)(Z^* \to \ell^+\ell^-)$, where ℓ is a charged lepton, a search for four-lepton final states has been made. For higher Higgs masses, the charged multiplicity of the decay products increases and the dominant final state becomes a hadronic jet. In the configuration $(H^0 \to \textit{hadrons})(Z^* \to \nu\bar{\nu})$ and in the Higgs mass range considered, the typical Higgs momentum is sufficiently large with respect to m_{H^0} for the monojet topology to be dominant: it still accounts for 80% of the final states when $m_{H^0} = 15\,\mathrm{GeV}/c^2$.

A search for two very energetic leptons recoiling against a low multiplicity and low mass jet is relevant in this mass range when the Z^* decays into two electrons or two muons. However, a non-negligible number of events with the same topology is expected to be produced from standard background processes such as $e^+e^- \to \ell^+\ell^-\ell'^+\ell'^-$ or $\ell^+\ell^-q\bar{q}$. Therefore, this search is not taken into account in the derivation of the Higgs mass limit but is reported for completeness.

5.1.3 High Higgs mass domain: $m_{H^0} > 11\,\mathrm{GeV}/c^2$.

Above the $b\bar{b}$ threshold, the dominant Higgs decay mode is into hadrons, but the branching ratio into τ pairs always remains above 6%. Therefore the searches for acoplanar τ pairs and for four-lepton final states remain relevant. Although the search for monojets retains substantial efficiency up to a Higgs mass of about $35\,\mathrm{GeV}/c^2$, a search for pairs of acoplanar, acollinear jets with missing energy becomes increasingly appropriate in the configuration $(H^0 \to \textit{hadrons})(Z^* \to \nu\overline{\nu})$ as the Higgs mass gets larger. When the Z^* decays into two electrons or two muons instead of neutrinos, it is appropriate to search for a pair of energetic, isolated (and thus well identifiable) leptons in hadronic events.

When the Z^* decays into two τs, a fraction of the energy of the τs is carried away by the decay neutrinos. Depending upon this fraction, the possible final state topologies are very different. In one extreme situation, the final state resembles the configuration $(H^0 \to \textit{hadrons})(Z^* \to \nu\overline{\nu})$, and the search for acoplanar jets therefore applies. In another extreme situation, the two τs may decay into energetic electrons or muons and the search for energetic leptons can be used. When the two τs decay into energetic charged particles, but now not necessarily leptons, the final state may be characterized by two charged particles isolated from a hadronic system. Finally, when the energy of one of the τs is carried mainly by a charged particle, while the energy of the other mainly by neutrinos, a search for isolated charged particles in hadronic events is performed. Of course, all these searches apply equally well in the configuration $(H^0 \to \tau^+\tau^-)(Z^* \to \textit{hadrons})$.

5.2 Common Features of the Analyses

5.2.1 Definitions and notations

All the good tracks, tracks from reconstructed V^0s, photons and neutral hadrons provided by the energy flow algorithm (section 3.4) are called "particles" in the following. These particles are used in the analyses to determine quantities such as missing momentum, visible mass, thrust axis, etc.

To define two jets, the events are divided into two hemispheres by a plane perpendicular to the thrust axis. The acollinearity η is the angle between the two jet directions, and the acoplanarity ψ the angle between the two jet directions projected onto $\mathcal{P}$, the plane transverse to the beam axis. In this definition two back-to-back jets have acollinearity and acoplanarity angles of 180°.

In the case of events induced by two-photon processes or by annihilation accompanied by hard initial state radiation, it may be preferable to work directly in the plane $\mathcal{P}$. For that purpose, all particle momenta are projected onto $\mathcal{P}$, a 2d-thrust axis is computed therein, and the event is divided into two 2d-jets with respect to that axis. The projected acoplanarity ψ_p is defined as the angle between the directions of the two 2d-jets. The projected transverse momentum ρ_p is defined as the scalar sum of the transverse components of the 2d-jet momenta, measured with respect to the 2d-thrust axis. A given part of an event may also be arbitrarily forced to produce any number n of jets, the jet clustering being performed with the LUCLUS algorithm [41].

Finally, although instrumented down to a polar angle of 2°, the very forward region of the detector, including ECAL/HCAL edges and the luminosity calorimeter (LCAL), is preferably avoided in searches for final states with missing energy since the boundaries between calorimeters are more numerous in this region and the energy resolution is therefore degraded. For vetoing purposes, the quantity E_{12}, defined as the total energy measured in the calorimeter cells within 12° of the beam axis, is used.

5.2.2 Monte Carlo samples

The selection procedures have been developed using appropriately weighted samples of fully simulated events, so that the efficiency for the H^0Z^* search is maximized while less than one background event is expected in the data sample.

The Monte Carlo samples used are the following: *(i)* 265,000 $Z \to$ *hadrons*, *(ii)* 30,000 $Z \to \tau^+\tau^-$, corresponding to three times the recorded integrated luminosity, *(iii)* 30,000 $e^+e^- \to (e^+e^-)q\bar{q}$, with $m_{q\bar{q}} > 4\,\mathrm{GeV}/c^2$, corresponding to an integrated luminosity of $\sim 25\,\mathrm{pb}^{-1}$, *(iv)* 20,000 $e^+e^- \to (e^+e^-)\tau^+\tau^-$, corresponding to an integrated luminosity of $\sim 50\,\mathrm{pb}^{-1}$, and *(v)* for various Higgs masses from 0 to $60\,\mathrm{GeV}/c^2$, at least 1,000 H^0Z^* events in each of the configurations studied.

5.2.3 Simulation of the production and of the decay of the Higgs boson

The H^0 production cross-section has been determined using the calculation of ref. [42] for the process $e^+e^- \to H^0\mu^+\mu^-$ where the Born approximation has been replaced by the "improved Born approximation" [43,44] and convoluted with an initial-state radiation spectrum computed to second order [45]. The correction to the cross-section due to a top quark loop at the ZZ^*H vertex, as calculated in ref. [46], has also been taken into account. When the Z^* decays into a charged lepton pair, the radiation of a photon by a final state lepton is simulated using an algorithm described in ref. [47]; when the Z^* decays into quarks, the Lund parton shower model [48,49,50] is used for the simulation of quark fragmentation.

In addition to the simple decay channels into massive fermion pairs, the simulation of the decays of the Higgs boson includes the decays into two photons and two gluons, a special treatment of the hadronic decays in the mass range $2m_\pi \leq m_{H^0} \lesssim 2\,\mathrm{GeV}/c^2$, and the first order QED and QCD corrections to the channels $H^0 \to f\bar{f}(\gamma)$ and $q\bar{q}(g)$ [51,52]. For large Higgs masses (above $45\,\mathrm{GeV}/c^2$), the hadronic decays have been modelled using the Lund parton shower algorithm, better suited to simulate the subsequent hadronization of the quark system than first order gluon radiation.

5.3 Topological Searches

5.3.1 Search for energetic acoplanar pairs

In this section, a search for energetic lepton pairs with missing energy, typical of a long-lived Higgs boson, is described. The backgrounds to such final states are $Z \to \tau^+\tau^-$, with each of the τs decaying to a single charged particle, $Z \to \ell^+\ell^-(\gamma)$, with $\ell =$ e or μ, and charged particle pairs produced in two-photon interactions.

Only events with exactly two good tracks are considered. The $Z \to \tau^+\tau^-$ and the two-photon interaction backgrounds are brought down to a negligible level by requiring that both charged particle momenta exceed $30\,\mathrm{GeV}/c$. Cuts are applied on the acoplanarity and on the acollinearity angles η and ψ between the two tracks to eliminate non-radiative dilepton events and dilepton events where a photon from initial or final state radiation is present but remains undetected. This happens when it is emitted below the LCAL acceptance or too close to the direction of one of the final leptons, in which case its energy deposit in ECAL is not resolved from that of the charged lepton. Both $\pi - \eta$ and $\pi - \psi$ are required to exceed 50 mrad.

The other radiative dilepton events are eliminated by requiring that E_{12} be zero, that the total energy of the ECAL neutral clusters be less than 1 GeV, and that the total energy of the HCAL neutral clusters situated in the regions of HCAL backing the boundaries between the ECAL modules be less than 500 MeV. To avoid vetoing a Higgs event because of a final state radiation or bremsstrahlung photon coming from one of the two leptons, any cluster

situated within $\pm 2^\circ$ in polar angle and within $+Q_\ell \times 6^\circ$ and $-Q_\ell \times 3^\circ$ in azimuth of the direction of a charged particle is ignored where Q_ℓ is the sign of the charge of the particle. (Asymmetric azimuthal cuts are made necessary by the curvature of the charged particle tracks in the magnetic field.)

No events survived in the data, while the selection efficiency for a massless, and therefore stable, Higgs boson is 30% when Z^* decays to $\mu^+\mu^-$ and 20% when Z^* decays to e^+e^-.

5.3.2 Search for acoplanar pairs

In this section the topology of interest consists of a pair of charged particles or τ decay products accompanied by missing energy. The search has been optimized for a 50 GeV/c^2 Higgs boson in the configuration $(H^0 \to \tau^+\tau^-)(Z^* \to \nu\overline{\nu})$, but it is also used for the two- or four-prong Higgs boson decays that occur below the $\tau^+\tau^-$ threshold.

To select this topology, events with two or four charged particle tracks and total electric charge zero are considered. τ candidates decaying into three charged particles are selected as triplets of tracks with a total electric charge ± 1 and an invariant mass smaller than 1.5 GeV/c^2. If more than one triplet fulfils these conditions, only the one with the lowest mass is considered. For simplicity, the τ triplets and the remaining charged particle tracks are referred to as leptons, and only the events with two leptons are further considered. At this stage, the main background sources are $e^+e^- \to \ell^+\ell^-(\gamma)$ and $e^+e^- \to (e^+e^-)\ell^+\ell^-$.

To avoid energy losses in the forward region of the detector, E_{12} is required to be zero and both lepton directions must form an angle θ with the beam axis such that $|\cos\theta| < 0.95$. To remove most of the $Z \to \ell^+\ell^-$ events, the acollinearity angle of the two leptons, η, must be smaller than 165°. In addition, if the angle θ between the direction of the total momentum of the leptons and the beam axis is such that $|\cos\theta| > 0.90$, it is required that $\eta > 2.5^\circ$ to remove e^+e^- pairs from photon conversions which occur preferentially at low angles with respect to the beam axis.

Events from $Z \to \ell^+\ell^-\gamma$ are eliminated by applying a "photon veto" which requires that no neutral particle with energy above 1 GeV be detected unless the angle of its direction with that of one of the leptons is smaller than 10°, or unless the invariant mass of it and one of the leptons is smaller than 2 GeV/c^2. However, to retain efficiency for low multiplicity monojets, the "photon veto" is not applied to events with a total visible mass smaller than 10 GeV/c^2.

Background from two-photon events can arise in which both spectator electrons remain below the inner boundary of the LCAL acceptance. Thus the component of the vector sum of the lepton momenta transverse to the beam axis is required to exceed 3.75% of the centre-of-mass energy. The same cut is applied to the transverse component of the total visible momentum. As it may also happen that a spectator electron escapes through the vertical crack of the LCAL but still remains below the inner boundary of the HCAL acceptance, a tighter cut at 5% of the centre-of-mass energy is also applied if the direction of the total missing momentum is within $\pm 10^\circ$ in azimuth of the vertical LCAL crack.

The background from $e^+e^- \to (e^+e^-)\tau^+\tau^-$ is not fully removed by the transverse momentum cuts because of the energy taken away by the neutrinos from the τ decays. These events appear almost coplanar, but with an acoplanarity potentially increased if at least one of the τs has emitted an energetic neutrino. This background is efficiently removed by rejecting events in which the projected transverse momentum ρ_p is smaller than 1.25 GeV/c. To preserve monojet-like events, this last cut is not applied when the 2d-thrust axis points between the two projected lepton momenta.

No events remained, while the efficiency for a 50 GeV/c^2 Higgs boson decaying to $\tau^+\tau^-$, with the Z^* decaying to $\nu\overline{\nu}$, is 41%.

5.3.3 Search for four-lepton final states

To select this topology, characteristic of the configuration $(H^0 \to \tau^+\tau^-)(Z^* \to \ell^+\ell^-)$ only events with four or six charged particle tracks are considered, and among them, only those with four leptons, as defined in section 5.3.2 are kept. The same E_{12} veto is also applied.

To remove the expected $e^+e^- \to 4$ *leptons* electroweak background, all pairs of leptons are required to have invariant masses in excess of $2\,\mathrm{GeV}/c^2$. In the signal events, it is expected that a substantial energy, carried away by the neutrinos coming from τ decays, should be missing. The four events remaining in the data, all identified as $ee\mu\mu$ and $\mu\mu\mu\mu$ final states, were removed by further requiring that the scalar sum of the charged particle momenta be less than $85\,\mathrm{GeV}/c^2$. For a $50\,\mathrm{GeV}/c^2$ Higgs boson decaying to $\tau^+\tau^-$ while the Z^* decays to e^+e^-, $\mu^+\mu^-$ or $\tau^+\tau^-$, the efficiency of this search is 54%.

5.3.4 Search for monojets

The monojet topology is characteristic of the configuration $(H^0 \to \textit{hadrons})(Z^* \to \nu\bar{\nu})$ in the intermediate Higgs mass domain. The analysis has been optimized for the search for a $10\,\mathrm{GeV}/c^2$ Higgs boson. The main backgrounds to this topology are two-photon processes and $e^+e^- \to \tau^+\tau^-$ when the energy of one of the τs is carried away by neutrinos. To reject most of the latter, only events with at least four good tracks are considered. For an event to be classified as a monojet, one of the two hemispheres defined with respect to the thrust axis is required to contain an energy smaller than 2 GeV, the other hemisphere being the "monojet".

By reinforcing the veto on the second hemisphere in requiring that no energy be measured in a cone of half angle 50° around the direction opposite to that of the monojet, most of the $e^+e^- \to \textit{hadrons}$ and all of the remaining $e^+e^- \to \tau^+\tau^-$ background events are removed. The remaining background comes mostly from two-photon processes and is expected to be produced at low polar angle. Therefore the direction of the monojet is required to form an angle θ with respect to the beam axis such that $|\cos\theta| < 0.9$ and E_{12} is required to be zero.

No events survived in the data after requiring that the total transverse momentum exceed 5% of the centre-of-mass energy. This cut eliminates most of the remaining background but, to remove the few background events still expected from the process $e^+e^- \to (e^+e^-)\tau^+\tau^-$, and although this is not needed by the data, the projected acoplanarity ψ_p is required to be smaller than 150°.

For an $11\,\mathrm{GeV}/c^2$ Higgs, the resulting efficiencies are 57% for $H^0 \to \textit{hadrons}$ and 13% for $H^0 \to \tau^+\tau^-$.

5.3.5 Search for acoplanar jets

In this section, the topology of interest consists of a pair of jets accompanied by missing energy. The search has been optimized for a $50\,\mathrm{GeV}/c^2$ Higgs boson in the configuration $(H^0 \to \textit{hadrons})(Z^* \to \nu\bar{\nu})$.

Backgrounds arise from events where some energy is either unseen or mismeasured in the detector. Therefore, performing cuts on energy related quantities might not be the best choice to eliminate standard sources of missing energy. However, as this missing energy is likely to be contained in jets (neutrinos from semileptonic decays, cracks in the calorimeters), the directions of the jets should still be well determined and reliable. Most of the cuts were thus performed on these jet directions, resulting in both a higher selection efficiency and a better selectivity.

To design these cuts, attention was first focused on hadronic events with energy actually lost, characterized by a visible mass smaller than $70\,\mathrm{GeV}/c^2$, at least five good tracks and a scalar sum of the momenta carried by the good tracks in excess of $8\,\mathrm{GeV}/c$. In addition, to

be complementary to the monojet analysis (section 5.3.4), the energies measured in the two hemispheres defined with respect to the event thrust axis are required to exceed 2 GeV.

For a substantial fraction of these events, energy is lost because a parton has been emitted close to the beam direction and some of its fragmentation products escape the detector. The fraction of the total visible energy measured beyond 30° of the beam axis is thus required to exceed 60%. Furthermore, to avoid dealing with the very forward region of the detector, E_{12} has to be smaller than 3 GeV.

Most of the remaining background is due to $Z \rightarrow$ *two jets*, where at least one of the jet energies is measured to be much smaller than the beam energy. Whatever the origin and the amount of energy lost, the two jets remain collinear while the two jets coming from a Higgs decay would be acollinear, as shown in fig. 5.2. The acollinearity angle η is therefore required to be smaller than 165°. However, if a hard photon is radiated in the initial state, the energy of this photon is lost and the two jets become acollinear. If the jet energies were perfectly determined for these events the total missing momentum would point along the beam direction. If α is the angle between the missing momentum and the beam axis some energy fluctuation in the two jets is allowed by requiring $\tan\alpha$ to be larger than 0.4 ($\alpha > 21.8°$).

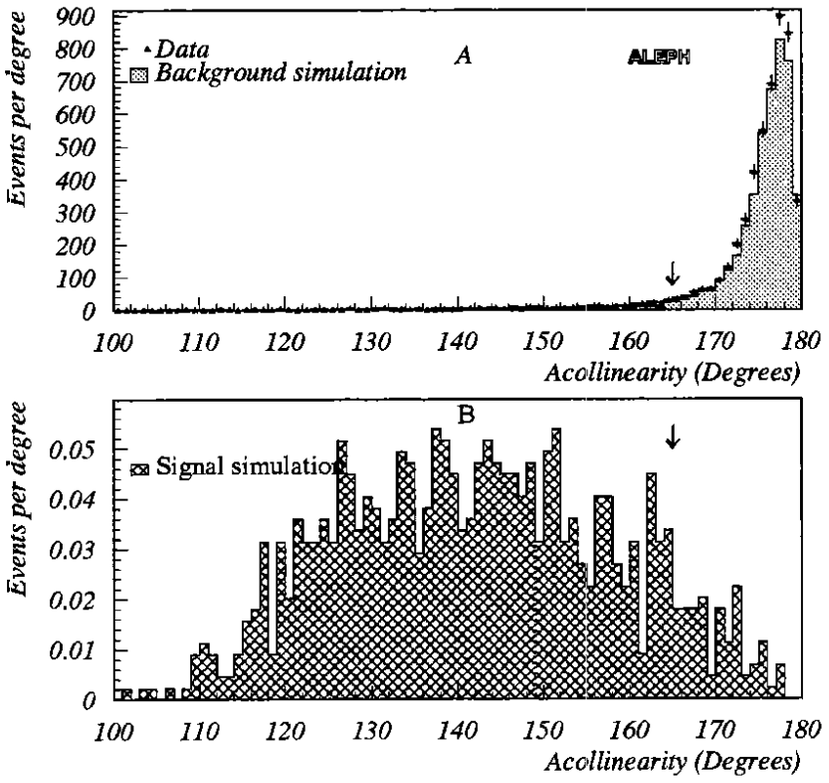

Figure 5.2: Distributions of the acollinearity angle η between the two jets in the acoplanar jet pair search: (A) for the data (points with error bars) and the simulated background processes (filled area) and (B) for the signal in the configuration $(H^0 \rightarrow \nu\overline{\nu})(Z^* \rightarrow hadrons)$. The arrows indicate the value of the cut.

The events surviving at this point are mostly three-jet events, where at least one of the jet energies is mismeasured, making the direction of at least one of the two hemispheres unreliable. Nevertheless, if only one jet "fluctuated", the total missing momentum should be contained in that jet, and thus not be isolated. The total energy measured in a cone of half-angle 25.8° around the missing momentum, E_{cone}, is therefore required to be smaller than 3 GeV.

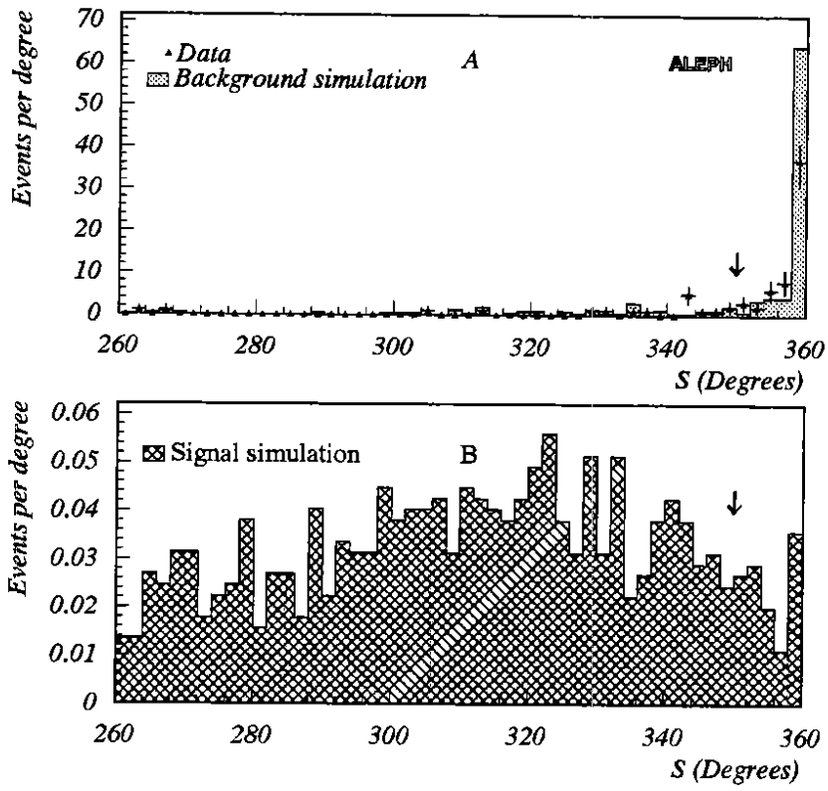

Figure 5.3: Distributions of the variable $\mathcal{S}$ (see text) in the acoplanar jet pair search: (A) for the data (triangles with error bars) and the simulated background processes (filled area) and (B) for the signal in the configuration $(H^0 \rightarrow \nu\overline{\nu})(Z^* \rightarrow hadrons)$. The arrows indicate the value of the cut.

For three-jet events with at least two fluctuating jets, the total missing momentum direction can no longer be used, but the directions of the three jets are still well determined. The jet reconstruction is thus forced to give three jets for each event in the remaining sample. Let θ_i be the angle between the directions of jet j and jet k, with $i, j, k = 1$, 2 or 3, and with $\theta_i < 180°$. Then as a consequence of momentum conservation, the three directions have to be contained in a given plane i.e. they have to fulfil the condition $\mathcal{S} = \sum_{i=1}^{3} \theta_i = 360°$. Two-jet events artificially forced to be reconstructed into three jets tend to have a value of $\mathcal{S}$ close to 360° if collinear, but not otherwise. As the Higgs signal events, even if three-jet like, are not expected to be planar, they always tend to be characterized by a value of $\mathcal{S}$ much smaller than 360°, as shown in fig. 5.3. $\mathcal{S}$ is therefore required to be smaller than 350°.

The remaining events from the processes $e^+e^- \rightarrow q\overline{q}$ or $\tau^+\tau^-$ are two-jet events with large fluctuations and accompanied by a hard initial state radiation. Therefore they have not been rejected by any of the previous cuts (in particular the $\tan\alpha$ cut is inefficient because the direction of the missing momentum is no longer determined by the energetic photon only). However, making use of the direction of the two jets again, the acoplanarity angle ψ of such events remains very close to 180°, whatever the fluctuations and the photon energy. Therefore ψ is required to be smaller than 175°.

To remove the last remaining background events coming from two photon processes, it is finally required, for events with a visible mass smaller than 25 GeV/c^2, that the total momentum transverse to the beam direction be larger than 5% of the centre-of-mass energy.

Although this analysis has been developed for events with a visible mass below 70 GeV/c^2, it is worth looking at its results when applied to the full sample. No events were observed

in the data over the whole mass range, thus rendering useless the 70 GeV/c^2 mass cut. The selection efficiency is about 68% for a 50 GeV/c^2 Higgs boson. It is worth noticing that, when applied to the $\tau^+\tau^-q\bar{q}$ final state and for a 50 GeV/c^2 Higgs boson, the efficiencies of this search are 9% in the configuration $(H^0 \to \tau^+\tau^-)(Z^* \to \textit{hadrons})$ and 5% in the configuration $(H^0 \to \textit{hadrons})(Z^* \to \tau^+\tau^-)$.

5.3.6 Search for energetic lepton pairs in hadronic events

This search has again been optimized for a 50 GeV/c^2 Higgs boson, but now for the configurations $(H^0 \to \textit{hadrons})(Z^* \to e^+e^-$ or $\mu^+\mu^-)$.

Energetic pairs, in events with at least seven good tracks carrying more than 10% of the centre-of-mass energy, are defined as pairs of oppositely charged good tracks with individual momenta in excess of 3 GeV/c, with a scalar sum of momenta greater than 20 GeV/c and with an invariant mass greater than 5 GeV/c^2.

To declare the pair isolated with respect to the recoiling hadronic system, the scalar sum of the transverse momenta of the two tracks calculated with respect to the thrust axis of the rest of the event has to exceed 15 GeV/c. In addition, at least one of the two tracks has to be topologically isolated from the other particles, namely: *(i)* there is no other charged particle track inside a cone of 18.2° half-angle around the direction of its momentum, and *(ii)* the sum of the energies of the neutral particles inside the same cone is smaller than 1 GeV. The clusters potentially coming from final state radiation or bremsstrahlung photons (section 5.3.1) are not counted in the sum.

In order to eliminate the remaining hadronic background events, a lepton identification is performed on both tracks, requiring one track to be "tightly" identified, and allowing the other to be only "loosely" identified, leading to zero events in the data.

For electron identification, the two estimators R_T and R_L are used (section 3.3.1). The tight identification is defined by $R_T > -4$ and $|R_L| < 4$. The loose criterion requires only $R_T > -6$, except when the charged particle track extrapolates to an ECAL crack, where R_T cannot be calculated reliably; in this case, the associated HCAL cluster, if any, must have fewer than six planes of streamer tubes fired.

For muon identification, the track is extrapolated through the HCAL up to the muon chambers and the number of HCAL planes fired inside a road 50 mm wide around the extrapolation of the track is compared to the number of instrumented planes in the corresponding HCAL region. The tight identification criterion requires, in regions where at least 15 planes are instrumented, at least a third of them to be fired, and at least one hit to be registered in the last three HCAL planes or in the muon chambers. The loose identification criterion requires *(i)* in regions where at least 10 planes are instrumented, at least one hit in the last 10 HCAL planes or in the muon chambers, and less than 15 GeV in the corresponding HCAL cluster, or *(ii)* in regions where fewer than 10 planes are instrumented or for the tracks with a momentum smaller than 5 GeV/c, no associated ECAL cluster or its $R_T < -5$.

A control analysis has been performed by looking for an $H^0e\mu$ signal in the data, requiring two leptons of which at least one is tightly identified, thus providing the possibility of testing the lepton identification criteria on an independent sample. This check identified deep inelastic scattering (with one tagged electron) as the main background to the $H^0e\mu$ final state (3.6 events expected, 3 events seen), and even to the H^0ee final state although the loose electron identification is much more selective against soft pions than the loose muon one (1.2 events expected, 0 events seen). To eliminate this ultimate background, it has therefore been required, in the final states with one electron tightly identified, that $Q_e.p_L$ be smaller than $15\%\sqrt{s}$, where p_L is the missing longitudinal momentum of the event and Q_e the sign of the charge of the most energetic electron. No $H^0e\mu$ events remained in the data.

The overall efficiency of this selection for a 50 GeV/c^2 Higgs boson is 74% in the channel ($Z^* \to \mu^+\mu^-$) and 69% in the channel ($Z^* \to e^+e^-$) .

Applying this analysis to the $\tau^+\tau^-q\bar{q}$ final state for a 50 GeV/c^2 Higgs boson, also allowing for $H^0 e\mu$ final states, the efficiencies are 7% in the configuration ($H^0 \to \tau^+\tau^-$)($Z^* \to$ *hadrons*) and 4% in the configuration ($H^0 \to$ *hadrons*)($Z^* \to \tau^+\tau^-$). These are added to the 9% and 5% obtained in section 5.3.5.

5.3.7 Search for isolated charged particle pairs in hadronic events

This search has been optimized for a 50 GeV/c^2 Higgs boson in the configurations ($H^0 \to$ *hadrons*)($Z^* \to \tau^+\tau^-$) and ($H^0 \to \tau^+\tau^-$)($Z^* \to$ *hadrons*), when the two τs do not necessarily decay into leptons. Thus the lepton identification can no longer be used and the isolation requirements have to be tightened to reject the background.

Only events with at least seven good tracks carrying more than 10% of the centre-of-mass energy are considered in the analysis. The energy E_{12} is required to be smaller than 3 GeV. At least two oppositely charged particles, with momenta $p_1 > 2.5$ GeV/c and $p_2 > 5$ GeV/c and with polar angles between 45° and 135°, have to be isolated from the other particles. To be isolated, a particle has to fulfil the conditions that there is no other charged particle track inside a cone of half-angle 25.8° around the direction of its momentum and the invariant mass of the particles contained in the cone has to be compatible with the τ mass, i.e. smaller than 1.5 GeV/c^2.

In the few remaining hadronic background events, there is no particular reason to observe any missing energy, while some missing energy is expected in the signal events due to the neutrinos coming from the τ decays. A missing energy of at least 20 GeV is therefore required, leading to zero events in the data.

For a 50 GeV/c^2 Higgs boson, the efficiencies of this selection are 10% in the channel ($H^0 \to \tau^+\tau^-$)($Z^* \to$ *hadrons*) and 4% in the channel ($H^0 \to$ *hadrons*)($Z^* \to \tau^+\tau^-$), bringing additional efficiencies of 6.5% and 3% (since the selections are not exclusive) to the 16% and 9% obtained with the analyses presented in sections 5.3.5 and 5.3.6.

5.3.8 Search for an isolated charged particle in hadronic events

Here the topology searched for is a charged particle accompanied by missing energy and momentum, both isolated from a hadronic system. Appropriate selection criteria have been developed and optimized to search for charged Higgs bosons in the channel $e^+e^- \to H^+H^- \to (c\bar{s})(\tau^-\bar{\nu}_\tau)$. Since this analysis is found to increase the selection efficiency in the configurations ($H^0 \to \tau^+\tau^-$)($Z^* \to$ *hadrons*) and ($H^0 \to$ *hadrons*)($Z^* \to \tau^+\tau^-$) when the energy of one of the τs is mostly carried away by decay neutrinos, it is described here.

Only events with at least six charged particles carrying more than 10% of the centre-of-mass energy are considered. The energy E_{12} is required to be smaller than 3 GeV. At least one charged particle with a momentum in excess of 2.5 GeV/c and with a polar angle between 45° and 135° has to be isolated from the other particles (with the same definition as in section 5.3.7). To further select events with isolated missing energy and momentum, the total transverse missing momentum of the event with respect to the beam axis is required to exceed 7 GeV/c and the total missing energy has to be larger than 10 GeV. Furthermore, the total energy measured in a cone of half angle 25.8° around the total missing momentum of the event has to be smaller than 3 GeV.

Since in the Higgs mass domain of interest here (40 GeV/$c^2 \lesssim m_{H^0} \lesssim$ 50 GeV/c^2) the standard Higgs boson and the Z^* also carry about half of the centre-of-mass energy each, the energy of the hadronic system (recoiling against the τ) is expected to be $\sim$ 45 GeV; it is thus required

to be smaller than 55 GeV, but no lower bound has been applied in order to allow for energy losses due for example to additional neutrinos.

No events remained in the data after these cuts, but a few background events survive in the Monte Carlo sample. These are eliminated by observing that they are three-jet events with a mismeasured missing momentum but in which the planar topology is preserved (while such a feature is not expected in the H^0Z^* signal). To determine the directions of the "non-τ" jets, the jet reconstruction of the event, from which the τ cone has been removed, is forced to give two jets. Then the sum, S, of the angles between the τ and the first jet, the τ and the second jet, and between the two jets, is expected to be close to 360° for planar events but not otherwise, and a cut on S at 359.5° is therefore applied.

For a 50 GeV/c^2 neutral Higgs boson, the efficiencies of the analysis are 7% in the channel $(H^0 \to \tau^+\tau^-)(Z^* \to hadrons)$ and 5% in the channel $(H^0 \to hadrons)(Z^* \to \tau^+\tau^-)$, bringing additional efficiencies of 3.5% and 3% to the 22.5% and 12% obtained with the analyses presented in sections 5.3.5, 5.3.6 and 5.3.7.

5.3.9 Search for energetic lepton pairs recoiling against a low multiplicity jet

This topology would result from a Higgs boson in the intermediate mass domain accompanied by a Z^* decaying into e^+e^- or $\mu^+\mu^-$. The search has been optimized for a 5 GeV/c^2 Higgs boson.

To select this topology, events with at least four good tracks are considered. The energetic lepton pair is defined as a pair of oppositely charged good tracks with individual momenta in excess of 30 GeV/c. Furthermore, these two tracks have to be identified as an electron pair or a muon pair using the critieria described in section 5.3.6.

At this level, the main background sources come from radiative dilepton events where the photon converts in the detector material and from $e^+e^- \to \tau^+\tau^-$ where at least one of the τs decays into three prongs or more. To eliminate the latter, the angle between each of the two leptons of the pair and the vector sum of the momenta of the other charged particles is required to exceed 14.1°. To remove photon conversions, events with an electron in the system recoiling against the lepton pair are removed if its charged multiplicity is lower than four. Here, the electron identification is performed using the two estimators R_T and R_I by requiring one of the three following conditions to be satisfied: *(i)* $R_I + R_T > -4$ if both estimators are measured, or *(ii)* $R_I > -3$ if only R_I is measured, or *(iii)* $R_T > -3$ if only R_T is measured.

Only two events remained in the data compared to 7.3 predicted from the standard processes $e^+e^- \to \ell^+\ell^-\ell'^+\ell'^-$ or $\ell^+\ell^-$ *hadrons*. For a 5 GeV/c^2 Higgs boson, the efficiency of this analysis is 32% when $Z^* \to e^+e^-$ and 38% when $Z^* \to \mu^+\mu^-$.

5.4 Search Efficiencies and Numbers of Events Expected from $e^+e^- \to H^0Z^*$

5.4.1 Very low mass domain : $0 \leq m_{H^0} < 2m_\mu$

In this mass range only two of the analyses presented above contribute. The search for energetic acoplanar pairs presented in section 5.3.1 applies for very light Higgs bosons which escape undetected, accompanied by a pair of electrons or muons from the Z^* decay. For higher masses, the Higgs lifetime becomes shorter so that some of the decays are expected to occur close enough to the interaction vertex for the search for acoplanar pairs described in section 5.3.2 to be efficient in the configuration $(H^0 \to e^+e^-)(Z^* \to \nu\overline{\nu})$. Table 5.1 shows the efficiencies of these two analyses as a function of the Higgs mass. The numbers of events expected are presented in that same table and in fig. 5.4. The total number of events expected exceeds 38 in the Higgs mass range considered; this domain is thus excluded at a confidence level much higher than 95%.

m_{H^0}	$H^0\nu\bar{\nu}$		$H^0e^+e^-$		$H^0\mu^+\mu^-$	
(MeV/c^2)	Eff.	N_{exp}	Eff.	N_{exp}	Eff.	N_{exp}
0	–	–	20.	17	30.	26
25	1.	5	16.	14	24.	21
50	3.	16	10.	9	15.	13
75	6.	31	5.	4.3	8.	6.5
100	9.	47	2.	1.7	3.	2.6
125	14.	73	1.	0.9	1.5	1.3
150	20.	104	–	–	–	–
200	28.	145	–	–	–	–
212	49.	253	–	–	–	–

Table 5.1: Efficiencies (in %) and expected numbers of signal events in the very low mass Higgs domain arising acoplanar pair searches described in sections 5.3.1 and 5.3.2 and applied to the three channels $e^+e^- \rightarrow H^0\nu\bar{\nu}$, $H^0e^+e^-$ and $H^0\mu^+\mu^-$.

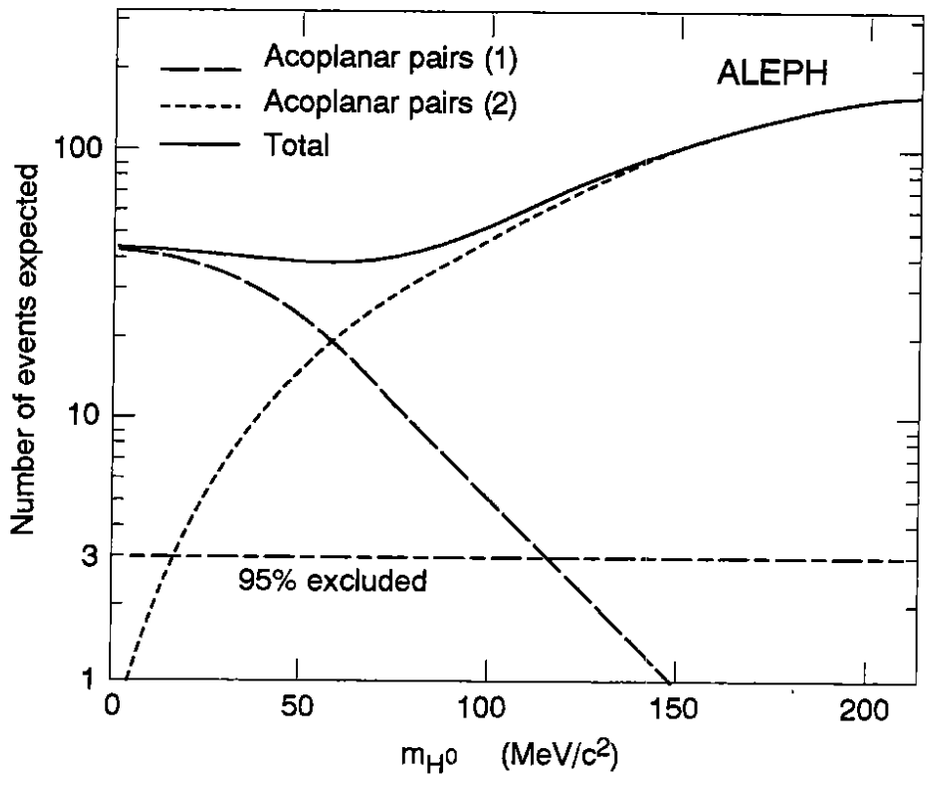

Figure 5.4: Number of signal events expected from the two acoplanar pair analyses for a Higgs boson mass below the muon threshold. Analysis (1) is described in section 5.3.1 and analysis (2) in section 5.3.2.

5.4.2 Intermediate mass domain : $2m_\mu < m_{H^0} < 15\,\mathrm{GeV}/c^2$

Between the muon threshold and $\sim 15\,\mathrm{GeV}/c^2$ the most relevant analyses are the acoplanar pair and the monojet searches applied to the $H^0\nu\overline{\nu}$ channel. The acoplanar pair selection is naturally efficient when the Higgs decays mostly into two or four charged particles, in particular for masses below the $D\overline{D}$ threshold. The additional efficiency brought by the monojet analysis increases progressively with the Higgs mass as shown in table 5.2. Fig. 5.5 shows the corresponding numbers of events expected to be observed if the Higgs mass were between $2m_\mu$ and $15\,\mathrm{GeV}/c^2$. In the whole mass range, a total of at least 32 events are expected while none was seen; this domain is thus also excluded with much more than 95% confidence. The analysis of section 5.3.9 has not been included in this mass range since it has a much higher level of background.

m_{H^0}	Acoplanar pairs		Monojets	
(GeV/c^2)	Eff.	N_{exp}	Eff.	N_{exp}
0.212	49.	253	–	–
0.300	36.	184	–	–
0.500	38.	189	–	–
0.800	35.	165	–	–
1.0	33.	149	–	–
1.2	32.	139	–	–
1.4	30.	125	0.5	2.1
1.6	31.	124	0.5	2.0
1.8	35.	134	1.	3.8
2.0	33.	121	2.	7.3
2.5	38.	125	4.	13
3.0	32.	96	9.	27
4.0	21.	52	26.	65
5.0	19.	41	28.	60
8.0	13.	19	40.	58
11.0	11.	11	42.	45
15.0	2.	1.3	43.	31

Table 5.2: Efficiencies (in %) and expected numbers of signal events for the acoplanar pair (section 5.3.2) and monojet (section 5.3.4) searches for a Higgs mass between $2m_\mu$ and $15\,\mathrm{GeV}/c^2$. Only the $e^+e^- \rightarrow H^0\nu\overline{\nu}$ channel has been used in this domain. The efficiencies and the numbers of events given for the monojet search are additional to the corresponding quantities in the acoplanar pair search.

5.4.3 High mass domain : $m_{H^0} > 11\,\mathrm{GeV}/c^2$

In order to be sensitive to the highest possible Higgs mass, all the topologies presented in sections 5.3.2 to 5.3.8 have been included to derive the final result. The most important final state (18.8% of the cases) is the $(H^0 \rightarrow \textit{hadrons})(Z^* \rightarrow \nu\overline{\nu})$ channel, leading to a monojet or an acoplanar pair of jets (sections 5.3.4 and 5.3.5). The other final states like *hadrons* $\ell^+\ell^-$ (3.1% for each lepton $\ell = e$ or μ, section 5.3.6), *hadrons* $\tau^+\tau^-$ and $\tau^+\tau^-$ *hadrons* (7.3%, sections 5.3.5, 5.3.6, 5.3.7 and 5.3.8), $\tau^+\tau^-\nu\overline{\nu}$ (1.2%, section 5.3.2) and $\tau^+\tau^-\ell^+\ell^-$ (0.6%, section 5.3.3), also contribute significantly. The efficiencies of the corresponding analyses for each channel are listed in table 5.3 together with the numbers of events expected to be found. The latter are summarized in fig. 5.6. The total number of events expected for a $48\,\mathrm{GeV}/c^2$ Higgs boson is 3.05. With no events observed such a Higgs boson is excluded with 95% confidence.

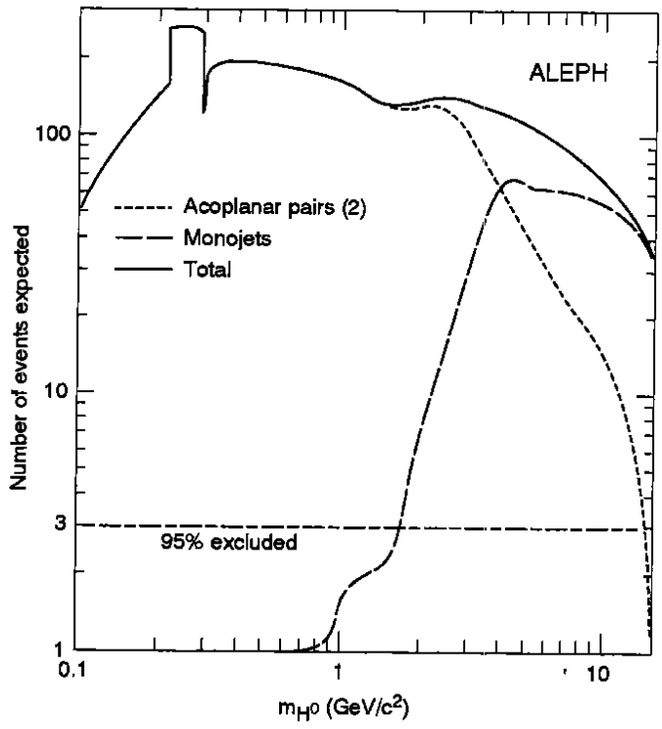

Figure 5.5: Number of signal events expected from the acoplanar pair analysis (section 5.3.2) and the monojet analysis (section 5.3.4) for a Higgs boson mass below 15 GeV/c^2.

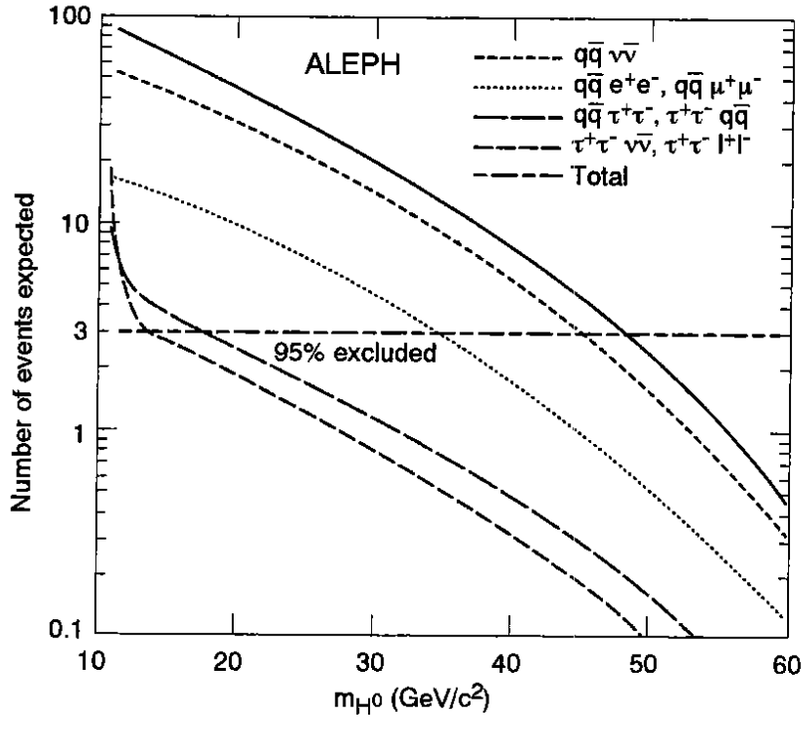

Figure 5.6: Total number of signal events expected from the analyses described in sections 5.3.2 to 5.3.8 for a Higgs boson mass above 11 GeV/c^2. Also indicated are the numbers of events expected in the various final states.

m_{H^0}	$Z^* \to \nu\bar{\nu}$		$Z^* \to e^+e^-$		$Z^* \to \mu^+\mu^-$		$Z^* \to \tau^+\tau^-$	
(GeV/c^2)	Eff.	N_{exp}	Eff.	N_{exp}	Eff.	N_{exp}	Eff.	N_{exp}
11	65.	54.5	60.	7.9	71.	9.4	21.	2.82
20	69.	29.5	70.	4.95	78.	5.51	22.	1.49
30	75.	13.2	75.	2.15	82.	2.35	23.	0.66
40	77.	5.11	73.	0.80	80.	0.88	20.	0.22
48	71.	1.99	71.	0.33	76.	0.36	17.	0.08
50	68.	1.49	69.	0.25	74.	0.27	15.	0.05
60	54.	0.31	63.	0.06	67.	0.06	7.	0.01

m_{H^0}	$Z^* \to hadrons$		$Z^* \to \nu\bar{\nu}$		$Z^* \to \ell^+\ell^-$	
(GeV/c^2)	Eff.	N_{exp}	Eff.	N_{exp}	Eff.	N_{exp}
11	7.	6.36	41.	11.0	54.	7.16
20	11.	1.03	41.	1.14	54.	0.73
30	17.	0.65	41.	0.46	54.	0.30
40	24.	0.35	41.	0.18	54.	0.11
48	26.	0.16	41.	0.08	54.	0.05
50	26.	0.12	41.	0.06	54.	0.04
60	25.	0.03	32.	0.01	54.	0.01

Table 5.3: Efficiencies (in %) and expected numbers of signal events for $m_{H^0} > 11\,\mathrm{GeV}/c^2$. Top—configurations where the Higgs boson decays into hadrons; bottom—configurations where the Higgs boson decays into a τ pair.

5.4.4 Systematics

No detailed systematic studies have been performed in the very low mass and in the intermediate mass domains since the total number of events expected to be seen is so large. In the high mass domain, about 85% of the Higgs events expected to be found come from the configurations ($H^0 \to hadrons$)($Z^* \to \nu\bar{\nu}$, e^+e^- or $\mu^+\mu^-$). The systematic errors have therefore been studied carefully for these final states only and assumed to be of the same order for the other channels (the relative contributions from these channels are very small, and the dominant systematic errors are common to all the channels).

The uncertainty on the number of multihadronic events in the data sample induces a systematic error of 0.6%. Another source of systematic error is the dependence on the top-quark mass of the $e^+e^- \to H^0Z^*$ cross-section: varying m_t from 90 to 200 GeV/c^2 gives rise to a 1% variation in the ratio of the $q\bar{q}$ to H^0Z^* cross-sections. The limited Higgs Monte Carlo statistics introduces a contribution of 0.7% to the error.

The most important uncertainty might originate from the hadronization of the $q\bar{q}$ pair coming from a scalar particle (the Higgs boson). In order to determine this uncertainty, the Higgs decay simulation has been performed both using the $H^0 \to q\bar{q}g$ matrix element on the one hand, and applying the Lund parton shower evolution to the quark pair, thus pretending that the two quarks are produced from a vector boson, on the other. This results in a variation smaller than 0.5% in the selection efficiencies. An additional error of 0.5% has been estimated by varying the QCD and fragmentation parameters (mainly Λ_{QCD}, σ_q and ϵ_b).

The electron and muon identification efficiencies ($H^0\ell^+\ell^-$ channel only) have been compared for data and simulation using samples of Bhabha and dimuon events. The difference between

the data and the Monte Carlo is less than 1%.

Adding the various uncertainties in quadrature, a total systematic error of 2% is obtained. Conservatively reducing by this amount the total number of events expected, the Higgs mass lower limit obtained is 48 GeV/c^2.

5.5 Summary

Using a data sample corresponding to approximately 185,000 hadronic Z decays, the process $e^+e^- \to H^0Z^*$ has been studied in most of the possible final states in order to search for the standard model Higgs boson H^0. No events have been found in any of these analyses. Combining all of them, the whole mass range between 0 and 48 GeV/c^2 is excluded at 95% c.l.

6 Non-minimal Higgs Bosons

In non-minimal versions of the standard model, additional Higgs fields are often introduced, for instance when the Peccei-Quinn mechanism is invoked to solve the problem of the violation of CP in the QCD sector of the theory, or in the context of supersymmetry. The tree-level value of ρ naturally remains equal to unity if these Higgs fields occur in $SU(2)_L$ representations not higher than doublets. This is what will be assumed in this section. Moreover, even when only two Higgs doublets are present, flavour changing neutral currents are almost unavoidable unless one of the doublets couples to up-type quarks only and the other one to down-type quarks and to charged leptons only. This also will be assumed here, and is indeed what occurs in supersymmetry. Although additional Higgs singlets are occasionally also introduced, this is not generally necessary; therefore, in the following, only the simplest non-minimal case with two Higgs doublets will be considered.

The physical spectrum in two Higgs doublet models [53] consists of three neutral bosons, the CP-even h and H and the CP-odd A, and of a pair of charged bosons $H^\pm$. These five physical states, together with the three longitudinal degrees of freedom carried by the massive W and Z result from the eight initial degrees of freedom of the two complex doublets H_1 and H_2 of Higgs fields. In the process of spontaneous breaking of $SU(2)_L \times U(1)_Y$, the neutral components of H_1 and H_2 develop vacuum expectation values v_1 and v_2, with $v_1^2 + v_2^2 = v^2/2$, such that the up-type quarks receive masses proportional to v_2, and the down-type quarks and the charged leptons masses proportional to v_1. The large top quark mass value leads to the expectation that $\tan\beta = v_2/v_1 > 1$. However, this will not be systematically assumed in the following.

6.1 Searches for Charged Higgs Bosons

The couplings of the charged Higgs bosons to the gauge bosons are completely determined [53,54] and therefore, once the mass $m_\pm$ of the charged Higgs boson is fixed, so also is the Z decay width to H^+H^-

$$\Gamma(Z \to H^+H^-) = 2(\frac{1}{2} - \sin^2\theta_W)^2\beta_\pm^3\Gamma_\nu$$

where $\beta_\pm = (1 - 4m_\pm^2/m_Z^2)^{1/2}$. On the other hand, the couplings of the charged Higgs bosons to matter fermions depend also on $\tan\beta$ in a way such that the partial $H^\pm$ decay widths read [53,54]

$$\Gamma(H^+ \to \ell^+\nu_\ell) = \frac{G_F\sqrt{2}}{8\pi} m_\pm m_\ell^2 \tan^2\beta$$

and

$$\Gamma(H^+ \to u_i\bar{d}_j) = 3|V_{ij}|^2 \frac{G_F\sqrt{2}}{8\pi} m_\pm (m_i^2 \cot^2\beta + m_j^2 \tan^2\beta)$$

where V_{ij} is the relevant Cabibbo-Kobayashi-Maskawa matrix element. For charged Higgs boson masses above $\sim 20\,\mathrm{GeV}/c^2$ (the only case which will be considered here since lower masses have been excluded at lower energy e^+e^- colliders [55]) the main decay modes are therefore $H^+ \to \tau^+\nu_\tau$ and $H^+ \to c\bar{s}$. Given the low value of $|V_{cb}|$ compared to $|V_{cs}|$, the $c\bar{b}$ final state can only compete with $c\bar{s}$ for very large values of $\tan\beta$, but in such a case the $\tau^+\nu_\tau$ mode dominates anyway. For $\tan\beta = v_2/v_1 > 1$ as usually expected, the branching ratio to $\tau^+\nu_\tau$ is greater than 30%.

In Z decays to H^+H^-, the final states are therefore purely leptonic ($\tau^+\nu_\tau\tau^-\bar{\nu}_\tau$), mixed ($\tau^+\nu_\tau c\bar{s}$ and $c\bar{s}\tau^-\bar{\nu}_\tau$), or purely hadronic ($c\bar{s}c\bar{s}$). Dedicated searches have been performed in each of these cases, the results of which will be presented in a way such that the dependence on the value of the hadronic branching ratio B_h is explicit. In all charged Higgs boson hadronic decay simulations, the Lund parton shower algorithm [56] has been used.

6.1.1 Search in the leptonic final state

For the purely leptonic final state, the search for acoplanar pairs, sensitive to the one-prong and three-prong decays of the τ, and developed in the context of the reaction $e^+e^- \to H^0\nu\bar{\nu}$ with H^0 decaying to $\tau^+\tau^-$, has been applied. No events were observed in the data while the efficiency for a $44\,\mathrm{GeV}/c^2$ charged Higgs boson decaying leptonically in 100% of the cases is 53%. The mass limit for such a charged Higgs boson is $45.3\,\mathrm{GeV}/c^2$, and the result as a function of B_τ is shown in fig. 6.1.

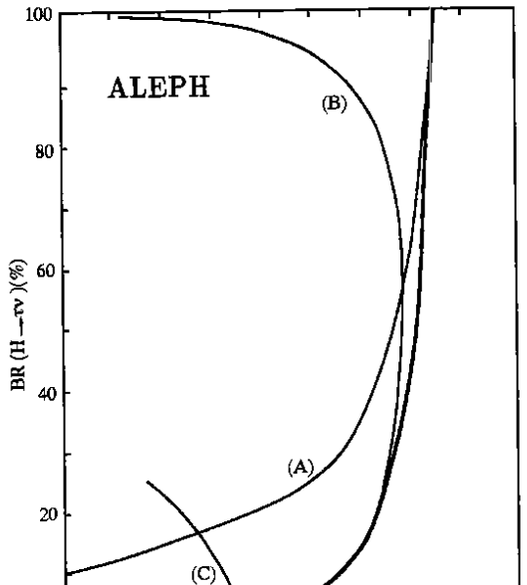

Figure 6.1: Results on charged Higgs bosons: boundaries of the domains excluded by the searches in purely leptonic final states (A), in mixed final states (B), and in purely hadronic final states (C). The heavy outer contour limits the domain excluded when combining these searches. ($B_h = 1 - B_\tau$.)

6.1.2 Search in the mixed final state

In the mixed lepton-hadron final state, a substantial amount of energy is taken away by the direct τ neutrino from the Higgs boson decay. The search for hadronic events with missing

energy, known as the search for acoplanar jets and developed in the context of the reaction $e^+e^- \rightarrow H^0\nu\bar{\nu}$ with $H^0 \rightarrow$ *hadrons*, can therefore be applied. No events survived in the data while the efficiency for a pair of 44 GeV/c^2 charged Higgs bosons decaying into the mixed state is 47%.

To take advantage of the characteristic topology of τ decays, a complementary analysis has been performed in which hadronic events with an isolated charged particle accompanied by missing energy are searched for. The relevant selection criteria have already been used and described in the context of the reactions $e^+e^- \rightarrow (H^0 \rightarrow$ *hadrons*$)(Z^* \rightarrow \tau^+\tau^-)$ and $e^+e^- \rightarrow (H^0 \rightarrow \tau^+\tau^-)(Z^* \rightarrow$ *hadrons*$)$. No events were observed in the data while this selection has an efficiency of 20% for a 44 GeV/c^2 Higgs boson mass. However 11% of these have already been detected in the above search so that, when added to the 47% from the acoplanar jet selection, the total efficiency is 56%. In the best case, when $B_\tau = 50\%$, the efficiency of the search in the mixed channel is 28% when calculated with respect to all the possible H^+H^- final states, and the corresponding mass limit is 44.7 GeV/c^2. The result as a function of B_τ is shown in fig. 6.1.

6.1.3 Search in the hadronic final state

For the purely hadronic final state, a search for a localized excess in the jet-jet mass distribution in 4-jet events has been performed, optimized to best discriminate between the signal from a high mass ($\gtrsim$35 GeV/c^2) Higgs boson and standard hadronic Z decays.

In events with at least five charged particles carrying more than 10% of the centre-of-mass energy the particles are clustered into jets using the JADE algorithm [57], with a y_{cut} value of 0.03 corresponding to a maximum jet mass of about 16 GeV/c^2. Only events with at least four jets are kept, and those with five jets or more are reduced to a four jet topology by merging into a single jet the jet pair with the smallest invariant mass until only four jets are left. To ensure that the four jets are well separated, it is required in addition that no jet-jet angle be less than 50°. To improve the jet energy resolution, the energies of the four jets are recalculated from their directions, imposing energy-momentum conservation and keeping the jet velocities fixed. It is then required that all jet energies be greater than $0.25E_{beam}$ and smaller than $0.70E_{beam}$.

For each of the three possible pairings in the four-jet system, the following angles are defined:

(i) the production angle θ^p formed by the common direction of the pairs with the beam axis,

(ii) the decay angles θ_i^d (with $i = 1$ or 2 labelling the jet pairs) between the direction of one of the jets of pair i and the direction of the pair itself, measured in the pair rest frame.

An accepted pairing has to fulfil the following conditions:

(i) $50° < \theta^p < 130°$, which takes advantage of the $\sin^2\theta^p$ distribution expected for the signal, in contrast to the $1 + \cos^2\theta^p$ distribution of the standard hadronic Z decays,

(ii) $50° < \theta_i^d < 130°$ for at least one of the pairs, which takes advantage of the isotropic angular distribution of the decay of spin-0 particles, in contrast to the QCD background in which daughter jets tend to be emitted at small angles with respect to their parent jets.

At this point, 1495 events are selected in the data while 1443 are expected from standard hadronic Z decays.

For each of the retained pairings, the sum $M = m_1 + m_2$ and the difference $m = |m_1 - m_2|$ of the two pair masses are calculated. Because of the overall energy-momentum conservation constraint imposed in the determination of the jet energies, these variables are much less correlated than m_1 and m_2, and the resolution is substantially better for M than for m. The probability for an event induced by the production of 41 GeV/c^2 mass charged Higgs bosons to lead to at least one combination in the bin ($|M - 2 \times 41\,\text{GeV}/c^2| < 2\,\text{GeV}/c^2, m < 10\,\text{GeV}/c^2$) is 18% if the hadronic branching ratio $B_h = 1$. The distribution of $M/2$, for $m < 10$ GeV/c^2,

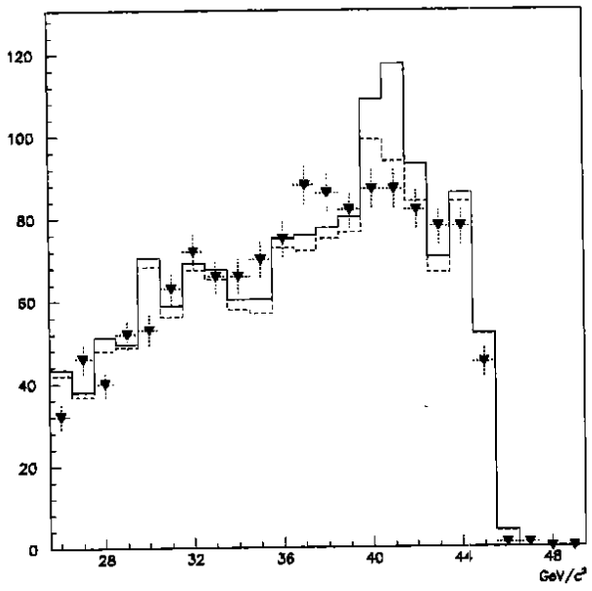

Figure 6.2: Distribution of the average jet-jet mass $M/2$ when the mass difference m is smaller than $10\,\mathrm{GeV}/c^2$. The dashed histogram is the expectation from standard hadronic decays of the Z while the full histogram is the same, with the expectation from a $41\,\mathrm{GeV}/c^2$ mass charged Higgs boson added (with $B_h = 100\%$). Triangles show the data.

is shown in fig. 6.2 for the data and for the QCD Monte Carlo (absolute normalization); the expectation from a $41\,\mathrm{GeV}/c^2$ mass Higgs boson is also shown (for $B_h = 1$).

The (M, m) plane is divided into overlapping bins of size $4 \times 10(\,\mathrm{GeV}/c^2)^2$, corresponding to about twice the resolution, and scanned in steps of $250\,\mathrm{MeV}/c^2$ in M and $625\,\mathrm{MeV}/c^2$ in m. A polynomial fit to the distibution in M and m expected from standard hadronic Z decays is performed in order to smooth out the fluctuations induced by the limited Monte-Carlo statistics. A local excess is then sought in the data by comparing in each bin the number of events observed to the expectation from the polynomial. The result of this comparison, measured in each bin as a signed number of standard deviations, is shown in fig. 6.3. The distribution is well described by a normalized Gaussian, showing that data and simulation are in good agreement. In particular, no excess, which would be signalled by large positive fluctuations, is observed in the data.

For a given charged Higgs boson mass $m_\pm$, the content N_{obs} of the bin ($|M - 2m_\pm| < 2\,\mathrm{GeV}/c^2, m < 10\,\mathrm{GeV}/c^2$) is compared to the expectation μ_{exp} from standard hadronic Z decays. A 95% c.l. upper limit for the expectation value of any contribution additional to μ_{exp} is then derived and, if the number of events expected in that bin from the production of such a charged Higgs boson, assumed to decay hadronically in 100% of the cases, is larger, this Higgs boson mass value is excluded at 95% c.l. Conservatively, N_{obs} has been used in the calculation instead of μ_{exp} whenever N_{obs} had fluctuated below μ_{exp}. In addition, a systematic error of 10% has been subtracted from the expected number of signal events to account for the limited Monte-Carlo statistics and for uncertainties in the modelling of quark hadronization. The effect of initial state radiation and the distribution of the integrated luminosity at the various energies of the scan around the Z peak have been taken into account to calculate the predicted numbers of signal events.

Assuming a 100% branching ratio for hadronic decays, the mass limit obtained this way is $41.7\,\mathrm{GeV}/c^2$, and the exclusion contour in the (B_h *vs* $m_\pm$) plane is shown in fig. 6.1.

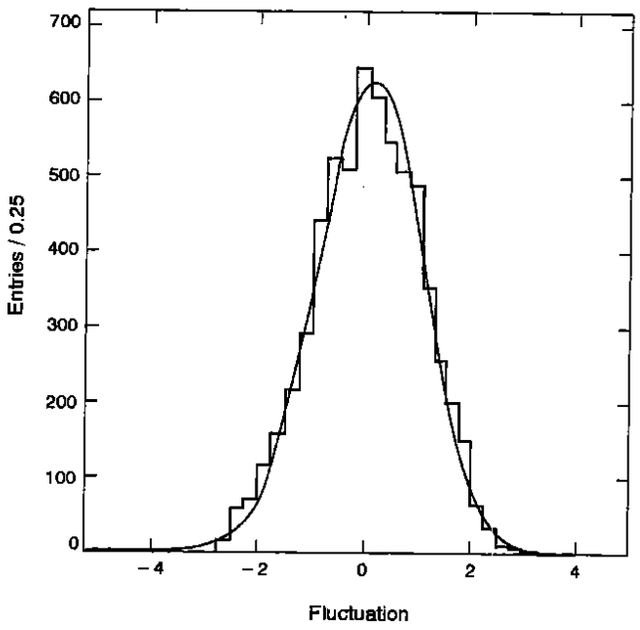

Figure 6.3: Distribution of the normalized fluctuation $(N_{obs} - \mu_{exp})/\sqrt{\mu_{exp}}$, where N_{obs} and μ_{exp} are the numbers of events observed in the data and expected from standard hadronic Z decays, respectively, in $4 \times 10(\,\mathrm{GeV}/c^2)^2$ bins in the (M, m) plane. There are 6336 entries. A Gaussian fit yields a mean of 0.04 and a σ of 0.99.

6.2 Searches for Neutral Higgs Bosons

The number of parameters needed to describe the neutral Higgs sector is larger [53]: three masses for the neutral Higgs bosons, the ratio $\tan\beta = v_2/v_1$, and α, a mixing angle in the CP-even sector.

Production and decay of neutral Higgs bosons

The phenomenology of the neutral Higgs bosons of two-doublet models in e^+e^- collisions near the Z peak can be easily inferred from their couplings to the Z and to the matter fermions [53,54]. The ZZA coupling vanishes if CP is conserved while the Zhh and ZAA couplings are forbidden by Bose statistics. The ZZh coupling is the same as the minimal standard model ZZH^0 coupling, except that it is reduced by a factor $\sin(\beta - \alpha)$. The CP-even h can therefore be searched for just like the minimal standard model H^0 in the process $e^+e^- \to H^0Z^*$, but with reduced sensitivity:

$$\frac{\Gamma(Z \to hZ^*)}{\Gamma(Z \to H^0Z^*)} = \sin^2(\beta - \alpha).$$

However, when this reduction is strong, the ZhA coupling, proportional to $\cos(\beta - \alpha)$, becomes substantial. This makes a search for the $Z \to hA$ decay promising since the partial width is large:

$$\Gamma(Z \to hA) = \frac{1}{2}\cos^2(\beta - \alpha) \cdot \Gamma_{\nu\bar{\nu}} \cdot \lambda^{\frac{3}{2}}\left(1, \frac{m_h^2}{m_Z^2}, \frac{m_A^2}{m_Z^2}\right)$$

where $\lambda(x, y, z) = (x^2 + y^2 + z^2 - 2xy - 2yz - 2zx)$. Therefore, the searches for $Z \to hZ^*$ and for $Z \to hA$ are to be considered as complementary.

The h decay widths into fermion pairs are readily deduced from the corresponding ones for H^0 by applying factors $f_d = \sin^2\alpha/\cos^2\beta$ for down-type quarks and charged leptons, and

$f_u = \cos^2\alpha/\sin^2\beta$ for up-type quarks. The A decay widths are obtained similarly, but with $f_d = \tan^2\beta$ and $f_u = \cot^2\beta$. For masses well above the $b\bar{b}$ threshold, the A decays mainly to $c\bar{c}$ pairs if $\tan\beta \ll 1$, and to $b\bar{b}$ pairs (but also to $\tau^+\tau^-$ in $\sim 6\%$ of the cases) if $\tan\beta \gtrsim 1$. Model building, particularly within the supersymmetric framework, suggests that the same holds for h decays in spite of the additional dependence on α [53] and this will be assumed in the following. For very light h and A, below the $\mu^+\mu^-$ threshold, the main decay to e^+e^- remains dominant if $\tan\beta > 1$, but the h lifetime is reduced compared to the H^0 lifetime; if $\tan\beta < 1$, the $\gamma\gamma$ decay mode is reinforced, and the lifetime is also modified.

Furthermore, if $m_h > 2m_A$, the CP-even h may decay into a pair of CP-odd A bosons. Indeed, except for some fortuitous choices of parameters such as $\tan\beta = 1$, this decay mode even tends to be dominant.

Higgs bosons in the MSSM

More detailed predictions can only be made in specific models, of which the most popular is the minimal supersymmetric extension of the standard model (MSSM) discussed in more detail in section 7. This model is the simplest of all possible supersymmetric models [58,59,60]: its field content and its number of parameters are minimal, but the attractive features of supersymmetry are maintained such as, for instance, the stabilization of the Higgs boson masses with respect to radiative corrections (this is known as the solution to the gauge hierarchy problem). As in any supersymmetric model, two Higgs doublets are needed in order to give masses to both up and down-type quarks, and also to cancel the gauge anomalies (the number of fermionic and bosonic degrees of freedom must be equal in the gauge-Higgs sector). However, the number of parameters is greatly reduced with respect to a general two-doublet model: only one Higgs boson mass, say m_A, and $\tan\beta$ (or alternatively another mass, say m_h) suffice. The other Higgs boson masses and the mixing angle α are then all determined.

When the Higgs potential is considered at the tree-level, interesting mass relations arise [53]. In particular, the charged Higgs bosons are always heavier than the W. One of the neutral CP-even states, h, is always lighter than the Z (in fact, $m_h < |\cos 2\beta| m_Z$), while the other, H, is heavier than the Z. The mass of the CP-odd state, m_A, is bound to lie between m_h and m_H and can be larger or smaller than m_Z. However, it has been recently realized [61,62,63,64,65,66,67] that large radiative corrections may occur at the one-loop level if the top quark mass is large. The main corrections [61,62,63,65,66,67] typically of order

$$\frac{3g^2}{8\pi^2\sin^2\beta}\frac{m_t^4}{m_W^2}\log\left(\frac{m_{\tilde{t}}^2}{m_t^2}\right),$$

affect principally the CP-even squared mass matrix (and thus m_h, m_H and α), whereas the charged Higgs boson and the A masses are much less affected [64,68] and the couplings very little [68], except through the modification of α. In the above expression, $m_{\tilde{t}}$ is the mass of the supersymmetric partners of the top quark, assumed to be mass degenerate. As a consequence of these corrections, the tree-level mass relations are significantly modified. In particular, the lighter CP-even state h can become heavier than the CP-odd A and need not be lighter than the Z.

6.2.1 Searches for $e^+e^- \to hZ^*$

The searches for the minimal standard model Higgs boson H^0 in the reaction $e^+e^- \to H^0f\bar{f}$ can be reinterpreted in the context of two-Higgs-doublet models as searches for h in $e^+e^- \to hf\bar{f}$. These searches, hereafter called "standard searches," have been optimized for the detection of a Higgs boson with mass $\sim 50\,\mathrm{GeV}/c^2$, either decaying into a τ pair and produced in association with a $\nu\bar{\nu}$, $\ell^+\ell^-$ or $q\bar{q}$ pair, or decaying hadronically and produced in association with a $\nu\bar{\nu}$ or

$\ell^+\ell^-$ pair (ℓ = e, μ or τ). For the hadronic decay channels, the multiplicity requirements are such that they imply a minimum detected charged multiplicity of five in the Higgs boson decay.

Assuming the selection efficiencies to be similar for the two processes, the only difference comes from the cross-section reduction by the factor $\sin^2(\beta-\alpha)$. Then, if N_{exp}^{SM} is the number of events expected to be observed in the standard model case for a Higgs boson with mass $m_{\mathrm{H^0}}$, a 95% c.l. upper limit on $\sin^2(\beta-\alpha)$ can be set at the value $3.0/N_{exp}^{SM}$ for $m_{\mathrm{h}} = m_{\mathrm{H^0}}$ (3.0 is the 95% c.l. upper limit on any signal when no events were observed). Indeed, the detection efficiencies are in general the same for h and $\mathrm{H^0}$ because the standard searches are sufficiently inclusive not to be affected, for instance, by the proportion of Higgs boson decays into $\mathrm{c\bar{c}}$ or $\mathrm{b\bar{b}}$. This is not the case, however, when $m_{\mathrm{h}} < 2m_\mu$ since the results of the $\mathrm{H^0}$ searches performed in this mass range are affected by the $\mathrm{H^0}$ lifetime. Therefore, no general limit on $\sin^2(\beta-\alpha)$ has been derived when $m_{\mathrm{h}} < 2m_\mu$.

In addition, if the decay $\mathrm{h} \to \mathrm{AA}$ can take place, the standard searches have to be reexamined according to the A decay modes. When $m_{\mathrm{A}} > 2m_{\mathrm{b}}$, their efficiencies are at least as large as if the $\mathrm{h} \to \mathrm{AA}$ channel were closed. On the other hand, for lighter A bosons, some of those searches, developed for a high mass $\mathrm{H^0}$, which is expected to decay to large multiplicity final states, may not apply efficiently since a substantial fraction of the Higgs boson decay final states then contains only four charged particles [52]. This is particularly true for $2m_\tau < m_{\mathrm{A}} < 2m_{\mathrm{b}}$ and $\tan\beta \gg 1$, a case where the decay mode $\mathrm{A} \to \tau^+\tau^-$ dominates.

These searches have therefore been slightly modified in order to cope with this specific configuration. For the $\mathrm{Z^*} \to \nu\bar{\nu}$ final state, the event is required to contain exactly four charged particle tracks originating from the beam crossing point, each making an angle θ with the beam axis such that $|\cos\theta| < 0.95$. In order to avoid energy losses in the beam pipe region, the total energy measured within 12° of the beam axis must not exceed 1 GeV. The event is then divided into two hemispheres by a plane perpendicular to the thrust axis. Each hemisphere has to contain a total energy of at least 2 GeV and exactly two charged particle tracks, with total electric charge zero. To remove low charged multiplicity hadronic Z decays, the acoplanarity angle between the directions of the total momenta of the two hemispheres is required to be smaller than 175°. Finally, to remove events from $\gamma\gamma$ interactions, the total momentum transverse to the beam axis must exceed 5% of the centre-of-mass energy unless the total mass of the event is larger than 25 GeV/c^2. For the $\mathrm{Z^*} \to \ell^+\ell^-$ final state, with ℓ = e or μ, the search for energetic lepton pairs in hadronic events has been repeated, but now requiring a multiplicity of exactly six charged particle tracks. No events were found in either of these searches, while 0.3 are expected from the background of standard processes. When combined with the standard searches, these analyses provide a 21% efficiency for the detection of a 48 GeV/c^2 h boson produced in the reaction $\mathrm{e^+e^-} \to \mathrm{hZ^*}$ and decaying into a pair of 6 GeV/c^2 A bosons. To be applicable for $m_{\mathrm{A}} < 2m_\mu$, these analyses should take the A lifetime into account, which has not been done here.

The upper limit on $\sin^2(\beta-\alpha)$ as a function of m_{h} obtained when combining all these searches is presented in fig. 6.4.

6.2.2 Results inferred from the Z width measurement

The cases not excluded by the searches for $\mathrm{e^+e^-} \to \mathrm{hZ^*}$ correspond to m_{h} too large or to $\sin^2(\beta-\alpha)$ much smaller than unity. In the latter instance, however, it is expected that $\mathrm{Z} \to \mathrm{hA}$ occurs at a substantial rate if kinematically allowed. Hence the Z width measurement provides constraints on this process.

In section 4 it was shown that any contribution to the Z width from non-standard processes is limited to less than $0.28\Gamma_\nu$ at 95% c.l., with Γ_ν the Z decay width into a neutrino pair. A 95% c.l. upper limit on $\cos^2(\beta-\alpha)$ can thus be derived for any (m_{h}, m_{A}). Taking into account

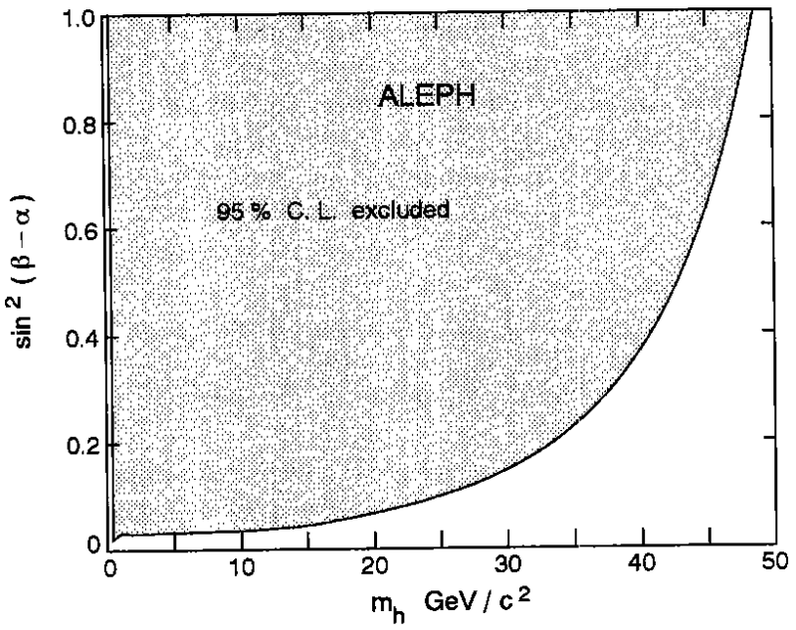

Figure 6.4: 95% c.l. upper limit on $\sin^2(\beta-\alpha)$, as a function of m_h, inferred from the searches for $e^+e^- \to hZ^*$. Here $m_h < 2m_A$ or $m_A > 2m_\mu$ have been assumed.

the upper limit on $\sin^2(\beta-\alpha)$ obtained for the same m_h from the searches for $Z \to hZ^*$ reported above, this (m_h, m_A) is excluded if the sum of these limits is less than unity. The resultant excluded region in the (m_h, m_A) plane is bounded by curve (A) in fig. 6.5.

6.2.3 Searches for $Z \to hA$

Even for $\sin^2(\beta-\alpha)$ substantially smaller than unity, it is not possible to obtain any limitation from the Z width measurement when m_h or m_A are sufficiently large. Direct searches for $Z \to hA$ must therefore be performed.

Search in four-jet final states

For sufficiently massive Higgs bosons, a search in the 4-jet topology is relevant, the final state being predominantly $c\bar{c}c\bar{c}$ when $\tan\beta \ll 1$, or $b\bar{b}b\bar{b}$ when $\tan\beta \gtrsim 1$. The search technique developed for charged Higgs bosons in the $c\bar{s}c\bar{s}$ final state can be used without modification since it was general enough to be sensitive to the pair production of unequal mass systems, each decaying to two jets, at least for masses $\gtrsim 20\,\mathrm{GeV}/c^2$ and for mass differences $\lesssim 30\,\mathrm{GeV}/c^2$.

The 95% c.l. upper limit on $\cos^2(\beta-\alpha)$ resulting from this search is shown in fig. 6.6 as a function of m_h and m_A for $\tan\beta \ll 1$, the case in which the $c\bar{c}c\bar{c}$ final state is dominant. The results for $\tan\beta \gtrsim 1$ are not shown because, in that case, more stringent limits can be obtained from the search in the $\tau^+\tau^- b\bar{b}$ final state.

Search in the $\tau^+\tau^-$ – hadrons final state

Some of the standard searches for $e^+e^- \to H^0Z^*$ had been developed to be particularly sensitive to the $\tau^+\tau^-$*hadrons* final state. The standard searches can therefore be efficiently applied to the $\tau^+\tau^- b\bar{b}$ final state resulting from $e^+e^- \to hA$ which contributes $\sim 12\%$ when $\tan\beta \gtrsim 1$, at least when $m_A > m_h/2$. For $m_h = m_A = 42\,\mathrm{GeV}/c^2$, the resulting efficiency is 25%. The 95% c.l. upper limit on $\cos^2(\beta-\alpha)$ thus obtained for $\tan\beta \gtrsim 1$ is shown in fig. 6.6 as a function of m_h and m_A.

However, if either h or A becomes light enough to decay predominantly to ≤ 4 charged

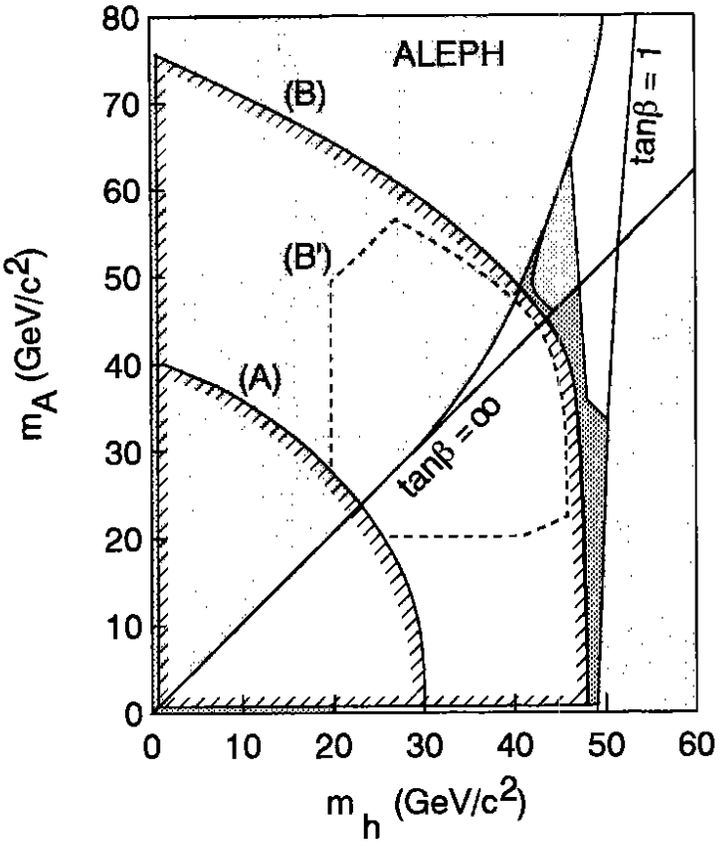

Figure 6.5: In the (m_A *vs* m_h) plane, domains excluded in general two-Higgs doublet models by the searches for $e^+e^- \to hZ^*$ combined with the Z width measurement (A) and with the direct searches for $Z \to hA$ when $\tan\beta \gtrsim 1$ (B) or $\ll 1$ (B'). Within the MSSM and for $\tan\beta > 1$, the region shown in light grey is theoretically forbidden when one-loop radiative corrections are taken into account with the following choice of unknown parameters: $m_t = 140\,\mathrm{GeV}/c^2$ and $m_{\tilde{t}} = 1\,\mathrm{TeV}/c^2$; any mixing among the supersymmetric partners of the top quark has been neglected. Under these assumptions, the excluded domain bounded by curve (B) is enlarged to comprise the dark grey region, and also the medium grey area for the lower of the two possible values of $\tan\beta$ allowed therein.

particles, the latter search becomes less efficient (with an efficiency of 15% for $m_h = 48\,\mathrm{GeV}/c^2$ and $m_A = 6\,\mathrm{GeV}/c^2$). Therefore a specific analysis has been developed for this case. The events are required to contain four or six charged particle tracks originating from the beam crossing point, with total electric charge zero, each making an angle θ with the beam axis such that $|\cos\theta| < 0.95$. The total energy measured within 12° of the beam axis must not exceed 1 GeV. The JADE algorithm [57] is then used to form jets, with a y_{cut} value of 0.01 corresponding to a maximum jet mass of about $9\,\mathrm{GeV}/c^2$. Events are selected with exactly three such jets, one of which contains a single positively charged particle and another a single negatively charged particle. Each of these two "τ-jets" is required to have a mass smaller than $1.8\,\mathrm{GeV}/c^2$. To remove the background from low multiplicity hadronic Z decays which tend to exhibit a back-to-back topology, the maximum angle between two jet directions must not exceed 165°. To take advantage of the missing energy carried away by the neutrinos in τ decays, the total energy has to be less than 85% of the centre-of-mass energy. Only two events survived at this stage, both identified as $\tau^+\tau^-\gamma$ final states with the photon converting into an e^+e^- pair in the detector material. Both of these events are eliminated using an algorithm designed to identify such converted pairs. No candidate event was found in any of the standard process background Monte Carlo samples. With this analysis taken into account, the overall efficiency

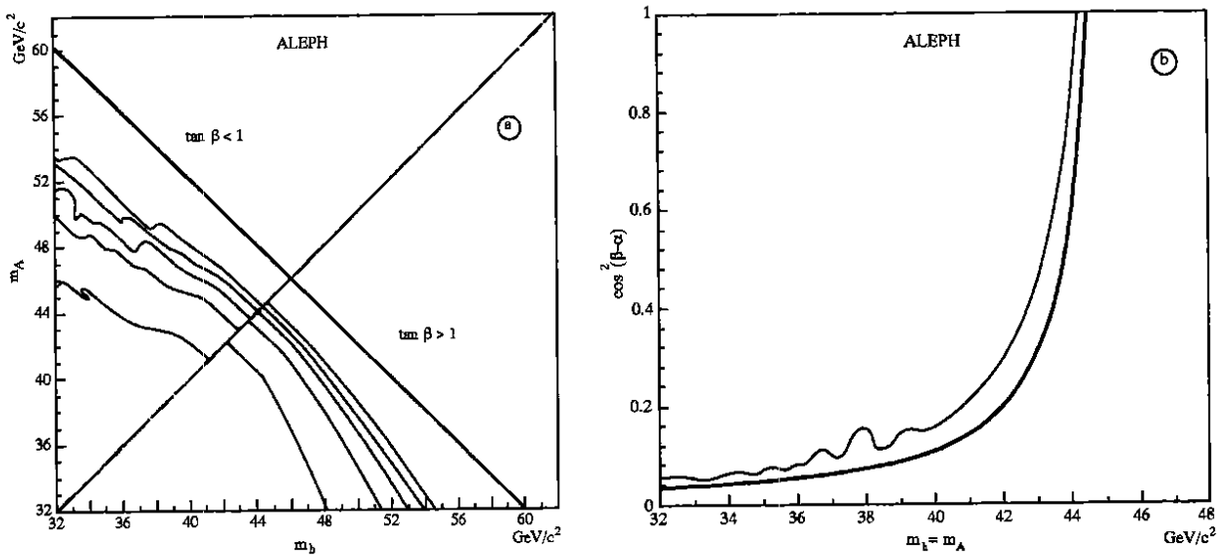

Figure 6.6: In the (m_A *vs* m_h) plane, (a) equal value contours for the 95% c.l. upper limit on $\cos^2(\beta-\alpha)$, inferred from the direct searches for $Z \rightarrow hA$. The contours are symmetric in the interchange of m_h and m_A, and have been drawn for $m_A > m_h$ when $\tan\beta \ll 1$, and for $m_A < m_h$ when $\tan\beta \gtrsim 1$. The innermost contour corresponds to a value of 0.2, and this value is to be increased by 0.2 for each new contour encountered when moving outwards. The heavy line is the kinematic limit in Z decays. Also shown (b), the 95% c.l. upper limit on $\cos^2(\beta-\alpha)$ when $m_h = m_A$ for $\tan\beta \gtrsim 1$ (thick line) and for $\tan\beta \ll 1$ (thin line).

becomes 30% for $m_h = 48\,\mathrm{GeV}/c^2$ and $m_A = 6\,\mathrm{GeV}/c^2$ (or *vice versa*), when h (or A) decays to a τ pair. This analysis does not apply if the h or A recoiling to the τ pair has a mass less than $2m_\mu$.

Search in the AAA *final state*

If $m_A < m_h/2$, the decay $h \rightarrow AA$ can take place, leading to a final state consisting of three A bosons. The ultimate topology then depends on m_A. If $\tan\beta \gtrsim 1$, the search for $\tau^+\tau^-$*hadrons* final states is applicable without any modification as long as $m_A > 2m_b$, but a new search had to be developed specifically for topologies consisting of three low multiplicity jets in order to cope with lower mass A bosons: if $2m_b > m_A > 2m_\tau$, each jet contains two τs, and thus two (four) charged particles in 72% (26%) of the cases; if $m_A < 2m_\tau$, the A-decay charged particle multiplicity is two (two or four) in $\gtrsim 20\%$ ($\gtrsim 70\%$) of the cases [52].

The events are required to contain six or eight charged particle tracks originating from the beam crossing point, with total electric charge zero, each making an angle θ with the beam axis such that $|\cos\theta| < 0.95$. The total energy measured within 12° of the beam axis must not exceed 1 GeV. The JADE algorithm is again used to form jets, with $y_{cut} = 0.01$. Exactly three such jets are required, each electrically neutral and containing two or four charged particles. The maximum angle between two jet directions must not exceed 165°. Finally, the total energy has to be smaller than 85% of the centre-of-mass energy. However, in order to retain efficiency if $m_A \lesssim 2m_\tau$, this last criterion is not applied if the three jet masses are smaller than $4.5\,\mathrm{GeV}/c^2$. No events satisfied these criteria, either in the data or in any of the standard process background Monte-Carlo samples, while the efficiency of this selection is 16% for $m_h = 48\,\mathrm{GeV}/c^2$ and $m_A = 6\,\mathrm{GeV}/c^2$, when h decays to an A pair and $\tan\beta \gtrsim 1$. Except for $m_A < 2m_c$, this analysis does not apply for $\tan\beta < 1$ because the typical A-decay multiplicity is too large when $A \rightarrow c\bar{c}$. It also does not apply if $m_A < 2m_\mu$.

6.2.4 Results

Results valid in general two-Higgs-doublet models

In any two-Higgs-doublet model of the class considered here, the 95% c.l. upper limit on $\cos^2(\beta-\alpha)$, obtained as a function of m_h and m_A from the Z width measurement and from the direct searches for $Z \to hA$, can be combined with the 95% c.l. upper limit on $\sin^2(\beta-\alpha)$ obtained for the same m_h from the searches for $e^+e^- \to hZ^*$: a given (m_h, m_A) pair is excluded at the 95% confidence level if the sum of these two upper limits is smaller than unity.

The domain thus excluded for $\tan\beta \gtrsim 1$ is limited by curve (B) in fig. 6.5. In particular, $m_h = m_A < 43.4\,\mathrm{GeV}/c^2$ is excluded at 95% c.l.

For $\tan\beta \ll 1$, the excluded domain is limited by curves (A) and (B'). In particular, $m_h = m_A > 42.9\,\mathrm{GeV}/c^2$ at 95% c.l. As mentioned previously, the search for four-jet final states reported in section 6.1.3 is not sensitive in the regions where m_h or $m_A \lesssim 20\,\mathrm{GeV}/c^2$ or $|m_h - m_A| \gtrsim 30\,\mathrm{GeV}/c^2$ or $m_h > 2m_A$, which explains the shape of curve (B').

As indicated in section 6.2.1, the regions $m_h < 2m_\mu$ and ($m_A < 2m_\mu$ with $m_h > 2m_A$) are not excluded.

Results valid in the framework of the MSSM

Within the MSSM, larger excluded domains can be inferred. For instance, $m_h = m_A < 44.4\,\mathrm{GeV}/c^2$ ($< 44.2\,\mathrm{GeV}/c^2$) would be excluded at 95% c.l. for $\tan\beta \gg 1$ ($\ll 1$) if the tree-level relations were valid. When one-loop radiative corrections are taken into account, the situation is more complicated as the prediction depends on a number of unknown parameters, with a particularly large sensitivity to the top quark mass [61,62,63,64,65,66,67]. As an example, the domain excluded for $\tan\beta > 1$, the only case considered in the literature [61,62,63,65,66,67], is shown in fig. 6.5 for $m_t = 140\,\mathrm{GeV}/c^2$, for $m_{\tilde{t}} = 1\,\mathrm{TeV}/c^2$ and for negligible mixing among the supersymmetric partners of the top quark. The same result is shown in fig. 6.7 as an excluded domain in the ($\tan\beta$ *vs* m_A) plane. This presentation has the advantage that the occasional twofold ambiguity in the values of $\tan\beta$ corresponding to a given (m_h, m_A) couple is removed.

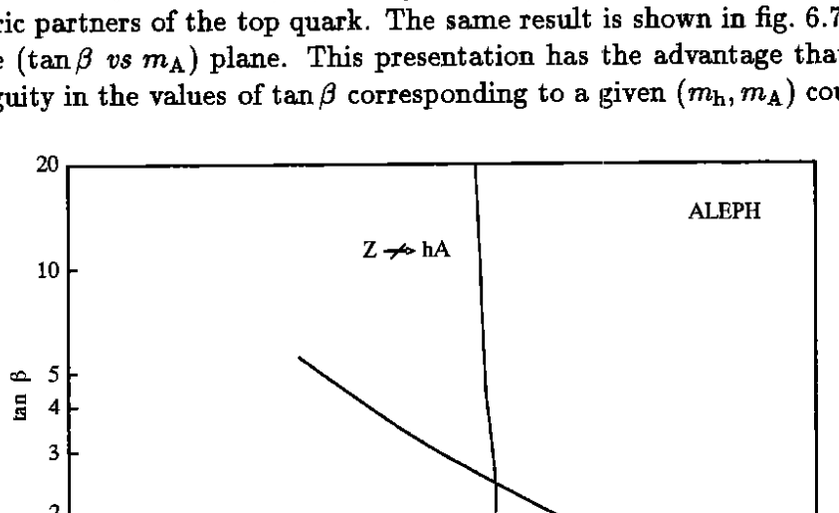

Figure 6.7: In the ($\tan\beta$ *vs* m_A) plane, domains excluded by the searches for $e^+e^- \to hZ^*$ and by the direct searches for $Z \to hA$. Here the MSSM is assumed, and one-loop radiative corrections are taken into account with the same choice of parameters as in fig. 6.5.

For the above choice of parameters, $m_h < 41\,\mathrm{GeV}/c^2$ and $m_A < 31\,\mathrm{GeV}/c^2$ are excluded at 95% c.l. It can also be seen that $\tan\beta = 1$ remains allowed when $m_A > 31\,\mathrm{GeV}/c^2$. Similarly

constraining limits are obtained when the top quark mass is varied. For instance, still with $m_{\tilde{t}} = 1\,\mathrm{TeV}/c^2$, m_h and m_A have to exceed 41 and 44 GeV/c^2 when $m_\mathrm{t} = 90\,\mathrm{GeV}/c^2$, or 44 and 25 GeV/c^2 when $m_\mathrm{t} = 190\,\mathrm{GeV}/c^2$. If $m_{\tilde{t}}$ is further allowed to vary from m_t to a few TeV/c^2 and m_t up to a few hundred GeV/c^2, 95% c.l. lower limits of 41 GeV/c^2 on m_h and of 20 GeV/c^2 on m_A remain valid.

Comment on light Higgs bosons in the MSSM

When $m_\mathrm{h} < 2m_\mu$ it turns out that, when one-loop radiative corrections are taken into account, A is light (actually $m_\mathrm{A} < m_\mathrm{h}$) and $\cos^2(\beta - \alpha)$ is close to unity. Thus $m_\mathrm{h} < 2m_\mu$ is excluded since $\mathrm{Z} \to \mathrm{hA}$ would give too large a contribution to the Z width.

When $m_\mathrm{A} < 2m_\mu$ it may, and indeed does, happen that the decay mode $\mathrm{A} \to \gamma\gamma$ has a substantial branching ratio and that the A lifetime is short enough for the decay photons not to escape undetected. Since no direct searches involving such photonic topologies have been performed, only the Z width measurement can be used to set limits on the rate of $\mathrm{Z} \to \mathrm{hA}$. For instance, with the choice of parameters of fig. 6.5, $m_\mathrm{h} < 20\,\mathrm{GeV}/c^2$ is excluded.

A complete analysis of this region is in progress and will be reported in a forthcoming publication.

6.3 Summary and Conclusions

The results from the various searches for charged Higgs bosons are summarized in fig. 6.1 where the domain excluded by the combination of all these searches is also shown. It can be seen that the charged Higgs boson mass has to exceed 41.7 GeV/c^2, irrespective of the value of the hadronic decay branching ratio, and 45.3 GeV/c^2 if leptonic decays dominate.

The results from the various searches for the neutral Higgs bosons of two-doublet models are summarized in figs 6.4 to 6.7. Within the MSSM, and with one-loop radiative corrections to the Higgs potential taken into account, excluded domains are obtained such as the ones shown in fig. 6.5 and 6.7 for typical values of the parameters of the model, and lower mass limits of 41 GeV/c^2 and of 20 GeV/c^2 have been established on the masses of the CP-even h and of the CP-odd A neutral Higgs bosons, respectively, except if $m_\mathrm{A} < 2m_\mu$.

These results improve on those previously obtained by ALEPH [69,70,26] and by the other LEP experiments [71,31,72,73,74,37].

7 Supersymmetric Particles

7.1 Introduction

The standard model of electroweak and strong interactions, based on the $SU(3)_C \times SU(2)_L \times U(1)_Y$ gauge group, with spontaneous breaking of $SU(2)_L \times U(1)_Y$ to $U(1)_{EM}$, has been confirmed to an impressive level of precision. It is however commonly accepted that this model can only be the low energy approximation of some more fundamental theory. One of the most compelling reasons is known as the "gauge hierarchy" problem, namely that the standard model Higgs boson mass receives quadratically divergent contributions in the renormalization process and that it cannot be stabilized near the scale of electroweak symmetry breaking without an extremely fine tuning of the Higgs potential parameters. The only known way to solve this problem while preserving the elementary nature of the Higgs field is supersymmetry.

Supersymmetry [59,75], a symmetry associated to transformations which change the spin by half a unit, has many attractive features—it is the only non-trivial extension of the Poincaré group and when realized locally, it provides a natural connection with gravitation (this is known as "supergravity"), and it can even be viewed as the low energy remnant of a more fundamental superstring theory. However, an inescapable consequence of supersymmetry is that the ordinary

particles appear in "supermultiplets" together with new particles differing by half a unit of spin, in a way such that, within each supermultiplet, the number of fermionic and bosonic degrees of freedom are equal.

More precisely [59], a matter spin-1/2 fermion f, which has two helicity states, is associated with two spin-0 partners, $\tilde{f}_L$ and $\tilde{f}_R$, in a "chiral supermultiplet". A massless vector boson like the photon (or a gluon), which also has two helicity states, is associated with a Majorana gauge fermion like the photino $\tilde{\gamma}$ (or a gluino $\tilde{g}$) in a "massless vector supermultiplet". On the other hand, a massive neutral vector boson like the Z, with three helicity states, has to be associated with two Majorana gauge fermions while a scalar Higgs boson H provides the otherwise missing bosonic degree of freedom to complete a "massive vector supermultiplet". Similarly, the W is associated with two Dirac gauge fermions and with a charged Higgs boson. The occurrence of charged Higgs bosons is indeed a feature common to all supersymmetric models since at least two Higgs doublets are needed to give masses to the up-type quarks on the one hand and to the down-type quarks and to the charged leptons on the other. As a consequence, there are at least two neutral Higgs bosons in addition to H, another CP-even h and a CP-odd A which are associated with a Majorana higgsino in a chiral supermultiplet. The search for these particles has already been discussed in section 6.

Supersymmetry must be broken since, for instance, there is no spin-0 particle degenerate in mass with the electron. Little is known *a priori* about the supersymmetry breaking mechanism but, if the "hierarchy problem" is to remain solved [76], the mass splittings within the supermultiplets cannot substantially exceed the Fermi scale. When supersymmetry is broken, not only is the mass degeneracy within the supermultiplets lifted, but also mixing occurs among the electroweak eigenstates. In particular, the supersymmetric partners of the $W^{\pm}$ and of the $H^{\pm}$ mix to form mass eigenstates called "charginos", the lighter of which is denoted $\chi^{\pm}$ in the following. Similarly, the photino, the higgsino(s) and the supersymmetric partners of the Z and of the H mix to form at least four mass eigenstates called "neutralinos", denoted χ, χ', χ'', etc. when ordered by increasing mass.

Although not generally necessary, a new quantum number called R-parity [77] is conserved in most supersymmetric models. Since $R = (-1)^{2S+3B-L}$, it can be seen that ordinary particles carry $R = 1$ while their superpartners have $R = -1$. As a result of R-parity conservation supersymmetric particles are produced in pairs and all supersymmetric particle decays ultimately lead to the lightest supersymmetric particle, (LSP). From cosmological arguments [78] it is expected that the LSP is electrically neutral and colourless. A natural candidate is χ, the lightest of the neutralinos, and this is what will be assumed in the following, unless explicitly stated. The interactions of the LSP with ordinary matter are mediated by the exchange of weak vector bosons or of the superpartners of the electron or of the quarks; since these have not yet been observed, they must be heavy and the LSP therefore behaves in a similar way to a neutrino. This is the reason for the signature which is at the basis of all searches for supersymmetric particles—the missing energy and momentum carried away by the LSP.

7.2 Searches for Scalar Leptons

For each charged lepton ℓ, there are two spin-0 supersymmetric partners. The electroweak interaction eigenstates are associated to the left and right helicity degrees of freedom of ℓ, and are therefore denoted $\tilde{\ell}_L$ and $\tilde{\ell}_R$. The mass eigenstates are usually practically identical to these interaction eigenstates and no distinction will be made in the following. On the other hand, mass degeneracy will not be assumed since, in most supergravity models, $m_{\tilde{\ell}_L}$ receives larger radiative corrections than $m_{\tilde{\ell}_R}$. All results will therefore conservatively be given for the spin-0 partner $\tilde{\ell}_R$ of the right-handed helicity degree of freedom of ℓ. The three spin-0 partners of the neutrinos, corresponding to the three lepton flavours, will be assumed to be mass degenerate [79].

The main production mechanism for charged or neutral scalar leptons in e^+e^- collisions at the Z peak is *via* Z decay to a scalar lepton pair [80]. Each light scalar neutrino and each light scalar charged lepton would contribute 50% and 20% of Γ_ν to the Z decay width, respectively. The t-channel χ exchange can in principle contribute to the production of scalar electrons, but at a rate which strongly depends on m_χ and on the field content of χ. Since there is no interference between the two production mechanisms at the Z peak, this additional contribution will be conservatively ignored. Scalar leptons will be assumed to decay promptly into their ordinary lepton partner and into the LSP χ. The final state topology is therefore a pair of acoplanar leptons of the same flavour in the case of charged scalar leptons, and purely invisible in the case of scalar neutrinos.

From the measurement of the Z invisible width by ALEPH [14] lower mass limits can be inferred for scalar neutrinos and also for scalar leptons, since the corresponding final state topology is retained in neither the hadronic nor the leptonic standard ALEPH selections since they fail the acollinearity cut in the lepton selection. The result is that $m_{\tilde{\nu}} < 41.1\,\mathrm{GeV}/c^2$ and $m_{\tilde{l}} < 24.5\,\mathrm{GeV}/c^2$ are excluded at 95% c.l. The decay of supersymmetric leptons results in final states containing acoplanar lepton pairs. No events of this type were found in the search described in section 5.3.2. This result can be interpreted as a limit on supersymmetric leptons by calculating the expected number of events in the $(m_{\tilde{l}}, m_\chi)$ plane. A Monte Carlo program based on the cross-sections given ref. [81] and containing the acoplanar pair cuts was used. Domains in this plane are excluded as shown in fig. 7.1. It can be seen in particular that $m_{\tilde{l}_R} \lesssim 45\,\mathrm{GeV}/c^2$ is excluded at 95% c.l. for $m_\chi \lesssim 41\,\mathrm{GeV}/c^2$ in the case of the $\tilde{e}$ and $\tilde{\mu}$ and for $m_\chi \lesssim 38\,\mathrm{GeV}/c^2$ in the case of the $\tilde{\tau}$.

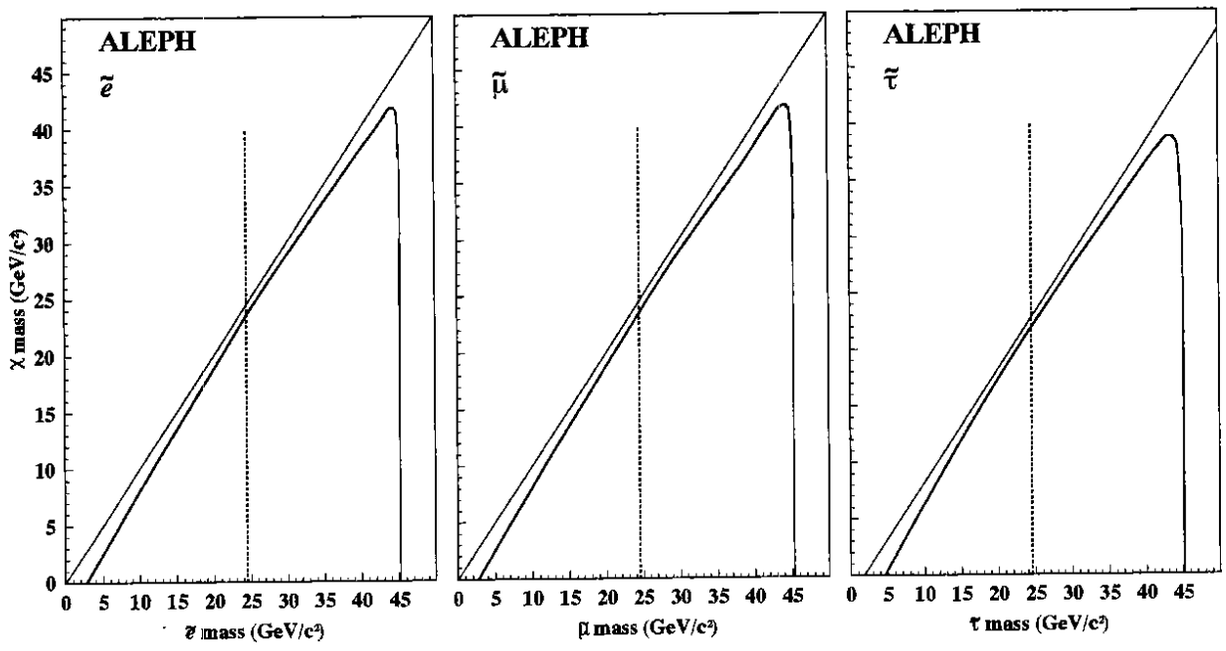

Figure 7.1: Excluded domains in the m_χ *vs* $m_{\tilde{l}_R}$ planes, for $\tilde{e}$, $\tilde{\mu}$ and $\tilde{\tau}$. Diagonal lines indicate the limit $m_{\tilde{l}} = m_\chi + m_l$. The region to the left of each vertical line is excluded by the invisible width measurement.

7.3 Searches for Charginos

If light enough, charginos can be abundantly produced in Z decays [80]. The partial Z decay width into $\chi^+\chi^-$ is $\sim 0.5\Gamma_\nu$ if the chargino is a pure higgsino (i.e. the supersymmetric partner

of the $H^{\pm}$), and as large as $4.5\Gamma_\nu$ if it is a pure wino (the supersymmetric partner of the $W^{\pm}$), at least when $m_{\chi^{\pm}} \ll m_Z/2$. For arbitrary field content, the rate lies between these extremes.

The charginos can decay to $\chi f_u \bar{f}_d$ *via* virtual W exchange or *via* $\tilde{f}_u$ or $\tilde{f}_d$ exchange where f_u and f_d are the members of any weak isospin doublet. Depending upon the field content of $\chi^{\pm}$ and on the masses of the scalar partners of the various matter fermions, the branching ratio for the decay of $\chi^{\pm}$ into leptonic final states can vary somewhat. When W exchange dominates, i.e. when all scalar partners are very heavy, the leptonic branching ratio is 10% for each lepton flavour. Depending upon whether both the χ^+ and the χ^- decay leptonically, or only one of them, or none, the final state topology is an acoplanar pair of leptons, an isolated lepton and missing energy in an hadronic event, or an acoplanar pair of jets.

The possibility of a light scalar neutrino has also been considered, but with the restriction that $m_{\tilde{\nu}} > 41\ \mathrm{GeV}/c^2$, the lower mass limit obtained above. If $m_{\tilde{\nu}} < m_{\chi^{\pm}}$, the decays $\chi^+ \to \ell^+ \tilde{\nu}_\ell$ are dominant, with ℓ = e, μ or τ with equal probabilities in the pure wino case, and $\ell = \tau$ in the pure higgsino case. The final state topology is then a pair of acoplanar leptons, not necessarily of the same flavour, and preferentially a τ pair if the higgsino component in $\chi^{\pm}$ is dominant.

Since the production rate for charginos is so large, interesting limits can already be derived from the Z width measurements. Any contribution to the Z width from non-standard processes must be less than $0.28\Gamma_\nu$ (section 4). More stringent limits can be inferred for "invisible" final states, defined as those final states which do not satisfy selection criteria for hadronic or leptonic Z decays, in which case the non-standard contribution has to be smaller than $0.13\Gamma_\nu$. The fraction of such "invisible" final states has been determined as a function of $m_{\chi^{\pm}}$ and of the mass of the LSP, leading to the excluded domains bounded by curves (A) in fig. 7.2.

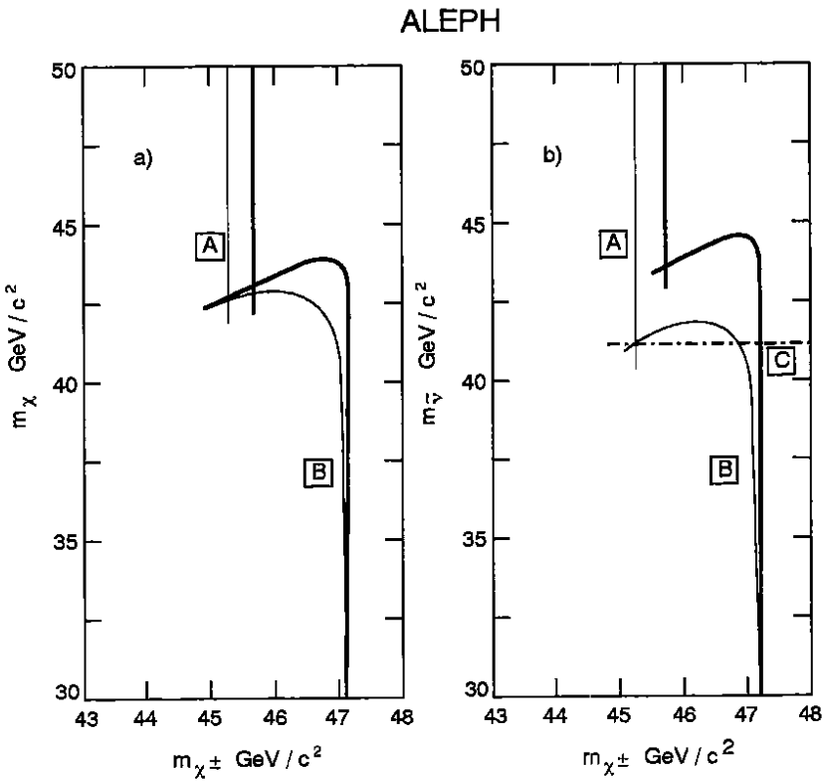

Figure 7.2: In the m_{LSP} *vs* $m_{\chi^{\pm}}$ plane, excluded domains from the Z width measurements (A), and from the direct searches (B) in the pure higgsino (light lines) and pure wino (heavy lines) cases, assuming: (a) $LSP = \chi$ and W exchange dominance in $\chi^{\pm}$ decays; (b) $LSP = \tilde{\nu}$. Notice that $m_{\tilde{\nu}} > 41\,\mathrm{GeV}/c^2$ from the Z invisible width measurement, assuming three mass degenerate scalar neutrinos (C).

To study charginos with higher masses, direct searches for the characteristic final state topologies arising from chargino pair production are necessary. They are, however, identical to those performed in the context of the searches for neutral and charged Higgs bosons, and have been described earlier. The results of those searches for acoplanar lepton pairs, for monojets and for acoplanar jets, and for isolated charged particles in hadronic events can be translated into excluded domains as shown in fig. 7.2.

Irrespective of the field content of $\chi^{\pm}$ and of the mass of the LSP, $m_{\chi^{\pm}}$ has to exceed $45.2\,\mathrm{GeV}/c^2$ at 95% c.l. The lower mass limit is $47\,\mathrm{GeV}/c^2$ if the LSP mass is $\lesssim 41\,\mathrm{GeV}/c^2$, irrespective of the leptonic branching ratio in $\chi^{\pm}$ decays.

7.4 Search for Neutralinos

In this section, the neutralinos other than χ, the lightest one, will be collectively denoted χ'. The relevant production mechanisms at the Z peak are [82]

$$\mathrm{e^+e^-} \to \mathrm{Z} \to \chi\chi \tag{7.1}$$

$$\mathrm{e^+e^-} \to \mathrm{Z} \to \chi\chi' \tag{7.2}$$

$$\mathrm{e^+e^-} \to \mathrm{Z} \to \chi'\chi'. \tag{7.3}$$

The Z partial width for the decay into $\chi_i\chi_j$, with χ_i and χ_j any two neutralinos, is:

$$\Gamma(Z \to \chi_i\chi_j) = (2-\delta_{ij})|C_{ij}|^2\Phi(m_i, m_j; \sqrt{s})\Gamma_\nu,$$

with Φ the phase space factor:

$$\Phi = \left(1 - \frac{(m_i^2+m_j^2)}{2s} - \frac{3\eta_{ij}m_im_j}{s} - \frac{(m_i^2-m_j^2)^2}{2s^2}\right)\left(1 - \frac{2(m_i^2+m_j^2)}{s} + \frac{(m_i^2-m_j^2)^2}{s^2}\right)^{\frac{1}{2}}.$$

Here, m_i and m_j are the masses of χ_i and of χ_j, respectively, and η_{ij} is the relative CP of χ_i and χ_j. The precise rate depends on the field contents of χ_i and χ_j through the value of the squared $\mathrm{Z}\chi_i\chi_j$ coupling $|C_{ij}|^2$ which reaches unity, its maximum value, when χ_i and χ_j are the appropriate combination of pure higgsino states, but is zero if χ_i or χ_j is a pure gaugino state.

While the $\chi\chi$ final state can be coped with only *via* its contribution to the Z invisible width, the final state topologies of the other reactions depend on the χ' decay pattern. In most cases, the main χ' decay mechanism is

$$\chi' \to \chi\mathrm{Z}^* \to \chi\mathrm{f\bar{f}}. \tag{7.4}$$

Since the χ escapes undetected, the signature of reaction (7.2) followed by (7.4) is an acoplanar pair of jets or a monojet, depending upon the masses of χ and of χ', or an acoplanar lepton pair. These same signatures also characterize, at least in some phase space regions, most of the final states resulting from reaction (7.3), and in particular those in which one of the χ' decays to $\chi\nu\bar{\nu}$. No events were observed in the searches for monojets and for acoplanar lepton or jet pairs reported in sections 5.3.2, 5.3.4 and 5.3.5. Within the same cuts defined for those searches the efficiencies for observing neutralino production and decay were calculated by Monte Carlo as a function of m_χ and $m_{\chi'}$ and for each of the two possible signs of η, the relative CP of χ and χ'. 95% c.l. limits at the level of a few 10^{-5} can be set in most of the domain kinematically accessible, on the products of branching ratios $B(Z \to \chi\chi') \times B(\chi' \to \chi\mathrm{Z}^*)$ and $B(Z \to \chi'\chi') \times B(\chi' \to \chi\mathrm{Z}^*)^2$. Unfolding the phase space factors, these results can be turned into the limits on the $\mathrm{Z}\chi\chi'$ and $\mathrm{Z}\chi'\chi'$ couplings shown in fig. 7.3, assuming $B(\chi' \to \chi\mathrm{Z}^*) = 100\%$.

Diagrams involving the exchange of scalar leptons or quarks in the χ' decay may also contribute to the same $\chi\mathrm{f\bar{f}}$ final states. Normally, the effect of these is simply to enhance the

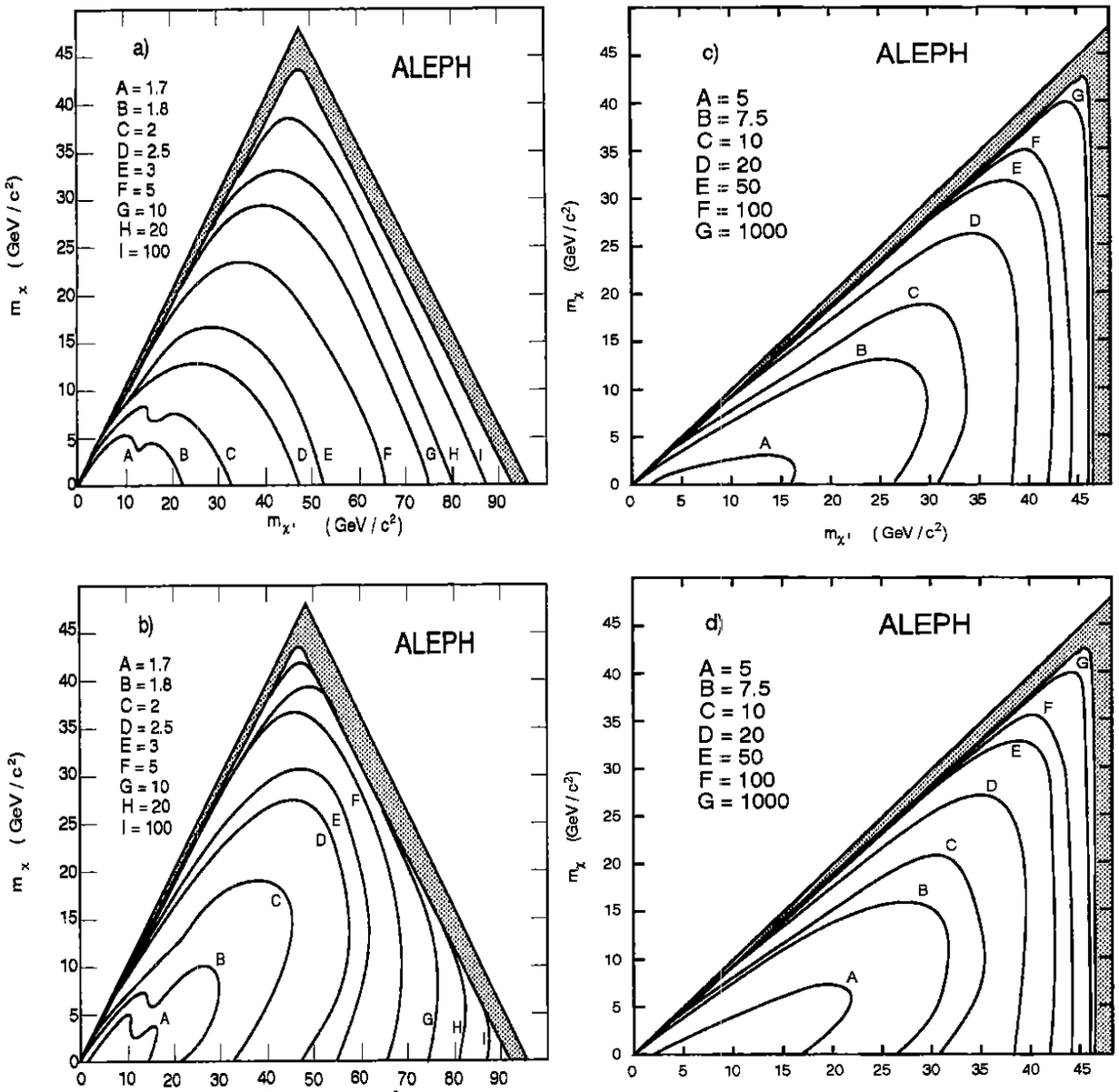

Figure 7.3: In the $(m_{\chi'}, m_{\chi})$ plane, equal value contours, labelled by capital letters, for the 95% c.l. limits on 10^4 times the squares of the couplings $Z\chi\chi'$ (a and b) and $Z\chi'\chi'$ (c and d). Here χ' is assumed to decay 100% to χZ^*. The relative CP of χ and χ' is positive in a) and c) and negative in b) and d).

leptonic final states, as scalar leptons are expected to be lighter than scalar quarks. This is harmless for the present analysis except if the scalar neutrino $\tilde{\nu}$ is light enough for the invisible decay mode $\chi' \to \nu\tilde{\nu}$ (with $\tilde{\nu} \to \nu\chi$) to become dominant.

It turns out, for particular neutralino masses and field contents, that the χ' decay to χ and a photon becomes significant, or even dominant, although it proceeds only *via* loop diagrams [83]. In such cases, the investigation of final states consisting of a single photon or of a pair of photons with missing energy, performed in the context of the search for excited neutrinos described in section 8.4, can be used. No signal was observed, and limits on the products of branching ratios $B(Z \to \chi\chi') \times B(\chi' \to \chi\gamma)$ and $B(Z \to \chi'\chi') \times B(\chi' \to \chi\gamma)^2$ can thus be derived, also at the level of a few 10^{-5}.

If kinematically accessible, the decays $\chi' \to \chi h$ or χA would be dominant. It has been verified that the efficiencies of the searches for monojets and for acoplanar jets are such that the limits in fig. 7.3 are unaltered if $\chi' \to \chi Z^*$ is replaced by $\chi' \to \chi h$ or χA. More restrictive results would even be obtained in such a case since the analysis would not suffer from the substantial invisible fraction of final states normally present because of the $\chi' \to \chi\nu\bar{\nu}$ decay.

Finally, if kinematically allowed, the decay channel $\chi' \to \chi^{\pm} W^* \to \chi^{\pm} f\bar{f}'$ followed by $\chi^{\pm} \to \chi f\bar{f}'$ should also be taken into account. However, this is normally disfavoured with respect to (7.4) as $m_{\chi^{\pm}} \gtrsim 45\,\mathrm{GeV}/c^2$.

7.5 Interpretation in the MSSM

In the minimal supersymmetric extension of the standard model (MSSM), the field content and the number of supersymmetry breaking parameters are minimal. In this model [58,60] the Lagrangian at the scale of grand unification is globally supersymmetric, except for a set of "soft breaking" terms. Among these, M_1, M_2 and M_3 are gaugino mass terms associated with the $U(1)_Y$, $SU(2)_L$ and $SU(3)_C$ gauge groups respectively. These mass terms are commonly assumed to be equal at the unification scale. However, they get renormalized differently, with in particular $M_1 = (5/3)M_2 \tan^2\theta_W$. Here, we will use the combination $M_{\tilde{\gamma}} = M_1 \cos^2\theta_W + M_2 \sin^2\theta_W$, which is associated with the photino field (for $\sin^2\theta_W = 0.23$, $M_{\tilde{\gamma}} = 0.61 M_2$). Another mass parameter not present in the minimal standard model is μ, the supersymmetric mass term which mixes the two Higgs superfields. Finally, the ratio v_2/v_1 of the vacuum expectation values of the two Higgs doublets completes the specification of the parameters relevant for the present study.

Within the MSSM, for any triplet of values for $M_{\tilde{\gamma}}$, μ and v_2/v_1, all the masses and couplings of the charginos and neutralinos can be computed. The total contribution of these to the Z decay width can be inferred and compared to the 95% c.l. upper limit on any new physics contribution derived in section 4. Further results can be obtained from the Z invisible width measurement by considering only the Z decay final states not retained by any of the standard hadronic and leptonic selections [14], and therefore classified as invisible. The most important of these is $\chi\chi$, but other decays such as $\chi\chi'$ followed by $\chi' \to \chi\nu\bar{\nu}$ also play some role. The results thus obtained are shown in fig. 7.4 as excluded domains in the $(M_{\tilde{\gamma}}, \mu)$ plane for various values of v_2/v_1.

Small additional domains are excluded by the direct searches for charginos. They correspond to cases where the lighter chargino is mostly higgsino-like, and therefore contributes less to the Z width than when it is mostly gaugino-like. As can be seen in fig. 7.4, a substantial increase of the excluded regions is obtained when the direct searches for neutralinos are taken into account. Here it has been assumed that the scalar neutrinos are heavy enough not to be produced in χ' decays. The results have been found to be insensitive to the precise value of the χ' radiative decay branching ratio. Cascade decays such as $\chi' \to \chi^{\pm} W^*$, kinematically allowed for some values of the MSSM parameters, have been explicitly taken into account.

It can be seen in fig. 7.4 that most of the kinematically accessible domain is thus excluded, at least for values of the "photino" mass $M_{\tilde{\gamma}}$ and of the "higgsino" mass μ not too large compared to the Z mass, as soon as $v_2/v_1 \gtrsim 2$. These results also lead to the 95% c.l. lower limits on the masses of χ and χ' shown in fig. 7.5 as a function of v_2/v_1. In particular, $m_{\chi} > 20\,\mathrm{GeV}/c^2$ and $m_{\chi'} > 45\,\mathrm{GeV}/c^2$ as soon as $v_2/v_1 > 3$. A massless χ can be excluded for $v_2/v_1 < 1.6$ only if these results are combined with the lower limit on the mass of the gluino obtained in $p\bar{p}$ collisions [84].

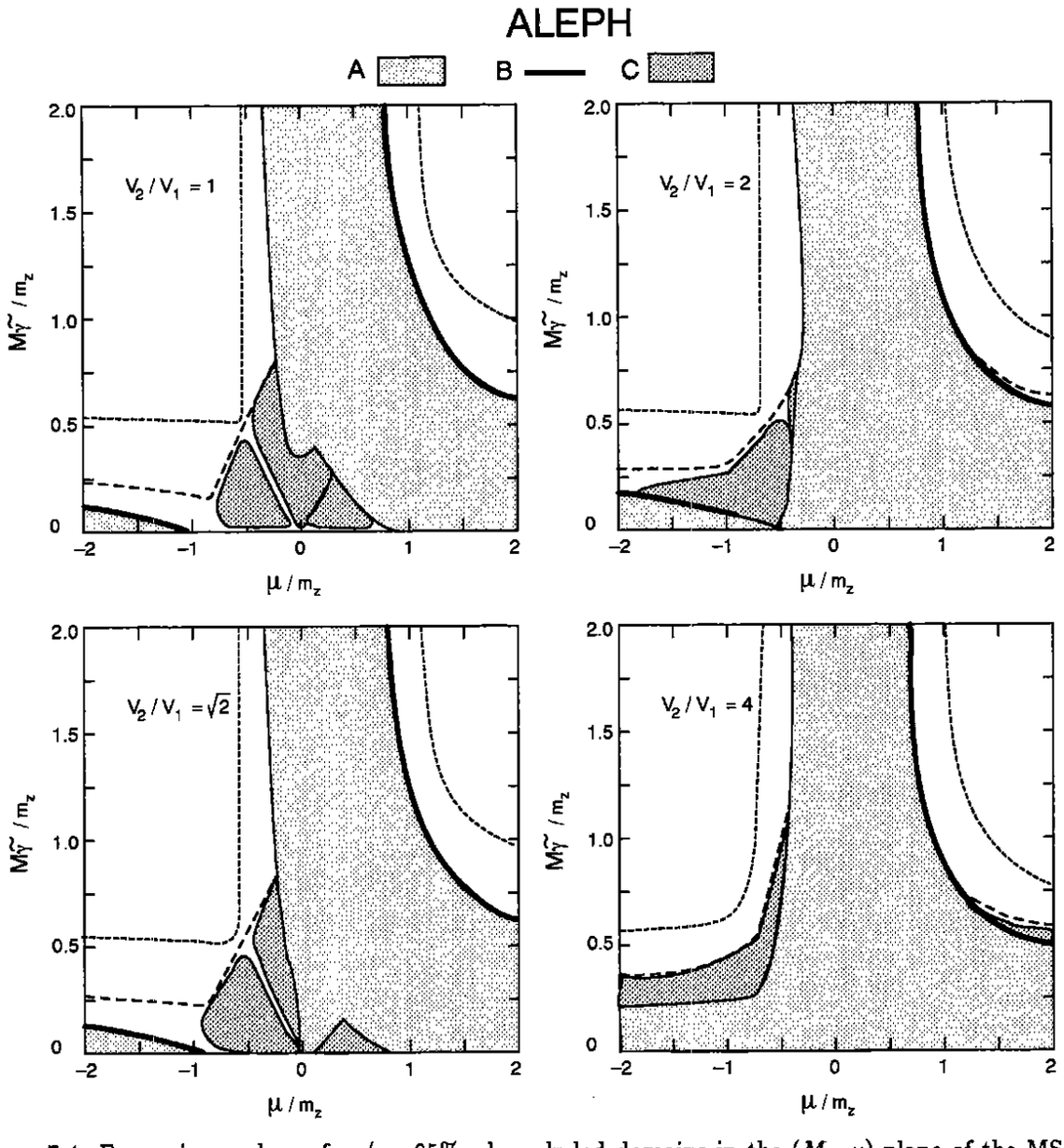

Figure 7.4: For various values of v_2/v_1, 95% c.l. excluded domains in the $(M_{\tilde{\gamma}}, \mu)$ plane of the MSSM: (A) from the Z width measurements, (B) from the direct searches for charginos and (C) from the direct searches for neutralinos. Dotted contour: limit of the domain kinematically accessible in Z decays into charginos and neutralinos. Dashed contour: the same, excluding the invisible mode $Z \rightarrow \chi\chi$.

7.6 Summary and Conclusions

From the Z invisible width measurement, a lower limit of 41 GeV/c^2 has been set on the mass of scalar neutrinos, assuming three mass degenerate species. If the mass of the LSP is $\lesssim$40 GeV/c^2 the masses of the supersymmetric partners of the charged leptons must exceed 45 GeV/c^2 and chargino masses must exceed 47 GeV/c^2. The Z decay branching ratio into neutralinos is restricted to be less than a few 10^{-5} in most of the domain kinematically accessible. Consequences of these results in the framework of the MSSM have been drawn; in particular, the lightest neutralino mass is larger than 20 GeV/c^2 as soon as $v_2/v_1 > 3$.

These results improve on those previously obtained by ALEPH [85,86] and by the other LEP experiments [87,88,89,90].

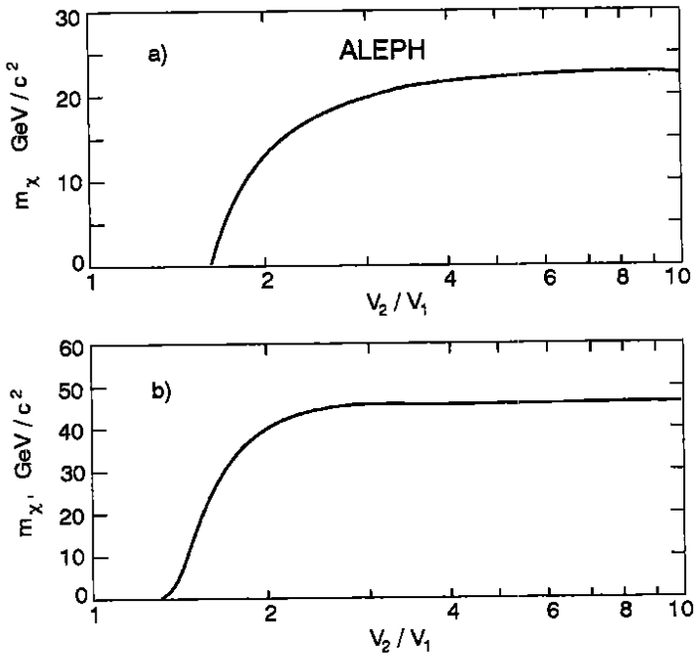

Figure 7.5: As a function of v_2/v_1, 95% c.l. lower limits derived in the MSSM for the masses of χ (a) and of χ' (b).

8 Compositeness

Compositeness is regarded as a possible solution to certain problems of the standard model such as the fermion spectrum, mass generation and the large number of arbitrary parameters. It supposes that some simple underlying structure can explain the lepton and quark family pattern and mass spectrum and possibly also that of the gauge bosons. Many such composite models exist but none has been able to give a satisfactory explanation of the above problems [91].

One effect of compositeness would be the existence of excited states of the known particles and much effort has been directed to the search for such states, particularly for excited fermions, f*, where f* may be an excited charged lepton (ℓ^*), an excited neutrino (ν^*) or an excited quark (q*). The simplest models of compositeness suppose that excited fermions form spin $\frac{1}{2}$ doublets and carry electroweak charges similar to the ordinary fermions. Such a particle will be readily produced at LEP as an $f^*\overline{f^*}$ pair if its mass, m^*, is less than $m_Z/2$. However, f* single production depends on the strength of the Zf*f coupling and the probability of observing a state with m^* between $m_Z/2$ and m_Z depends both on this coupling and the decay branching ratios. If the Z boson is composite a spectrum of states is again expected including both isoscalar (Y) and excited vector bosons (Z*). In addition new couplings and decay modes forbidden at lowest order can occur.

In this section we first review limits on composite fermions that can be established from Z width measurements. This is followed by a description of direct searches for ℓ^*, ν^* and q* states and a study of the reaction $e^+e^- \to \gamma\gamma$ for evidence of virtual e* exchange. In section 8.6 we describe the search for evidence for four-boson couplings by looking for the decays $Z \to gg\gamma$ and $Z \to \gamma\gamma\gamma$.

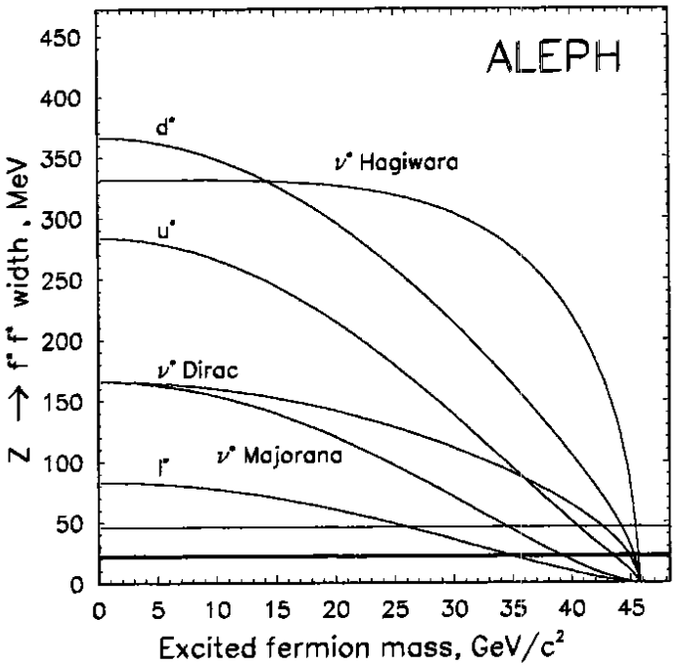

Figure 8.1: Variation of the width $Z \rightarrow f^*\overline{f^*}$ as a function of f^* mass. The horizontal lines show the total, non-hadronic and invisible width limits derived in section 4.

8.1 Mass Limits from Z Width Measurements

The limits obtained on Z partial widths in section 4 can now be applied to the production of excited fermion pairs $e^+e^- \rightarrow Z \rightarrow f^*\overline{f^*}$ in order to deduce limits on the f^* mass. The cross-section at tree-level for this process is well known (e.g. ref. [43]). Terms dependent on the fermion mass, unimportant for the known fermions, become significant as m^* approaches $m_Z/2$. Thus the width $\Gamma(Z \rightarrow f^*\overline{f^*})$ is

$$\Gamma = \frac{N_C G_\mu}{24\sqrt{2}\pi} m_Z^3 \beta \left[\frac{1}{2}(3+\beta^2)(g_L^2+g_R^2) + 3(1-\beta^2) g_L g_R\right]$$

where the velocity β depends on m^*, and g_L and g_R are the left- and right-handed standard model $Zf\bar{f}$ couplings of the corresponding ordinary fermions.

For excited neutrinos three types of coupling are considered: *(i)* $g_L = 1, g_R = 0$ (Dirac-type neutrino); *(ii)* $g_L = -g_R = 1$ (Majorana neutrino – in this case the width is divided by 2 to account for the presence of two identical neutrinos); *(iii)* $g_L = g_R = 1$ (model of Hagiwara *et al.* [92] discussed in detail in section 8.2).

The dependence of the predicted width Γ on m^* is plotted in fig. 8.1 for excited charged leptons, neutrinos and quarks of the up and down type. Horizontal lines indicate the limits on the total, non-hadronic and invisible widths. Mass limits derived from these are given in table 8.1. Those obtained from the total width are valid irrespective of f^* decay topology.

In addition, the mass limits for excited leptons are also derived under the assumption of purely radiative decays. This assumption may not be true since the decays *via* a virtual Z or W boson can also occur [92,93]. Radiative decays of excited charged leptons lead to a "non-hadronic" topology while excited neutrinos are "invisible". The corresponding width limits (table 4.1) are translated into mass limits in table 8.1.

Excited fermion	any decay topology	topology dependent limit
u-type quark	40.6	-
d-type quark	44.2	-
charged lepton	26.1	34.6
Dirac neutrino	42.6	44.9
Majorana neutrino	34.6	39.3
neutrino of Hagiwara *et al.*	45.4	45.5

Table 8.1: Limits on excited fermion masses in GeV/c^2 derived from the ALEPH Z lineshape measurements. The first limit is independent of the decay modes of the f*; the second assumes purely radiative decays of excited leptons.

8.2 Single Production of Excited Leptons

The theory of single excited lepton production has been discussed by several authors [92,94]. We have followed the formulation of Hagiwara *et al.* [92] in the analyses described here.

The general form of the effective Lagrangian for the l^*lV transitions is written

$$\mathcal{L}_{\rm eff} = \sum_{V=\gamma,{\rm Z},{\rm W}} \frac{e}{\Lambda}\overline{L}\sigma^{\mu\nu}(c_{VLl} - d_{VLl}\gamma^5)l^*\partial_\mu V_\nu + {\rm h.c.}$$

where Λ is the compositeness scale.

To high accuracy the $g-2$ measurements imply $|c| = |d|$ and the absence of electric dipole moments require c and d to have the same phase. It is usual to assume that the excited electron and neutrino form a weak doublet, L, which couples to the left-handed electron doublet, l_L, by the interaction Lagrangian

$$\mathcal{L} = \frac{gf}{\Lambda}\overline{L}\sigma^{\mu\nu}\frac{\tau}{2}l_L\partial_\mu W_\nu + \frac{g'f'}{\Lambda}\overline{L}\sigma^{\mu\nu}Yl_L\partial_\mu B_\nu + {\rm h.c.}$$

Here g and g' are the standard model $SU(2)$ and $U(1)$ coupling constants, τ are the Pauli matrices and $Y = -1/2$ is the hypercharge.

The differential cross-section for the process $e^+e^- \to \ell^*\ell$ (where $\ell^*\ell \equiv \ell\overline{\ell^*} + \overline{\ell}\ell^*$) to lowest order in α derived from the above is given in full by Hagiwara *et al.* including a term for t-channel photon exchange in e* production. In the special case of s-channel Z exchange the differential cross-section is given by

$$\frac{{\rm d}\sigma}{{\rm d}t} = \frac{4\pi\alpha^2}{s\Lambda^2|D_{\rm Z}|^2}\left[(a^2+b^2)(c^2+d^2)\left(m^{*2}(s-m^{*2})+2tu\right) + 4abcd\,m^{*2}(t-u)\right]$$

where a and b are the standard model couplings of the electron:

$$a = \frac{1}{4\sin\theta_W\cos\theta_W}, \qquad b = \frac{1-4\sin^2\theta_W}{4\sin\theta_W\cos\theta_W};$$

$1/D_{\rm Z}(s)$ is the Z propagator, with $|D_{\rm Z}(s)|^2 = (s-m_{\rm Z}^2)^2 + m_{\rm Z}^2\Gamma_{\rm Z}^2$.

In this model the coupling constants all satisfy $c = d$ with

$$c_{\gamma e^* e} = -\frac{1}{4}(f+f'); \qquad c_{{\rm Z}e^*e} = -\frac{1}{4}(f\cot\theta_W - f'\tan\theta_W);$$

$$c_{\gamma\nu^*\nu} = \frac{1}{4}(f-f'); \qquad c_{{\rm Z}\nu^*\nu} = \frac{1}{4}(f\cot\theta_W + f'\tan\theta_W).$$

8.3 Search for Excited Charged Leptons

The production and radiative decay of heavy excited objects like ℓ^* (where ℓ = e, μ or τ) is characterized by an acollinear lepton pair and one or two energetic photons. Backgrounds arise from standard radiative processes; the selection criteria have therefore been chosen to keep a good global detection efficiency for ℓ^* processes but to reduce the radiative background.

8.3.1 The process $e^+e^- \to (e^\pm)e^\mp\gamma$

This reaction has a large t-channel cross-section and has also been used to search for the on-shell production of an e^* through the direct interaction between a quasi-real photon emitted by one beam, along its direction, with the other beam. This process, known as quasi-real Compton scattering [95,96], is characterized by a single energetic charged track and an energetic photon; both particles are in a plane containing the beam direction and the expected visible energy is larger than the beam energy. Due to the imbalance in the initial state between the photon and the beam momenta, the event is boosted in the direction of the beam of the same sign as the detected charged particle.

The overconstrained kinematics of the process makes these events rather easy to separate from any background. Two initial cuts were applied: *(i)* the photon was required to be coplanar within $\pm 1^\circ$ with the observed electron and the beam; *(ii)* the total final state energy had to be greater than 92.5% of the centre-of-mass energy. At this stage 291 events remain. However there is an accumulation of events with the photon and the charged track almost back to back. These events arise from large angle Bhabhas where one of the final state electrons radiates a very hard photon along its direction of flight and is not detected in the TPC. This background was removed by requiring fewer than 13 ITC hits when the opening angle is larger than 140°. To prevent similar contamination at low angles both the charged track and the photon angles to the beam were required to be larger than 25.8°.

The final sample consists of 75 events. A calculation [97] of the standard t-channel process including soft bremsstrahlung and virtual corrections predicts 75.1 events. The $e\gamma$ invariant mass distributions for the data and Monte Carlo samples are shown in fig. 8.2(a).

8.3.2 The processes $e^+e^- \to \ell^+\ell^-\gamma$ and $e^+e^- \to \ell^+\ell^-\gamma\gamma$

To look for ℓ^* production through the reactions $e^+e^- \to \ell^*\ell$ and $e^+e^- \to \ell^*\overline{\ell^*}$ followed by the decay $\ell^* \to \ell\gamma$, events were selected with one or two isolated photons with energy above 5 GeV accompanying acollinear e^+e^-, $\mu^+\mu^-$ and $\tau^+\tau^-$ final states. Only events with two or four tracks were considered. For the two-prong topology, the acollinearity was required to be between 10° and 170°. To be considered as isolated, a photon had to be at least 30° away from any charged track.

No event with two photons survived the acollinearity cut giving zero candidates for any of the pair production processes with a global efficiency of about 75% independent of ℓ^* mass.

The selection of the $e^+e^-\gamma$ final state was made as follows. The ECAL energy due to the charged tracks was required to be larger than $0.75(\sqrt{s} - E_\gamma)$, this condition alone isolating with high efficiency final states where electromagnetic energy dominates. Then, to remove the remaining background, in particular $\tau\tau\gamma$ events, the total visible energy was required to be associated only to the charged tracks and to the photon i.e. the sum of the charged particle momenta as measured by the TPC, the energies of the associated ECAL clusters and of the photon, normalized to twice the total centre-of-mass energy, was required to be larger than 70%. Finally at least one charged track was required to pass the standard electron estimators (section 3.3.1). No event, either data or Monte Carlo, failed this last test.

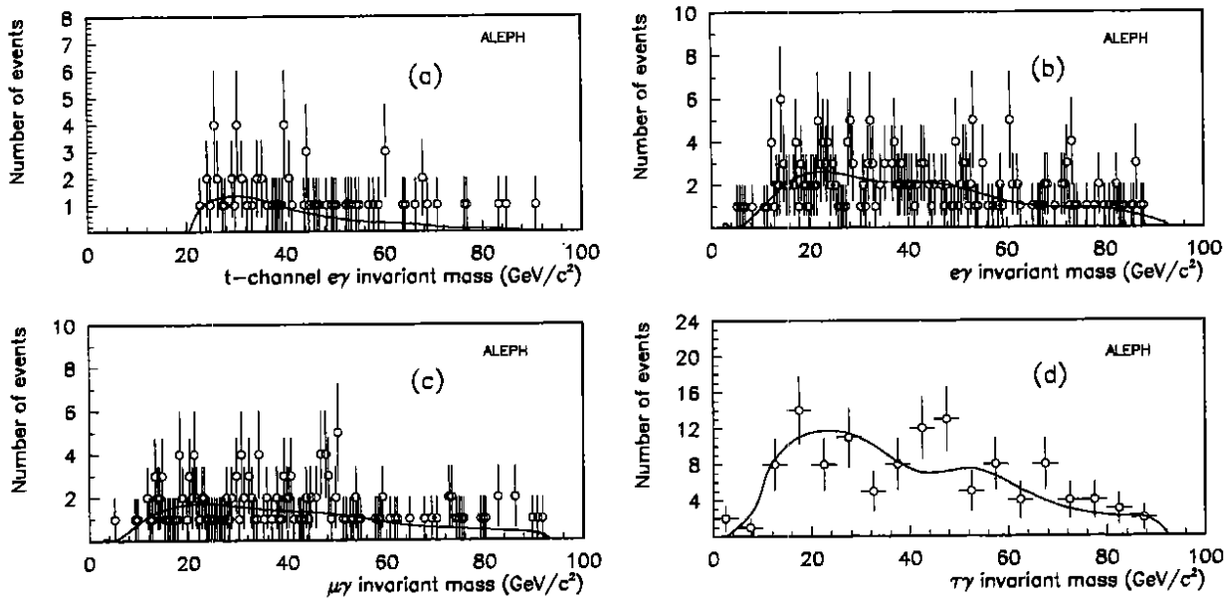

Figure 8.2: Invariant $\ell\gamma$ mass distribution for the final states (a) $e^{\pm}\gamma$, (b) $e^+e^-\gamma$, (c) $\mu^+\mu^-\gamma$ and (d) $\tau^+\tau^-\gamma$. The solid points represent the data, the lines are the QED expectations. There are two entries per event except for (a).

The final sample consists of 120 eeγ events compared to 131.1 predicted from the hard radiative QED reaction $e^+e^- \to e^+e^-\gamma$ calculated using the Monte Carlo program BABAMC [98,99]. The eγ invariant mass distributions are shown in fig. 8.2(b).

To select $\mu\mu\gamma$ events it was first required that the total ECAL energy deposited by the two charged tracks was less than $0.10(\sqrt{s}-E_\gamma)$. This cut removed all the Bhabha events and a large fraction of the $\tau\tau$ events. A second cut to select those events where the sum of the charged particle momenta and the photon energy is larger than 80% of the total centre-of-mass energy removed all remaining background. Finally at least one track was required to satisfy the muon requirements (section 3.3.2) removing one event from the data sample.

The final $\mu\mu\gamma$ sample consists of 83 events compared to a prediction of 87.7 from the hard radiative QED process $e^+e^- \to \mu^+\mu^-\gamma$ and 0.3 from the process $e^+e^- \to \tau^+\tau^-\gamma$, the latter calculated using the Monte Carlo program KORALZ [100]. The comparison of the $\mu\gamma$ invariant mass distributions is shown in fig. 8.2(c).

Events with two or four good tracks were used for the $\tau\tau\gamma$ selection. To remove events from the reactions $e^+e^- \to e^+e^-\gamma$ and $e^+e^- \to \mu^+\mu^-\gamma$ in the two track topology the missing mass squared was required to be larger than $2500\,(\,\mathrm{GeV}/c^2)^2$. Tau candidates decaying into three charged particles were selected as triplets of tracks with a total electric charge ± 1 and an invariant mass smaller than $1.6\,\mathrm{GeV}/c^2$ (the pion mass being assumed for the charged particles). To remove remaining background from two photon events the missing mass squared was required to be positive but smaller than $6000\,(\,\mathrm{GeV}/c^2)^2$. Finally two more cuts were applied on all events to remove remaining backgrounds: *(i)* the sum of the charged particle momenta was required to be larger than 10% of the total available energy (after subtraction of the radiated photon energy) to remove the remnant contribution from $e^+e^- \to (e^+e^-)\ell^+\ell^-\gamma$; *(ii)* the sum of the charged particle momenta and of the associated ECAL cluster energies, normalized to the available centre-of-mass energy after subtraction of the photon energy, was required to be less than 0.80. (This cut removes the tail of $e^+e^- \to e^+e^-\gamma$ events where, for example, another hard photon is emitted along the track direction.)

The final $\tau\tau\gamma$ sample consists of 61 events. The hard QED part of the reaction $e^+e^- \to$

$\tau^+\tau^-\gamma$ predicts 55.2 events while 0.8 events are predicted to arise from the reaction $e^+e^- \rightarrow e^+e^-\gamma$. Distributions for these events are shown in fig. 8.2(d).

8.3.3 Invariant mass reconstruction

In single production, a limit curve is extracted from a comparison between the observed $\ell\gamma$ invariant mass distribution and that predicted for radiative processes. Maximum sensitivity is obtained by achieving the best mass resolution possible.

For the t-channel reaction, $e^+e^- \rightarrow (e^{\pm})e^{\mp}\gamma$, the $e\gamma$ invariant mass was calculated using only the measured angular variables of the charged particle and of the photon. Due to the excellent angular resolution of ALEPH, the mass resolution is less than $0.5\,\mathrm{GeV}/c^2$ FWHM independent of energy and of the e* mass.

The invariant mass for the final states $e^+e^-\gamma$ and $\mu^+\mu^-\gamma$ was calculated by supposing an undetected photon to have been radiated in the initial state along the beam direction and then constraining this four body final state to recalculate the charged particle momenta and the photon energy. In this procedure the calculated momentum of the undetected photon has a mean of zero and a σ of $250\,\mathrm{MeV}/c$; the ℓ^* mass resolution is less than $0.5\,\mathrm{GeV}/c^2$ (FWHM) and independent of ℓ^* mass.

The invariant mass of $\tau\gamma$ combinations is more difficult to reconstruct because of unobserved neutrinos. However the τ momenta can be calculated by assuming that the original τ directions are the same as those of their visible decay products and rescaling their momenta by imposing energy and momentum conservation. A Monte Carlo study established the validity of this procedure and showed that the invariant mass resolution is $2.7\,\mathrm{GeV}/c^2$ and varies very little with τ^* mass.

The invariant mass distributions of fig. 8.2 have been plotted with bin size approximately equal to the resolution.

8.3.4 Extraction of mass limits

The detection efficiency for $\ell^*\overline{\ell^*}$ production was determined using a Monte Carlo generator based on the differential cross-section for the production of massive fermion pairs for each value of $\sqrt{s}$ at which we have data. Each ℓ^* was allowed to decay uniformly in its rest frame to $\ell\gamma$ and for the $\tau^*\overline{\tau^*}$ channel τ decays were generated using LUND 7.3. A photon finding probability of 93% was applied and all photons, including those from π^0 decay in τ^* events, were allowed to convert in the material around the beam with a 6% probability. The expected number of events as a function of mass is shown in fig. 8.3. Since no $\ell^*\overline{\ell^*}$ event is seen in any channel the 95% c.l. limit is set at three events corresponding to mass limits of $46.1\,\mathrm{GeV}/c^2$, $46.1\,\mathrm{GeV}/c^2$ and $46.0\,\mathrm{GeV}/c^2$ for the e*, μ^* and τ^* channels respectively.

8.3.5 Extraction of coupling limits

The cross-section for single production has been calculated using the Hagiwara formalism (section 8.2). The detection efficiency was determined using the following generators: *(i)* the e*e channel was simulated using the generator of Martinez *et al.* [101] and a modified version of this program was used for the quasi-real Compton scattering channel; *(ii)* for the $\mu^*\mu$ channel we used the generator of Berends *et al.* [102]; *(iii)* for $\tau^*\tau$ we used a modified version of the Berends program to decay τs using the Lund generator.

Events were generated at a number of ℓ^* masses and passed through the full ALEPH simulation and reconstruction program chain. For e* and μ^* the efficiency determined this way is around 60% and for τ^* it is about 50%. It varies very little with ℓ^* mass beginning to fall only within about $3\,\mathrm{GeV}/c^2$ of $\sqrt{s}$.

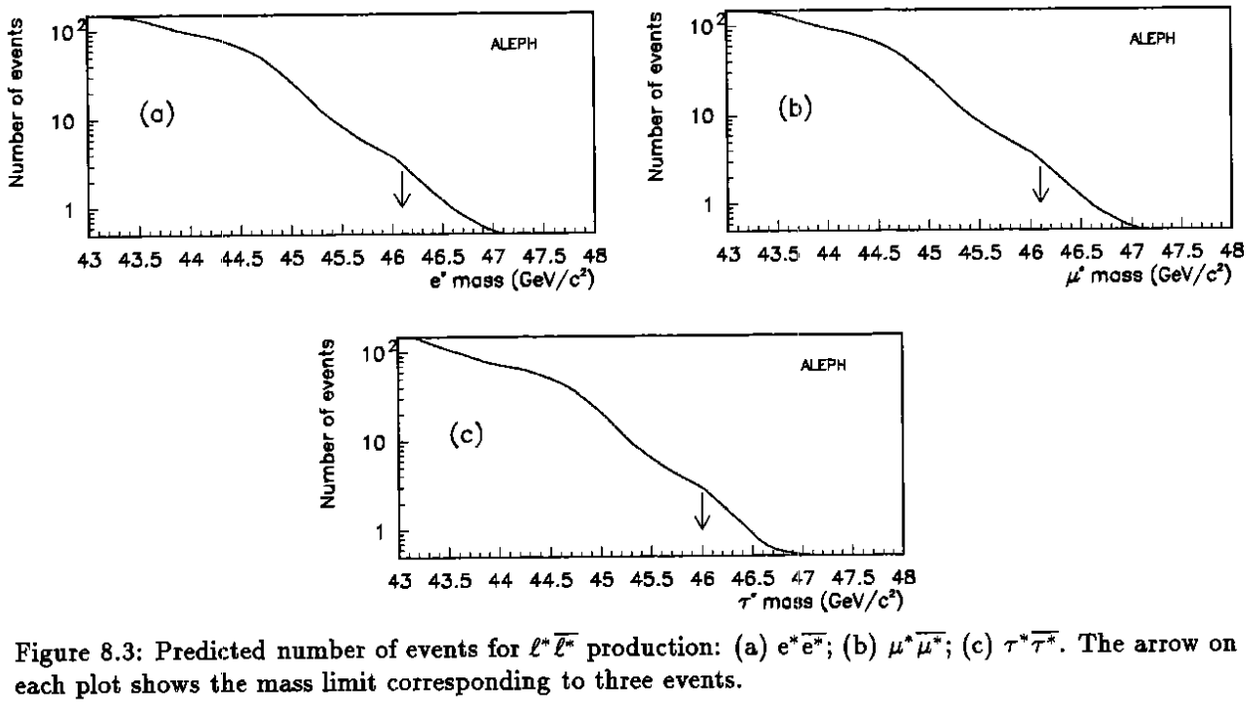

Figure 8.3: Predicted number of events for $\ell^*\overline{\ell^*}$ production: (a) $e^*\overline{e^*}$; (b) $\mu^*\overline{\mu^*}$; (c) $\tau^*\overline{\tau^*}$. The arrow on each plot shows the mass limit corresponding to three events.

The only significant background comes from radiative lepton pair events. For each channel and at each value of $\sqrt{s}$ a number of events was generated corresponding to a luminosity 5 to 10 times the experimental luminosity. The predicted number of background events (sections 8.3.1 and 8.3.2) and the corresponding invariant mass distributions were produced by mixing these events in the correct proportions. The results are shown together with the data in fig. 8.2; there is good agreement between data and background Monte Carlo for all four channels.

Limits on the $\gamma e^* e$ coupling determined at lower energy machines and at LEP have normally been given in terms of the quantity $\lambda/m^* \equiv \sqrt{2}c_{\gamma e^* e}/\Lambda$. Similar, but inconsistent, definitions of λ_{Ze^*e} have been used in the first publications of limits on $\ell^*\ell$ production at LEP. We have therefore chosen to express our coupling limits in terms of the parameters c of the Hagiwara model and give limits on $c_{\gamma e^* e}/\Lambda$ and $c_{Ze^* e}/\Lambda$. These limits are shown as a function of m^* in fig. 8.4 for the assumption that the branching ratio of ℓ^* to $\ell\gamma$ is 100%.

These results update previous limits published by ALEPH [103]. Similar results have been published by other LEP experiments [104,105,106,107].

8.3.6 The reaction $e^+e^- \to \gamma\gamma$

The reaction $e^+e^- \to \gamma\gamma$ proceeds *via* the exchange of a virtual electron in the t–channel and so provides a clean test of QED, electroweak corrections being negligible. The reaction could also occur *via* the exchange of a virtual excited electron e^* of mass m^*. Then [108]

$$\frac{d\sigma}{d\Omega} = \frac{\alpha^2}{s}\frac{1+\cos^2\theta}{1-\cos^2\theta}\left(1+\frac{s^2}{2}\left(\frac{\lambda}{m^{*2}}\right)^2\left(1-\cos^2\theta\right)H(\cos\theta)\right)$$

where λ is the $\gamma e^* e$ coupling parameter previously discussed in section 8.3.5 and

$$H(\cos\theta) = \left(1+\frac{s}{2m^{*2}}\frac{1-\cos^2\theta}{1+\cos^2\theta}\right)\left(\left(1+\frac{s}{2m^{*2}}\right)^2-\left(\frac{s}{2m^{*2}}\right)^2\cos^2\theta\right)^{-1}.$$

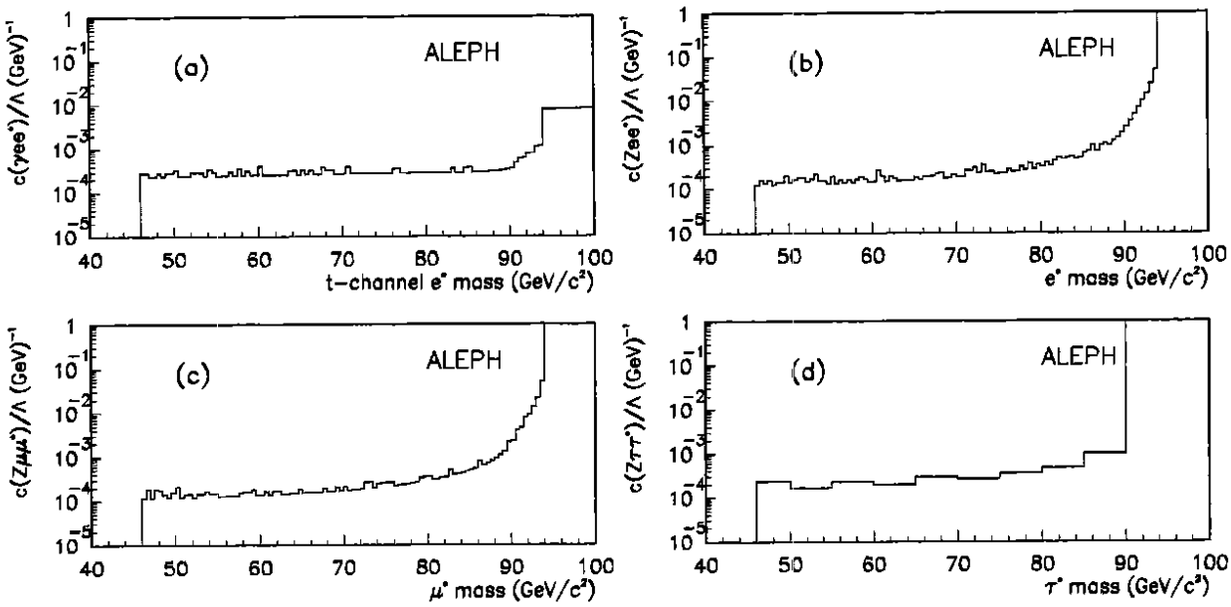

Figure 8.4: Coupling limits for single ℓ^* production as a function of m^*: (a) t-channel e*e, (b) s-channel e*e, (c) $\mu^*\mu$ and (d) $\tau^*\tau$ assuming 100% branching ratio for ℓ^* to $\ell\gamma$. The limit from $e^+e^- \to \gamma\gamma$ (section 8.3.6) is shown in (a).

The event sample used in this analysis had a total integrated luminosity of $8.47\,\mathrm{pb}^{-1}$. Selection of $\gamma\gamma$ events was performed demanding at least two ECAL modules with wire energy > 20 GeV associated with two reconstructed ECAL clusters each with $|\cos\theta| < 0.95$, the angle in space between the two most energetic ECAL clusters greater than 120° and no good tracks in the event. All 309 events satisfying these criteria were scanned and as a result two were rejected, one an $e^+e^-\gamma\gamma$ and the other a $\gamma\gamma\gamma\gamma$.

The detection efficiency and the expected number of events for the process was determined by Monte Carlo simulation using the multiphoton Monte Carlo generator of Berends and Kleiss [109] which gives QED calculations for this process to order α^3. The measured cross-section corrected to lowest order for $|\cos\theta| < 0.95$ as a function of $\sqrt{s}$ is shown in fig. 8.5(a) and listed in table 8.2(a). The figure also shows the lowest order QED prediction. The differential cross-section for the events summed over all energies is shown in fig. 8.5(b) and listed in table 8.2(b) together with the lowest order QED prediction at 91.3 GeV, the weighted mean energy of our data. The number of events predicted to order α^3 is 291.1 compared to the 307 observed. One possible source of background, low angle Bhabhas where both electron and positron tracks are not reconstructed, was evaluated by processing 30,000 Monte Carlo events; none satisfied the selection criteria.

The limit curve of $c_{\gamma e^* e}/\Lambda\ (= \lambda/\sqrt{2}m^*)$ *vs* m^* was extracted using the log-likelihood method, fitting to the differential cross-section including e* exchange. The likelihood function was defined as

$$\mathcal{L}(c/\Lambda) = \frac{1}{\sqrt{2\pi}\Delta N} \exp\left(-\frac{1}{2}\left(\frac{1-N}{\Delta N}\right)^2\right) \prod_{i=1}^{10} P\left(\alpha_i, \eta_i\left(c/\Lambda, N\right)\right)$$

where P is the Poisson probability, α_i and η_i are the observed and predicted (to order α^3) number of events in each bin of $\cos\theta$ and N is the overall normalization factor. N was allowed to vary with a standard deviation $\Delta N = 2.4\%$, the estimated systematic error. The limit curve obtained is shown on fig. 8.4(a) for m^* values above the region of sensitivity of the direct search. For $\lambda = 1$ the corresponding value of m^* is $99\,\mathrm{GeV}/c^2$.

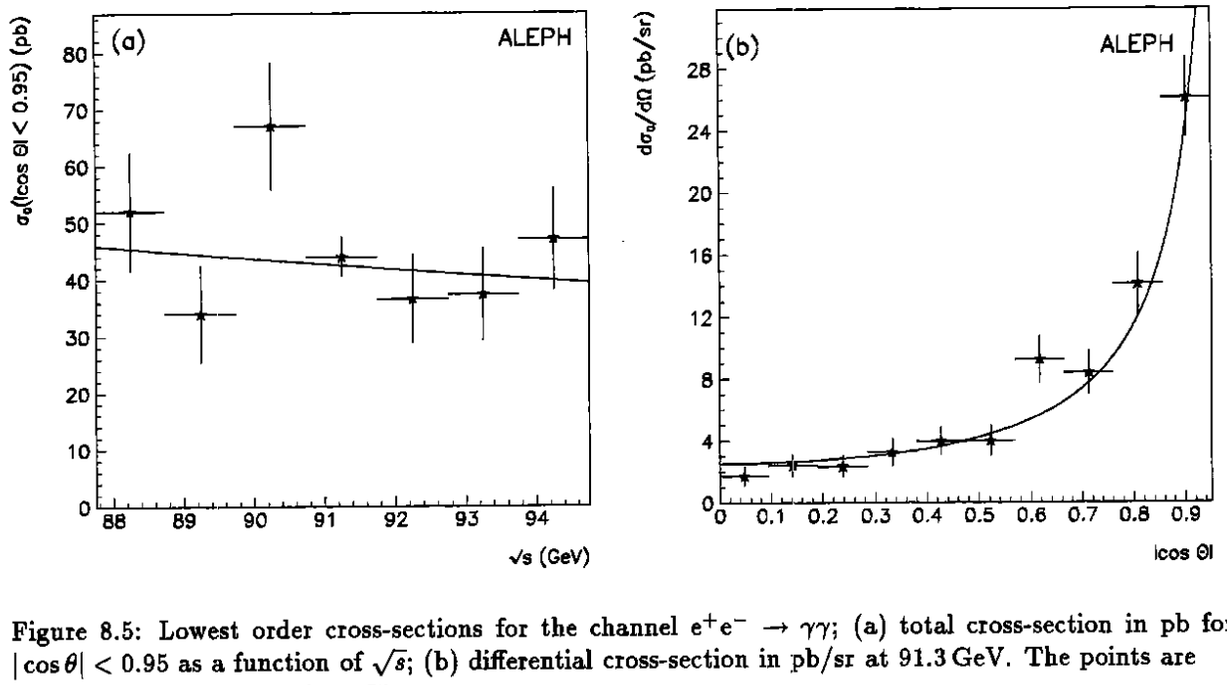

Figure 8.5: Lowest order cross-sections for the channel $e^+e^- \to \gamma\gamma$; (a) total cross-section in pb for $|\cos\theta| < 0.95$ as a function of $\sqrt{s}$; (b) differential cross-section in pb/sr at 91.3 GeV. The points are the data, the curves are for QED.

$\sqrt{s}$	Events		Cross-section
(GeV)	Data	MC	(pb)
88.2	25	21.8	52.0 ± 10.4
89.2	16	20.9	34.0 ± 8.5
90.2	36	23.3	67.1 ± 11.2
91.2	159	153.6	44.0 ± 3.5
92.2	22	25.0	36.6 ± 7.8
93.2	21	22.8	37.4 ± 8.2
94.2	28	23.7	47.1 ± 8.9

	Events		$\frac{d\sigma_0}{d\Omega}$
$\lvert\cos\theta\rvert$ range	Data	MC	
0.000 - 0.095	8	11.6	1.7 ± 0.6
0.095 - 0.190	11	11.9	2.4 ± 0.7
0.190 - 0.285	12	14.4	2.3 ± 0.7
0.285 - 0.380	14	13.4	3.3 ± 0.9
0.380 - 0.475	19	17.3	4.0 ± 0.9
0.475 - 0.570	17	18.7	4.0 ± 1.0
0.570 - 0.665	37	22.4	9.3 ± 1.5
0.665 - 0.760	35	32.2	8.4 ± 1.4
0.760 - 0.855	51	43.7	14.1 ± 2.0
0.855 - 0.950	103	105.5	26.1 ± 2.6

Table 8.2: Total cross-section in pb for $|\cos\theta| < 0.95$ and differential cross-section in pb/sr for the reaction $e^+e^- \to \gamma\gamma$, both to lowest order. The number of events observed and the number predicted to order α^3 are also given.

Any deviation from expected QED behaviour is sometimes expressed in a more general form in terms of two so-called QED cutoff parameters, Λ_+ and Λ_-, where

$$\frac{d\sigma}{d\Omega} = \frac{\alpha^2}{s}\frac{1+\cos^2\theta}{1-\cos^2\theta}\left(1 \pm \frac{s^2}{2\Lambda_\pm^4}\left(1-\cos^2\theta\right)\right)$$

A maximum-likelihood fit has also been made to this distribution. The parameters used in maximizing $\log\mathcal{L}$ were N and $1/\Lambda^4$, rather than Λ_+ and Λ_- since, unlike the latter parameters, it is normally distributed. The fitted value of $1/\Lambda^4$ was $1.9 \times 10^{-9}\,\mathrm{GeV}^{-4}$ with 95% c.l. limits at $+5.7 \times 10^{-9}\,\mathrm{GeV}^{-4}$ and $-5.2 \times 10^{-9}\,\mathrm{GeV}^{-4}$ from the fitted value, corresponding to $\Lambda_+ = 107\,\mathrm{GeV}$ and $\Lambda_- = 132\,\mathrm{GeV}$. Similar limits on on Λ_+ and Λ_- have been published by other LEP collaborations [110,111,112]. The LEP limits are significantly higher than those from the

lower energy e^+e^- colliders, TRISTAN [113,114,115], PETRA [116,117,118,119,120,121] and PEP [122,123].

8.4 Search for Excited Neutrinos

Excited neutrinos, expected to be the lightest excited particles, could be produced at LEP singly or in pairs, depending upon mass and couplings. Since the search is for the radiative decay of excited neutrinos, final states containing one or two photons and nothing else are studied. The data sample used corresponds to an integrated luminosity of $8.45\,\mathrm{pb}^{-1}$.

8.4.1 Event selection and photon reconstruction

Events were first selected which satisfied the following conditions. There were no good tracks, one or two ECAL barrel modules with wire energy E_W greater than 7 GeV, and no other ECAL module with E_W larger than 200 MeV. For each module, the ratio of the tower to wire energies had to be between 0.7 and 1.3. The event time, measured from a sampling of the rise time of the ECAL wire signal, had to coincide with the beam crossing time within ± 100 ns. Finally, the LCAL energy had to be less than 300 MeV (from randomly triggered events, the probability per bunch crossing of observing such LCAL energies is 0.4%). Two additional criteria were now applied to the photon candidates in these events. The transverse compactness, F_4 (section 3.3.1), had to be larger than 0.75 and the line of flight, reconstructed from storey energies and wire profile of the shower, was required to be closer than 500 mm to the beam crossing point.

The efficiency of photon identification was determined from both simulated events and a reference sample of photons coming from $e^+e^-\gamma$ and $\mu^+\mu^-\gamma$ events to be $(96.5 \pm 1.5)\%$.

8.4.2 Single excited neutrino production

The search for single-photon events has been restricted to the barrel part of the electromagnetic calorimeter (polar angles between 42° and 138°) in order to avoid a large background from radiative Bhabha events in which only the photon is detected. Ten events with a minimum photon energy of 7 GeV survive the selection cuts.

Background has been simulated using event generators for reactions $e^+e^- \to \nu\bar{\nu}\gamma$ [124], $e^+e^- \to e^+e^-\gamma$ [125] and $e^+e^- \to \gamma\gamma\gamma$ [109]. Events were processed through the standard ALEPH simulation and reconstruction programs, followed by the event selection described above. The expected number of background events from the three reactions is 12.4. The energy distribution of photons from the background is compared with the data in fig. 8.6 and a good agreement is observed. Above 17 GeV less than one background event is expected and no event is detected. This corresponds to an upper limit of three single excited neutrino events at 95% confidence level.

Single-photon events coming from the reaction $e^+e^- \to \nu^*\nu$ were generated according to the differential cross-section given in section 8.2 at several values of excited neutrino mass and at each beam energy. Initial state radiation is included in the generator; it modifies considerably the cross-section for excited neutrino masses close to m_Z. The overall acceptance for single ν^* events is 66% for large ν^* mass, m^*, mainly determined by the geometrical acceptance. The minimum energy cut at 17 GeV does not affect the acceptance for large m^* since the energy spectrum of photons from ν^* decay is flat and extends from $m^{*2}/2\sqrt{s}$ to $\sqrt{s}/2$ as is seen in fig. 8.6 for $m^* = 70\,\mathrm{GeV}/c^2$. At lower masses this cut decreases the acceptance down to 45% for m^* values close to zero.

The expected number of events for a given mass is calculated combining all energies and luminosities, and compared with the experimental upper limit of three events at 95% confidence level. We present our results in terms of the coupling $c_{Z\nu^*\nu}/\Lambda$ which is independent of any

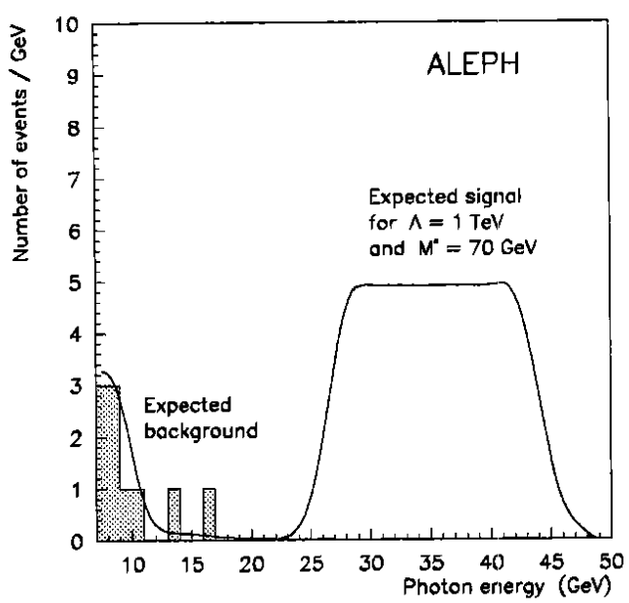

Figure 8.6: Distribution of photon energy in selected single photon events compared with expected contribution of residual background and predicted signal for the reaction $e^+e^- \to \nu^*\nu$.

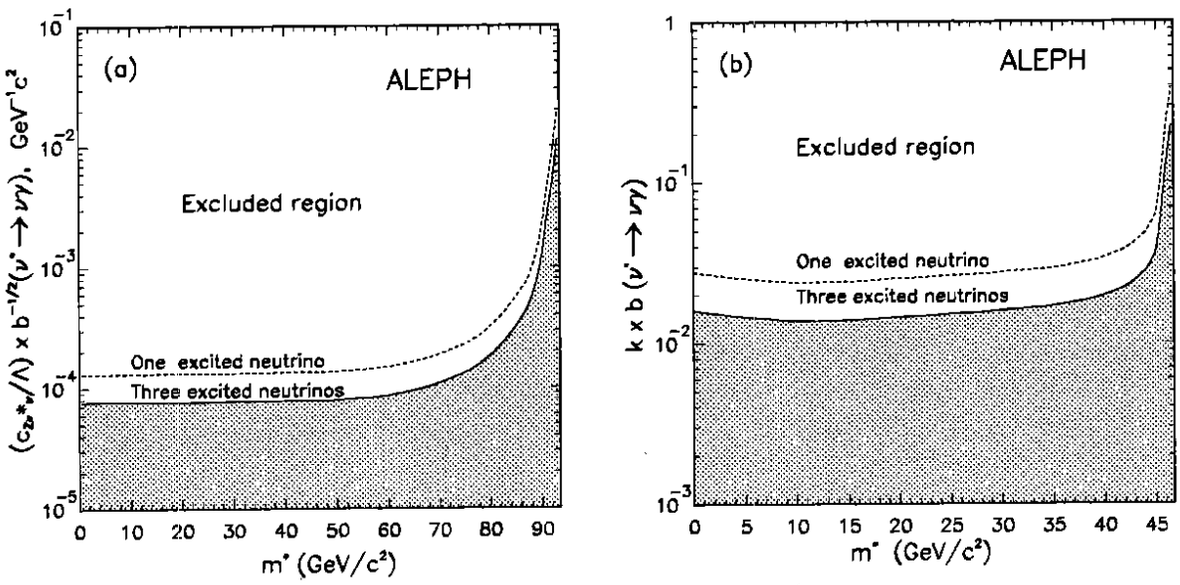

Figure 8.7: (a) Region excluded at 95% c.l. in the plane $(c_{Z\nu^*\nu}/\Lambda)B^{1/2}(\nu^* \to \nu\gamma)$ *vs* m^* extracted from the search for single ν^* production. (b) Region excluded at 95% c.l. in the plane $k \times B(\nu^* \to \nu\gamma)$ *vs* m^* extracted from the search for ν^* pair production.

assumption about f and f' (section 8.2). Since the branching ratio of ν^* decay into a photon and a neutrino, $B(\nu^* \to \nu\gamma)$, is unknown the predicted single-photon cross-section is proportional to $(c_{Z\nu^*\nu}/\Lambda)^2 B(\nu^* \to \nu\gamma)$. For each mass, an upper limit is derived for this quantity and fig. 8.7(a) shows the region excluded at 95% c.l. in the plane $(c_{Z\nu^*\nu}/\Lambda)B^{1/2}(\nu^* \to \nu\gamma)$ versus m^*. The limit curve is reduced by a factor $\sqrt{3}$ if we assume excited lepton universality for three mass-degenerate families. The one family limit is $B(Z \to \nu^*\nu) \times B(\nu^* \to \nu\gamma) < 2.7 \times 10^{-5}$ for low ν^* masses. These results improve previous limits published by ALEPH [126] and L3 [127].

8.4.3 Excited neutrino pair production

The production of an excited neutrino pair followed by radiative neutrino decays leads to a final state which is neither hadronic nor leptonic and is excluded by the Z lineshape measurement for branching ratios larger than 0.9%. A much better limit can be obtained from a direct search. Events with two photons having an energy > 7 GeV are used. The background of the QED reaction $e^+e^- \to \gamma\gamma$ is removed by requiring that the sum of the energies of the two photons be less than 45 GeV or that their acoplanarity be less than 179°. The cuts produce a negligible loss of efficiency for $\nu^*\overline{\nu}^*$ detection, except for a very light ν^* where the two photons tend to be aligned. The expected residual background is estimated using the $e^+e^- \to \gamma\gamma(\gamma)$ generator of ref. [109] and found to be 0.9 event. Experimentally, no two-photon event is left and thus the 95% c.l. limit for observing an excited neutrino pair production is three events.

The detection efficiency for the $\nu^*\bar{\nu}^*$ signal is determined by simulating the reaction kinematics and the detector response and applying the selection criteria. Initial state radiation is fully simulated. The models of $\nu^*\bar{\nu}^*$ production, discussed in section 8.1, predict a ν^* angular distribution of the form $1 + B\cos^2\theta$ with $0 < B < 1$ depending upon the ν^* mass and type of coupling. We have chosen the most pessimistic case $B = 1$. The ν^* decay is assumed to be isotropic. The detection efficiency varies from 40% for high ν^* masses to 24% in the worst case of $m^* = 1\,\mathrm{GeV}/c^2$.

An upper limit at 95% confidence level is deduced for the product of the branching ratios. A conservative limit for any ν^* mass is $B(Z \to \nu^*\overline{\nu}^*)B^2(\nu^* \to \nu\gamma) < 5 \times 10^{-5}$. To a large extent, this result is model independent and holds for the production of a pair of heavy neutral objects decaying into a photon and a light invisible particle. It excludes the existence of an excited neutrino having the standard model couplings and a mass up to $47\,\mathrm{GeV}/c^2$ (half of the highest LEP energy).

This limit can be interpreted in terms of a model which assumes that the $Z\nu^*\nu^*$ coupling is k times smaller than the standard model coupling for a massive Dirac-type neutrino. The expected number of events is calculated as a function of the factor k and compared to the experimental upper limit of three observed events. An upper limit for the quantity $k \times B(\nu^* \to \nu\gamma)$ is derived as a function of the ν^* mass. Fig. 8.7(b) shows the excluded region for one and three mass-degenerate excited neutrino families. If the ν^* decay is purely radiative, then the $Z\nu^*\nu^*$ coupling cannot exceed 3% of the standard model value up to ν^* masses close to $m_Z/2$. This limit is decreased by a factor $\sqrt{3}$ for three mass-degenerate families.

8.5 Search for Excited Quarks

Excited quarks with the same couplings as standard quarks and with deexcitations $q^* \to q + \gamma$ and $q^* \to q + g$ are expected in many composite models [91]. The branching ratios to the two channels are model dependent but in the absence of any special constraints the gluonic branching ratio has been estimated by Renard to be 92% [128]. The differential cross-section for the single production of excited quarks in combination with ordinary quarks of the same flavour is [129]

$$\frac{\mathrm{d}\sigma}{\mathrm{d}\Omega} = \frac{6\alpha^2 p^*\sqrt{s}}{m^{*2}}\left\{G^+\left[2EE^* + p^{*2}\sin^2\theta - 0.5(s - m^2 - m^{*2})\right] + G^- mm^*\right\}$$

where the asymmetry term is omitted and for the Z contribution only

$$G^\pm = \frac{(|a_e|^2 + |b_e|^2)(|a|^2 \pm |b|^2)}{|D_Z|^2}$$

with $D_Z = s - m_Z^2 + im_Z\Gamma_Z$ while a_e and b_e are the standard model Zee couplings and a and b are the Zq^*q couplings. Thus the effective strength parameter of the Zq^*q coupling is $\lambda_q^2 = (|a|^2 + |b|^2)/(|a_q|^2 + |b_q|^2)$.

8.5.1 The decay $q^* \to q + g$

Separate analyses were carried out to search for pair and single production. For each search three samples of events were subjected to the same analysis: *(i)* the ALEPH hadronic event sample of 185,000 events selected as described in [130], *(ii)* a Monte Carlo background sample of 265,000 events generated using the ALEPH hadronic event generator described in ref. [18], *(iii)* Monte Carlo signal samples generated using adapted versions of this hadronic event generator. For pair production around 1800 events were generated at q^* masses of 36 GeV/c^2, 40 GeV/c^2 and 44 GeV/c^2, $q^*\overline{q^*}$ generation being followed by parton showering then the decay $q^* \to q + g$, each decay being followed by new, separate parton showers. For single production about 1500 events were generated at q^* masses of 40 GeV/c^2 and 70 GeV/c^2, q^*q generation being followed by the decay $q^* \to q + g$ and then parton showering from each quark and gluon.

All Monte Carlo events were subject to full detector simulation and reconstructed in the same way as the data. The ALEPH energy flow algorithms (section 3.4) were used and all subsequent analysis conducted using the energy flow objects, both tracks and neutral particles. The detection efficiency at intermediate masses was obtained by interpolation.

The $q^*\overline{q^*}$ analysis was carried out as follows. Events were discarded if they had aplanarity less than 0.02 or thrust greater than 0.875. The remaining events were forced into a 4-jet configuration using the Lund cluster algorithm. Any event in which a jet had fewer than three charged tracks was rejected. The jet energies were rescaled using energy and momentum conservation and the dijet invariant mass M_{ij} was computed for all combinations of jet pairs from the four jets. Motivated by the search for properties associated with high invariant masses and symmetry between the two q^* candidates, the following event configuration variables were calculated and used: *(i)* the dijet combination giving the lowest difference between the two jet-pair invariant masses, ($|M_{ij} - M_{kl}|$), was chosen as generating the q^* pair and was required to be less than 15 GeV/c^2; *(ii)* the opening angles θ_1^{op} and θ_2^{op}, defined as the angles between the two jets forming each q^* candidate were required to satisfy $|\theta_1^{op} - \theta_2^{op}| < 45°$; *(iii)* the decay angles θ_1^d and θ_2^d, defined as the acute angles measured in the rest frame of the q^* between the directions of each q^* candidate and the back-to-back jet pair, had to satisfy $\cos\theta_1^d \cos\theta_2^d < 0.25$. The efficiency was calculated at 2 GeV/c^2 mass intervals between 30 and 45 GeV/c^2 and varies smoothly from 28% to 42% over this mass range. The variation with quark flavour is small but has been taken into account when setting limits.

The q^*q analysis was carried out as follows. Events were discarded from all three samples if they had thrust greater than 0.925. Remaining events were forced into a 3-jet configuration using the Lund cluster algorithm. Events with three jets were discarded if the lowest energy jet did not contain a charged particle or if either of the other two jets did not contain at least three charged particles. From the data and background Monte Carlo samples described above 63,216 and 84,210 events respectively survived these cuts. The efficiency for the signal Monte Carlo is around 90% for masses up to 80 GeV/c^2 then falls rapidly to reach 20% by 90 GeV/c^2. The jets were projected onto the plane defined by the thrust and major axes (the event plane) and then rescaled using energy and momentum conservation. The dijet invariant mass M_{kl} was computed for all selections of jet pairs from the three jets.

Cross-sections were calculated for pair production of excited up-type quarks at intervals in the mass range 30–46 GeV/c^2 at each of our energies using the distribution given in section 8.1. Similar cross-sections were calculated for single excited quarks in the range 40 to 90 GeV/c^2 using the formula given in section 8.5.

Fits were made to two dimensional distributions for the two channels—for $q^*\overline{q^*}$ these were $M_{ij} - M_{kl}$ *vs* $M_{ij} + M_{kl}$ and for q^*q the lowest and next lowest M_{ij} values (two entries per event) *vs* the corresponding $\cos\theta^d$. Distributions were fitted using a χ^2 fitting procedure with $\chi^2 = \Sigma_i[D_i - f_1 B_i - f_2 S_i]^2/\sigma_i^2$ where D_i, B_i and S_i are the number of events in bin i in the

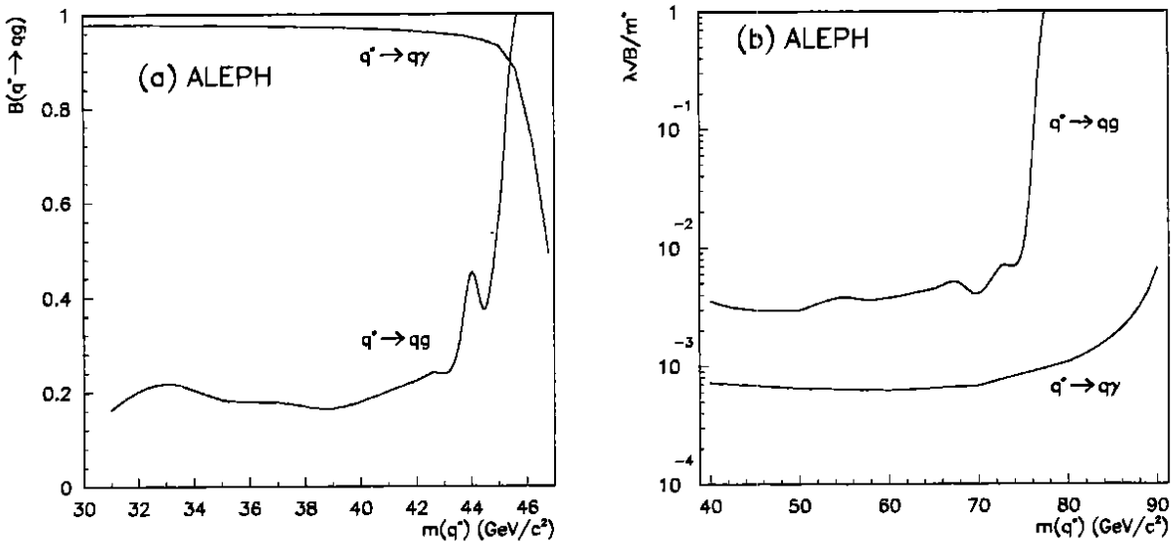

Figure 8.8: (a) Branching ratio limits as a function of q* mass from pair production and (b) limits on $\lambda_q\sqrt{B}/m^*$ as a function of q* mass for $Z \to q^*q$. The two curves give the limits for $q^* \to qg$ and $q^* \to q\gamma$ for a single up-type q*; in (a) the scale for $B(q^* \to q\gamma)$ is $1 - B(q^* \to qg)$.

data, smoothed background Monte Carlo and signal Monte Carlo respectively, and σ_i^2 is the variance; f_1 and f_2 are the fitted fractions of background Monte Carlo and signal. Thus 95% c.l. limits were set on the branching ratio, B, for $q^* \to q+g$ in $q^*\overline{q^*}$ production (fig. 8.8(a)) and $\lambda_q\sqrt{B}/m^*$ in single production (fig. 8.8(b)). These plots give the limits for the most conservative assumption, namely the existence of a single excited u-type quark. Thus for a branching ratio $B(q^* \to q+g)$ of 100% any q* is excluded at 95% c.l. up to 45 GeV/c^2. The coupling limit for single production is improved by factors of approximately 1.15, 1.5 and 2.4 for a single excited d-type quark, one generation of q* and five excited quarks respectively.

8.5.2 The decay $q^* \to q+\gamma$

The background process to this channel is radiative $q\overline{q}$ production, $Z \to q\overline{q}\gamma$, with either initial-state radiation (ISR) or final-state radiation (FSR). Studies of this process have been published by both ALEPH [131] and OPAL [132,133]. The photons from both ISR and FSR tend to be at small angles with respect to their parent particles and to have low energy, thus differing markedly from the expectation for excited quark decay. Accordingly, this background can be reduced with cuts on photon isolation and energy without a large effect on the signal efficiency. The search described here is for pair-production with both q*s decaying to $q\gamma$ and both photons seen, and single-production with the q* again decaying to $q\gamma$.

Background Monte Carlo was produced using version 7.3 of the Lund generator with an initial cut to ensure the presence of a final-state radiated photon of 3 GeV or more. This sample corresponds to almost two million hadronic decays of the Z. Signal Monte Carlo events were generated using modified versions of LUND 7.3 in which the q* decays by photon emission and the quarks are allowed to shower and fragment within the Lund scheme. Events were fully simulated and reconstructed for $q^*\overline{q^*}$ at $m_{q^*} = 36$, 40 and 44 GeV/c^2, and for q*q at $m_{q^*} = 40$, 50, 60, 70 and 80 GeV/c^2.

Hadronic events were defined in a very simple manner by requiring eight or more good tracks. No momentum cut was imposed, nor any cuts on thrust or total visible energy. Events

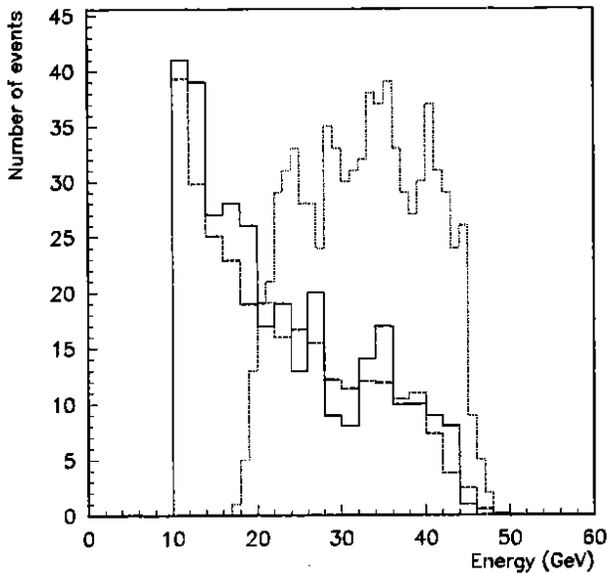

Figure 8.9: Isolated photon energy spectrum. The solid line is the data, the dashed line the best fit of the background to the data and the dotted line is the unnormalized Monte Carlo prediction for a q* of mass 60 GeV/c^2.

were selected with photons above 10 GeV and no other ECAL cluster or good track with an energy of 0.5 GeV or more within 30°. Applying this selection yielded 316 events. None has two photons satisfying the isolation and identification criteria. The energy spectrum of the photons in these events is shown in fig. 8.9 together with the expectation for a singly-produced q* with a mass of 60 GeV/c^2.

Since no events are observed in the two-photon final state a signal of more than three events is excluded at 95% c.l. The production cross-section is calculated from the standard model formula (section 8.1) for $Z \to f\bar{f}$ with heavy fermions. The efficiency as measured by Monte Carlo is $\sim$ 50% between $m_{q^*} = 36$ and 44 GeV/c^2. The branching ratio limits are shown in fig. 8.8(a). From these curves it is seen that whatever the q* branching ratio to the two channels its mass limit is 45 GeV/c^2.

To place a limit on $\lambda_q\sqrt{B/m^*}$ for single q* production the photon energy distribution is used. The distribution is fitted with a linear combination of the background from LUND 7.3 and the signal given by the q* Monte Carlo after simulation and reconstruction at masses of 40, 50, 60, 70, and 80 GeV/c^2. The limit obtained is shown in fig. 8.8(b) for a single excited u-type quark. This limit is again improved for all other assumptions about the number and type of excited quarks.

8.5.3 Summary

By searching for q* decay *via* both gluon and photon emission the present analysis excludes the existence of excited quarks up to a mass of 45 GeV/c^2 and limits on $\lambda_q\sqrt{B/m^*}$ have been obtained for both $q\gamma$ and qg decays of a q* of higher mass. These limits extend those obtained previously. In particular, an earlier mass limit for pair produced q* of about 22 GeV/c^2 has been published by CELLO [134] derived from the gluon decay channel assuming a branching ratio of at least 90%. A mass limit of 39 GeV/c^2 was derived by the same collaboration from the search for single production [134] using both decay channels but assuming unit coupling strength for $\gamma q^* q$. The OPAL collaboration at LEP has also derived a limit for single production from the photon channel only [132].

8.6 Searches for Composite Z Boson Effects

If the Z boson is composite then it will have additional couplings *via* its constituents—to the photon from electric charge and to the gluon from colour charge. Thus $Z\gamma\gamma\gamma$ and $Zgg\gamma$ couplings may appear [135]. Predicted rates for these processes are model dependent but are typically in the range 10^{-2}–10^{-5} [91].

8.6.1 The three gamma final state

The standard model predicts a branching ratio for the decay $Z \to \gamma\gamma\gamma$ of 1.0×10^{-9} [136]. The background process is radiative e^+e^- annihilation into two photons, $e^+e^- \to \gamma\gamma\gamma$, a pure QED process. The energy and $\cos\theta$ spectra for this background differ markedly from those expected for the signal thereby making this an ideal channel in which to search for a composite Z.

The event selection was based on ECAL clusters as follows. Events were required to have no good tracks, at least two ECAL clusters with energy ≥ 15 GeV and a third ECAL cluster with energy ≥ 0.2 GeV; the three highest energy ECAL clusters had to be in separate modules at least 10° apart. A small number of cosmic ray events was removed by demanding energy balance in the event to within 35%. After applying these cuts to the data 13 events were left.

Two Monte Carlo generators were used, one for the QED background and one for the compositeness signal. The QED background was calculated using a generator for $e^+e^- \to \gamma\gamma\gamma$ which produces unweighted events [109]. These events were passed through the ALEPH simulation and reconstruction programs and then subjected to the analysis cuts. About 400 events survived the full selection. The generator was run only at the Z peak and the predicted rate obtained by appropriate scaling of the cross-section and weighting with the luminosity at each scan point.

The compositeness signal was generated using a phase space generator for multiphoton events [137] and weighting them using a contact term matrix element [91]. In this model the matrix element depends only on the photon energies not their $\cos\theta$ values, and favours three photons of equal energy over configurations with two hard photons and one soft photon. The total cross-section is controlled by a compositeness scale factor, Λ and is proportional to Λ^{-8}.

Fig. 8.10 shows the energy and $|\cos\theta|$ distributions for the data, the background and the compositeness Monte Carlo. The background is normalized to the total integrated luminosity and is therefore an absolute prediction while the compositeness signal is normalized to the total number of events in the data, purely for the purposes of comparison. As can be clearly seen, the data favour the background. The $\cos\theta$ spectrum is forward peaked and the energy spectrum shows a peak at small energy, typical of bremsstrahlung processes. The compositeness signal is flat in $\cos\theta$ and has no peak at low photon energies.

The cuts as defined above are not optimized for the purpose of producing a limit on the presence of a signal. To arrive at the best possible limit on the compositeness scale, Λ, the signal and background Monte Carlos alone were used to find the $\cos\theta$ and energy cuts which gave maximum sensitivity to the compositeness signal. This procedure gave optimised cuts at $\cos\theta_{max} = 0.92$ and $E_{min} = 12.2$ GeV. The energy cut is quite hard, but is very effective against the QED background whilst not cutting much of the signal. The efficiency for the compositeness signal is 62%.

Fig. 8.11 shows the scatter plot of energy *vs* $|\cos\theta|$ for the lowest energy photon in each event; the optimised cuts are marked on the plot. The predicted QED background for these cuts is 2.5 events while two are actually observed in the data. This corresponds to a limit on the signal of 4.6 events, and a limit of $\Lambda \geq 24.4$ GeV for the contact term model of Renard, or, expressed as a branching ratio, $B(Z \to \gamma\gamma\gamma) \leq 1.9 \times 10^{-5}$. Limits on this branching ratio have also been published by the other LEP experiments [110,111,112].

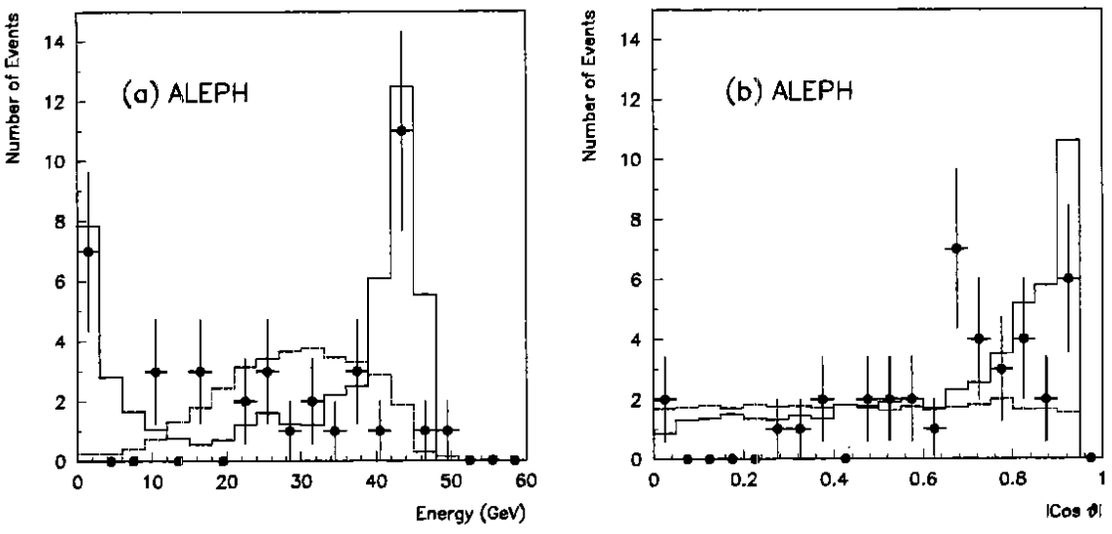

Figure 8.10: Photon distributions in $e^+e^- \to \gamma\gamma\gamma$ (three entries per event): (a) energy; (b) $|\cos\theta|$. Points–data, full line–QED, dashed line–composite model described in the text.

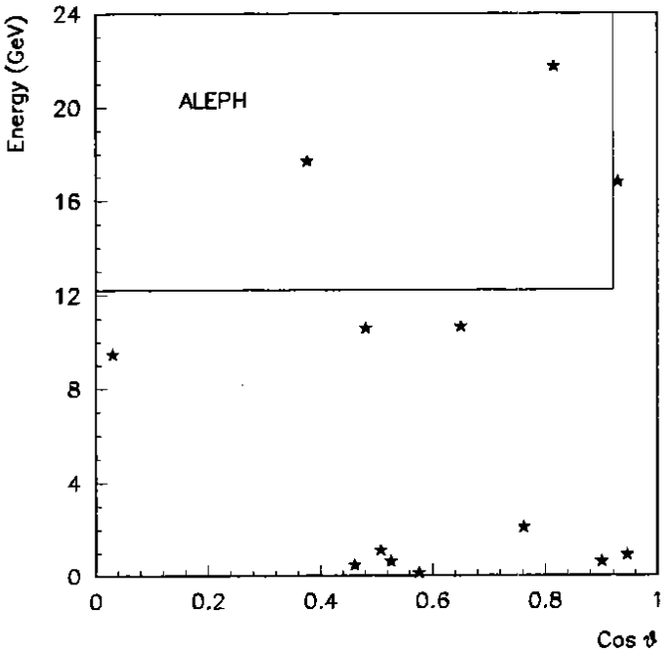

Figure 8.11: Photon energy *vs* $|\cos\theta|$ for the lowest energy photon in each event of the data. The two lines show the optimum values of $\cos\theta_{max}$ and E_{min} for determining the best limit on the compositeness scale.

8.6.2 The gluon gluon gamma final state

The data sample from the excited quark search in the photon decay channel (section 8.5.2) has also been used to put a limit on the branching ratio for the decay $Z \rightarrow gg\gamma$. The matrix element used to generate Monte Carlo events for this decay was the same as for the $\gamma\gamma\gamma$ study described in the last section. The efficiency for the observation of this process with the cuts used is 77%. The observed energy spectrum (fig. 8.9) was fitted to a linear combination of the predicted spectra from the Lund generator and the "composite Z" spectrum to give a branching ratio limit for $Z \rightarrow gg\gamma$ of 2.5×10^{-4}.

The OPAL collaboration has previously published a limit on this decay mode [132].

8.7 Summary

No evidence for compositeness has been found in the searches described in this section. The existence of excited charged leptons has been excluded for masses up to $46\,\mathrm{GeV}/c^2$ and for excited quarks up to $45\,\mathrm{GeV}/c^2$. Excited neutrinos decaying by photon emission have been excluded to $47\,\mathrm{GeV}/c^2$. Limits have been set on the couplings for the single production of all of these excited states. No evidence has been found for enhanced four-boson couplings predicted in composite models.

9 Leptoquarks

Leptoquarks are colour-triplet objects having a Yukawa-type coupling to a lepton-quark pair. They appear naturally in many theoretical schemes beyond the standard model, such as grand unifying models [138,139], composite models [140,141,142], technicolour [143,144,145] and E6 models inspired by superstring theories [146,147,148]. Their existence could be revealed in rare meson decays *via* flavour-changing neutral currents, in rare lepton decays, and in e^+e^- experiments in direct pair-production and in modifications to the cross-section and the forward-backward asymmetry of $q\bar{q}$ produced by the leptoquark exchanged t-channel diagrams [149,150].

Prior to the LEP experiments, mass limits for leptoquarks have been given by JADE at the PETRA e^+e^- collider [151], AMY at the TRISTAN e^+e^- collider [152] and UA1 at the CERN $\bar{p}p$ collider [153].

Although leptoquarks predicted by different models have different quantum numbers, most of them decay into a lepton-quark pair. They can be pair-produced in e^+e^- collisions and identified by their decays which produce the same distinctive final state topologies in many models. For the purpose of evaluating mass limits we have chosen the model giving the most conservative production cross-section, the superstring-inspired E_6 models [147], containing colour triplet, SU(2) singlet, spin 0, charge -1/3 particles, D_0 and $\overline{D_0^c}$ and their supersymmetric partners $D_{1/2}$.

Pair production arises from s-channel γ, Z (and in E_6 Z′) exchange and from t-channel u quark exchange. In the region of the Z peak the dominant contribution is from s-channel Z exchange and the cross-section is given by:

$$\frac{\mathrm{d}\sigma}{\mathrm{d}\cos\theta} = \frac{3\pi\alpha^2}{8s}\beta^3 \sin^2\theta \sum_{j=L,R} |C_j|^2 \qquad (9.1)$$

where

$$C_j = \sum_V g_V^2 Q_V(D) \frac{s}{s - m_V^2 + i m_V \Gamma_V} Q_V^j(e),$$

β is the centre-of-mass velocity of the D_0, θ is the production angle with respect to the beam direction, and g_V, $Q_V(D)$ and $Q_V^{L,R}(e)$ characterize the couplings of the D_0 and lepton to the neutral vector bosons [147].

In the superstring model family number is conserved and three leptoquarks are expected, each decaying into a lepton-quark pair of its own generation:

$$\begin{aligned} D_0 &\rightarrow u_R + \ell_R \\ \overline{D}_0^c &\rightarrow u_L + \ell_L \\ &\rightarrow d_L + \nu_{\ell L} \end{aligned}$$

with the up quark always coupling to the charged lepton and the down quark to the neutrino. The decay widths are

$$\Gamma(D_0 \rightarrow u\ell) = \lambda_L'^2 m_D/16\pi$$
$$\Gamma(\overline{D}_0^c \rightarrow q\ell) = \lambda_L^2 m_D/16\pi$$

where the unknown coupling constants λ_L and λ_L' are expressed in terms of their ratio to the electromagnetic coupling constant.

Depending upon whether the leptoquark decay goes through the charged lepton or neutrino mode there are three final state topologies:

- two jets with two opposite charged isolated leptons ($e^+e^- \rightarrow q\ell + \overline{q}\overline{\ell}$);
- two jets with an isolated lepton and missing energy ($e^+e^- \rightarrow q\ell + \overline{q}\overline{\nu}$);
- two jets with missing energy and missing transverse momentum ($e^+e^- \rightarrow q\nu + \overline{q}\overline{\nu}$).

In the analysis of the first two topologies the third generation has not been studied, since the charged lepton always couples to the top quark whose mass is greater than the available energy.

9.1 Event Selection

The analysis considers first and second generation leptoquarks and thus relies on the identification of electrons and muons. For electron identification loose cuts on the ECAL estimators were used (section 3.3.1), applying no cut on R_L and requiring $R_T > -5$. No upper limit was imposed on the latter in order not to reject electrons which have emitted hard bremsstrahlung photons or which overlap with other calorimetric energy deposits. The standard muon selection criteria were used (section 3.3.2). For final states with missing energy an energy flow algorithm was used (section 3.4).

In order to develop methods to separate leptoquark signal events from known backgrounds and to measure the signal detection efficiency, a Monte Carlo program was written to produce pairs of leptoquarks according to equation 9.1, including the simulation of initial state radiation. Each leptoquark was made to decay into a lepton and a quark and the quarks were fragmented using the Lund generator with the Peterson fragmentation function [154]. The generated events were processed through the ALEPH detector simulation and the standard reconstruction program. Backgrounds were estimated from a Monte Carlo data sample of 172,000 hadronic events generated using the LUND 6.3 code.

9.1.1 Two jets and two isolated leptons

Two opposite charged isolated leptons with hadrons form a clear signature for leptoquark pair production, particularly at large D_0 masses where the leptons are predominantly produced at large transverse momentum. At lower masses the efficiency falls off as the leptons begin to merge with the jet particles. Based on a study of the leptoquark Monte Carlo events the following cuts were applied to the data. An event must contain more than four good tracks including two oppositely charged lepton candidates of the same generation, identified according to the criteria given above; if there was more than one candidate of either charge, only the one with

the highest momentum was taken. The momentum of each lepton candidate had to exceed 7 GeV/c and the isolation angle (defined as the angle between the lepton and the closest hadron with momentum greater than 800 MeV/c) had to be greater than 25°. The invariant mass of the two leptons had to exceed 3 GeV/c^2.

One e^+e^- event and no $\mu^+\mu^-$ events passed the cuts while one $\mu^+\mu^-$ and no e^+e^- candidates were found in the QCD Monte Carlo. The efficiencies for the selection of lepton pair events are shown as a function of mass in fig. 9.1(a).

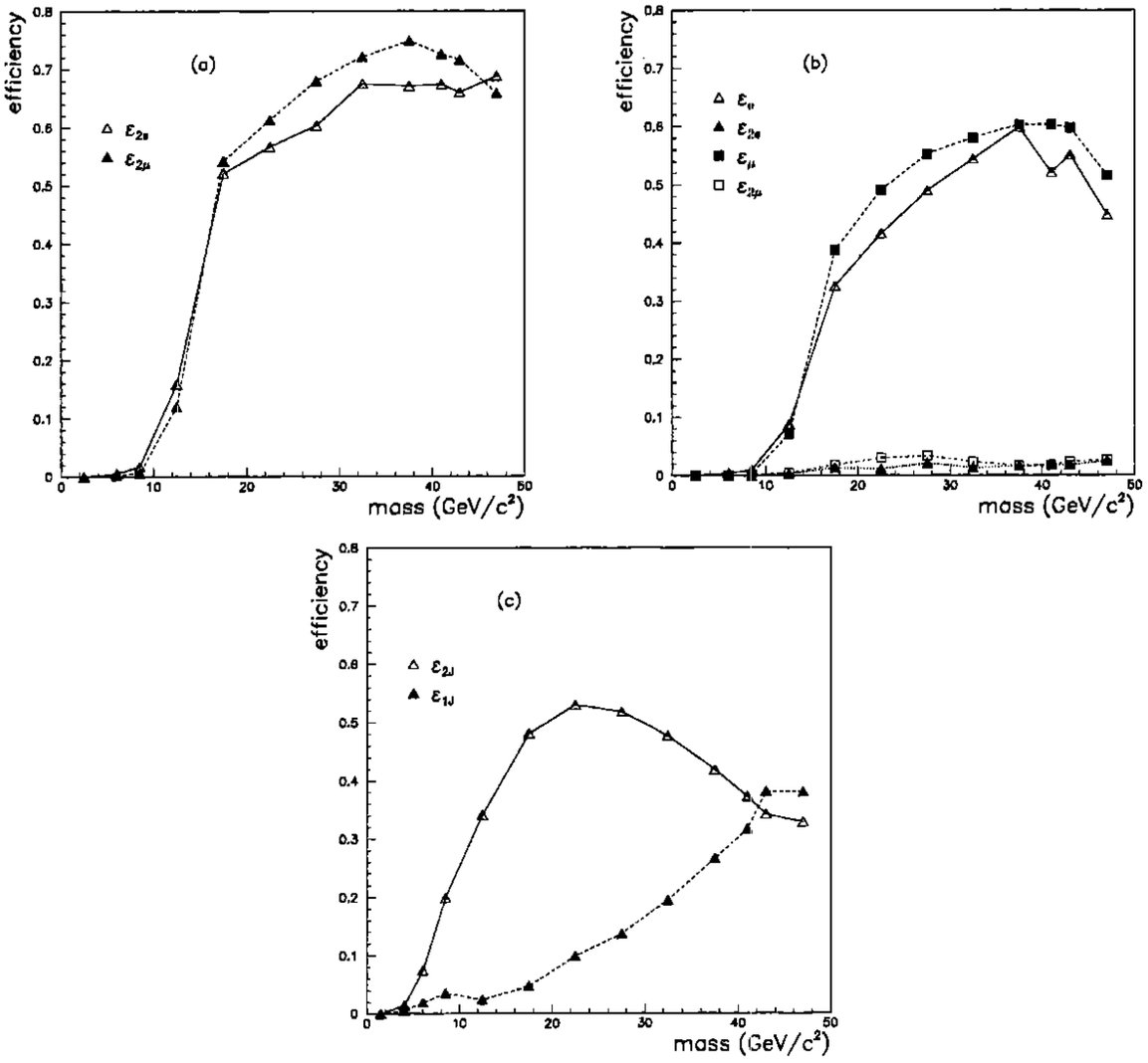

Figure 9.1: Detection efficiencies as a function of leptoquark mass for (a) the lepton pair selection (b) the single charged lepton selection and (c) the missing energy selection.

9.1.2 Two jets with an isolated lepton and missing energy

For this analysis the energy flow algorithm was used to calculate the physical quantities of the unobserved neutrino. In addition to the lepton from the leptoquark decay the event could contain one or more charged leptons originating from quark semileptonic decays or from other sources such as conversions and pion or kaon decays. If an event had only one charged lepton then the following cuts were applied. The momentum of the lepton must be greater than 7 GeV/c, the transverse momentum of the lepton with respect to the thrust axis had to be greater than 4 GeV/c and the isolation angle of the lepton had to be greater than 26°.

If an event had more than one charged lepton then these were ordered in decreasing momentum. If the first two had opposite charge then the highest momentum lepton was required to pass the above cuts and the second lepton to have a momentum less than 7 GeV/c (if its momentum were greater than 7 GeV/c it would have been classified as a 2 lepton + 2 jet event and treated according to the criteria of the previous topology). If the charge of the second lepton was the same as that of the first then only the cuts of the previous paragraph were applied to the first lepton.

In all cases the cuts applied to the missing neutrino were as follows. Its calculated momentum had to be greater than 10 GeV/c, its transverse momentum with respect to the thrust axis had to be greater than 7 GeV/c and its isolation angle had to be greater than 10°. The missing energy of the event had to be between 10 and 50 GeV and the angle between the seen and missing leptons had to be less than 150°.

When these cuts were applied to the data one muon candidate and two electron candidates survived. From the analysis of the QCD Monte Carlo data, we expect one muon and five electron candidates. To determine the selection efficiencies it is necessary to consider not only the channel where one leptoquark decays into a charged lepton and the other into a neutrino, but also the case where both leptoquarks decay into charged leptons in which one lepton is missing (mainly because of inefficiencies in lepton identification and detector acceptance). To find the effect of feedthrough from the two charged lepton channel, the analysis was performed for each leptoquark mass hypothesis on the two charged lepton Monte Carlo events which failed to pass the criteria for the topology with two charged leptons and two jets. The selection efficiencies are shown in fig. 9.1(b), where ϵ_ℓ represents the efficiency for finding the genuine single charged lepton events and $\epsilon_{2\ell}$ the efficiency for two charged lepton events.

9.1.3 Two acoplanar jets with missing energy

Events with no identified charged leptons (subject to the isolation cuts described above) were divided into two hemispheres by a plane perpendicular to the thrust axis, thus defining two "jets". If the sum of the energies in either hemisphere was below 2 GeV the event was classified as a monojet (the particles in the opposite hemisphere constituting the "monojet"). If the energy in each hemisphere was greater than 2 GeV the event was classified as a 2-jet candidate and subjected to a complementary analysis to the former case. In this scheme low mass leptoquark events where the jets are produced at low transverse momentum were mainly classified as two-jet candidates. At high leptoquark masses the quarks are emitted at large transverse momentum with the jets often falling in the same hemisphere, and a larger proportion of events was assigned to the monojet category. The monojet and 2-jet analyses employ a number of cuts (sections 5.3.4 and 5.3.5) designed to eliminate background from hadronic, $\tau^+\tau^-$ and two-photon events.

The efficiencies for the selection of the monojet (ϵ_{1J}) and two-jet events (ϵ_{2J}), determined from the first and second generation leptoquark Monte Carlo for various leptoquark masses, are shown in fig. 9.1(c). The overall efficiency is obtained from the sum of ϵ_{1J} and ϵ_{2J} since the analyses are strictly complementary. The same analysis has been applied to third generation leptoquarks where neutrinos couple to b quarks and the efficiency $\epsilon_{1J} + \epsilon_{1J}$ is found to be 70.1% at the highest mass.

9.2 Determination of the Leptoquark Branching Ratio Limits

Given the total luminosity, the signal detection efficiencies and the leptoquark production cross-sections, and assuming that the only possible decay channels are $D_0 \to q\ell$ and $D_0 \to q\nu$, we compute for each leptoquark mass hypothesis the branching ratios corresponding to the Poisson 95% c.l. limit for the number of observed signal events.

The branching ratio limits are displayed as contour plots in the branching ratio-mass plane in fig. 9.2. In general there are two solutions for each mass value due to the quadratic nature of the equations. Both solutions are given for the single charged lepton channels if they lie in the physical domain, while for the other channels only one physical solution exists. The data exclude the regions $M(\mathrm{D_0})$ from $\sim$ 4 to 44 GeV/c^2 and $\sim$ 6 to 44 GeV/c^2 for first and second generation leptoquarks respectively. Third generation leptoquarks are excluded at 95% c.l. up to 45 GeV/c^2 assuming no mixing of this generation.

Similar limits have been published by the other LEP experiments [155,156,157]. The UA2 experiment has recently set a mass limit for first generation leptoquarks as a function of the branching ratio to qe which is superior to the limits from the LEP experiments for values of this branching ratio greater than 12% [158].

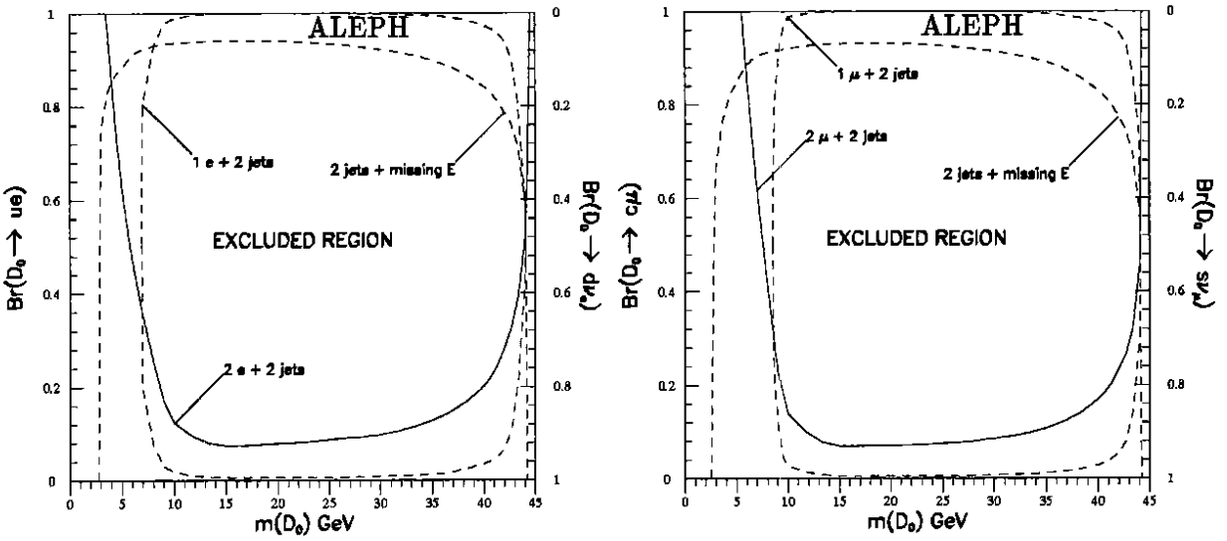

Figure 9.2: The 95% c.l. contours in the plane of mass and branching ratio for first and second generation leptoquarks.

10 New Weakly Interacting Particles

In section 5 the searches for a standard model Higgs boson were described. Here we present the results of a more general search for a new particle which couples to the Z but with unknown production and decay coupling strengths. However, such a particle has a *maximum stability* since it can decay by the same mechanism as it is produced, coupling to two virtual Z bosons (fig. 10.1). Within the framework of the standard model the $\mathrm{X^0}$ can also decay to two W bosons which further reduces the lifetime. For example, if the $\mathrm{X^0}$ has third component of weak isospin, I_3 greater than $\frac{1}{2}$, then such a decay is required and is also studied. The analysis procedure considers the two possibilities that the $\mathrm{X^0}$ decays within the detector or that it escapes before decaying.

The decay width for $\mathrm{X^0} \rightarrow \mathrm{Z^*Z^*}$ has been given by Kleiss [159]:

$$\Gamma_{\mathrm{X^0}} = \frac{1}{9216\pi^5}\frac{61}{504}\frac{m_{\mathrm{X}}^7 g^2}{m_{\mathrm{Z}}^8}\sum_{f_1,f_2} C_{f_1}C_{f_2}(v_{f_1}^2+a_{f_1}^2)(v_{f_2}^2+a_{f_2}^2) \qquad (10.1)$$

where g = decay constant $\times$ m_{Z} and $v_{f_{1,2}}$ and $a_{f_{1,2}}$ are the vector and axial vector couplings respectively of the virtual Z bosons to the fermions, $f_{1,2}$ and $C_{f_{1,2}} = 1$ or 3 for leptons or quarks

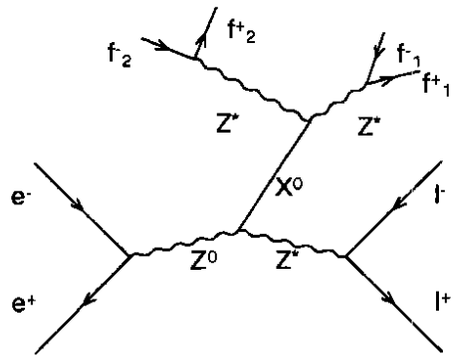

Figure 10.1: Feynman diagram for the process $e^+e^- \to \ell^+\ell^- X^0$

respectively. The value of the ZZ^*X^0 coupling which is excluded is then a function of luminosity, efficiency and the Z^* decay channel considered.

The reaction $e^+e^- \to Z^*X^0$, where $Z^* \to \ell^+\ell^-$ and the X^0 escapes from the detector before decaying, produces a pair of acollinear leptons and no isolated energy in the calorimeters. The search for such events has already been described in section 5.3.1 with no events surviving the cuts.

Monte Carlo event samples a factor 2.6 times larger than the data were generated for the following background processes:

1. $e^+e^- \to e^+e^-(\geq 1\gamma)$	2. $e^+e^- \to \mu^+\mu^-(\geq 1\gamma)$	3. $e^+e^- \to \tau^+\tau^-(\geq 0\gamma)$
4. $e^+e^- \to (e^+e^-)e^+e^-$	5. $e^+e^- \to (e^+e^-)\mu^+\mu^-$	6. $e^+e^- \to (e^+e^-)\tau^+\tau^-$.

A total of five Monte Carlo events passed the cuts giving a predicted background of 1.9 events from these processes after normalization.

Monte Carlo studies of the signal process $e^+e^- \to \ell^+\ell^- X^0$ for a completely stable X^0 show that the efficiency is almost constant as a function of m_X at about 25%. Once the X^0 has an appreciable probability to decay inside the detector the efficiency for detecting it with this method decreases exponentially with a mean distance $\bar{x}$ given by

$$\bar{x} = \frac{c\tau_{X^0}}{m_X}\bar{p},$$

where $\bar{p}$ is the average momentum of an X^0 whose mass is m_X.

The quantity $R = B(Z \to X^0\ell^+\ell^-)/B(Z \to \ell^+\ell^-)$ is related to the production coupling ZZ^*X^0. The 95% c.l. limit on R as a function of m_X, taking into account the reduction in detection efficiency as a function of lifetime, τ_{X^0}, is shown in fig. 10.2(a), curve B. A maximally stable X^0 is excluded up to $8.0\,\mathrm{GeV}/c^2$ for a value of $R \geq 7.2 \times 10^{-4}$. At this mass, the curve approaches an asymptotic value, corresponding to the production coupling which is excluded when the two virtual Zs each decay to two neutrinos and are unobserved in the detector. The sharp rise at $8.0\,\mathrm{GeV}/c^2$ is due to two effects—as the mass increases the lifetime decreases, but then the value of the coupling which can be excluded increases. These two factors multiply to create a very fast variation of the limit.

The results of the Higgs search in the channel $h \to q\bar{q}$, $Z^* \to \nu\bar{\nu}$ (section 5.3.5) can be used to set a limit on R by assuming that the X^0 decays to hadrons as would a Higgs particle. The resulting 95% c.l. limit is shown as a function of the X^0 mass in figure 10.2, curve A. Thus curve B corresponds to the case where X^0 decays inside the detector, while curve A is for the case where it escapes the detector without being detected. The crossover point of the two analyses clearly depends on the lifetime of the X^0, since, as the lifetime decreases and more events decay inside the detector they cannot be excluded by the acoplanar pairs search but are detected by the two jets + two leptons analysis. To illustrate this point, fig. 10.2(b) shows

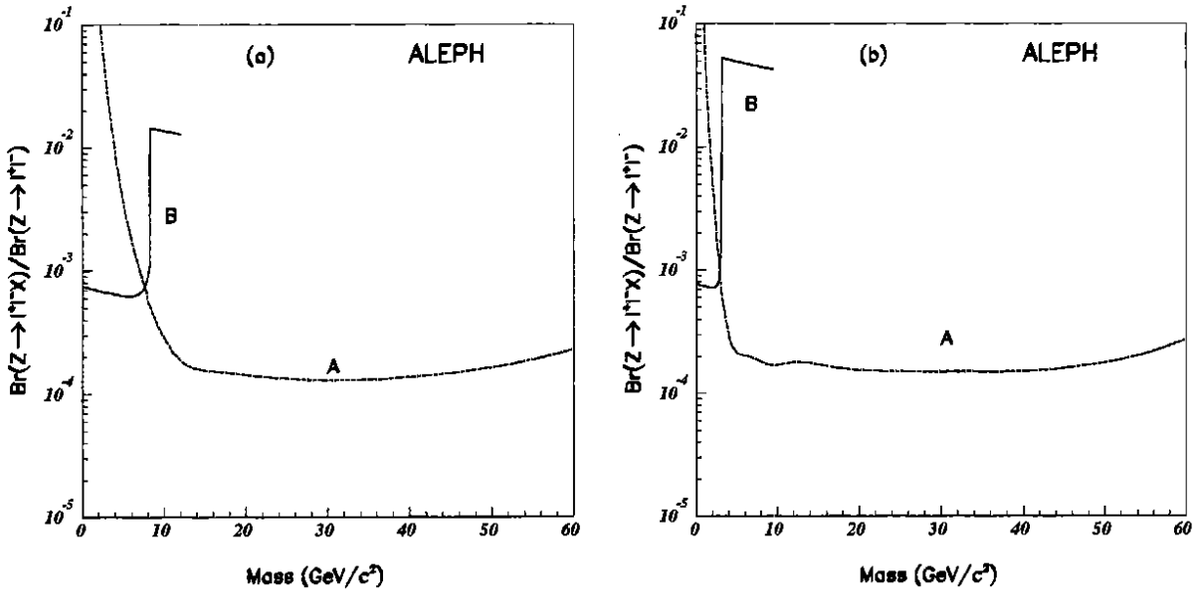

Figure 10.2: Branching ratio limits for X^0 decay: (a) maximally stable X^0, (b) additional coupling to W^*W^*. In both figures curve B is derived from the acoplanar pairs search and curve A from the two jets + two leptons search.

the limits when the X^0 is in addition allowed to decay to two W bosons. While the crossover point between the two analyses is shifted to 3 GeV/c^2 in m_X the limit is unchanged. The region excluded has $R \geq 7.2 \times 10^{-4}$ for all masses, and in the high mass region an even lower value of R is excluded.

In summary, any new particle whose sole decay mode is to two virtual gauge bosons and whose coupling to the Z is such that $R \geq 7.2 \times 10^{-4}$ has been excluded up to a mass of 60 GeV/c^2. Although this analysis has been performed for a scalar X^0, it is also valid if X^0 is not a scalar, provided that its decay characteristics do not preclude its observation in the above analysis. This result improves on an earlier limit published by ALEPH [160].

11 Rare Decay Modes of the Z

Many "rare" decay modes of the Z are sensitive to physics beyond the standard model [161] and some have already been discussed in section 8.6 in the context of compositeness. In this section others are discussed which are currently expected to have branching ratios $\sim 10^{-10}$ or less, or to be absolutely forbidden. Examples of the former are decays of the Z into a pseudoscalar plus a vector boson. Examples of the latter are the lepton flavour violating decays such as $Z \to e\mu$, $e\tau$ and $\mu\tau$. Searches for these processes are described here and branching ratio limits given.

11.1 Z Decays to Pseudoscalar plus Vector Particles

Branching ratio estimates for these decays have been estimated by several authors. Arnellos *et al.* [162] made the first calculations in 1982, parametrizing strong interaction effects in terms of hadronic form factors. As an example they obtained $B(Z \to \pi^0\gamma) = 3 \times 10^{-11}$. Manohar [163], using an operator product expansion, calculated $B(Z \to \pi^{\pm}W) = 3 \times 10^{-10}$ and $B(Z \to \pi^0\gamma) \sim 4 \times 10^{-11}$. Branching ratios in this range are too small by many orders of magnitude to allow detection at LEP. However, interest was stimulated by papers by Jacob and Wu [164] and Ghosh and Chatterjee [165] who claimed that the branching ratios of these channels may by greatly enhanced to values $\sim 10^{-3}$ by suppression of the form factor effect in moving from the photon

to the Z mass. Later West [166] refuted this argument showing that the branching ratio for $B(Z \to \pi^0\gamma)$ must be less than 10^{-4} and probably less than 5×10^{-6}. Chatterjee and Ghosh [167] then recalculated the rate and again found a lower rate compared to their earlier estimate. The present sensitivity of the LEP experiments is now $\sim 10^{-4}$ and searches for the decays $Z \to \pi^0\gamma$, $\eta\gamma$ and $\eta'\gamma$ have already been reported by the LEP collaborations [168,169,110,111,112]. Here we update the ALEPH limits on these branching ratios and also report the first limit on the decays $Z \to \pi W$ and $Z \to \rho W$.

The detection efficiency for all channels studied was calculated using Monte Carlo generators producing an angular distribution proportional to $1+\cos^2\theta$. Decays of the pseudoscalar mesons were produced with the LUND 7.3 generator and followed by full simulation and reconstruction.

11.1.1 The decay $Z \to \pi^0\gamma$

The first experimental limit on the branching ratio $Z \to \pi^0\gamma$, 4.9×10^{-4}, was reported by ALEPH in 1990 [168], significantly below the Jacob and Wu limit but well above that of West.

The events used for this search were the 307 discussed in section 8.3.6. The background is the QED process $e^+e^- \to \gamma\gamma$ which has a cross-section of the form $1/s$, while the cross-section for $\pi^0\gamma$ follows the line shape of the Z. Since at 45 GeV a π^0 cannot be distinguished from a photon on an event by event basis the search for this decay is based on this difference in s dependence.

To extract a limit on the branching ratio of $Z \to \pi^0\gamma$ the predicted number of $\gamma\gamma$ events to order α^3 as a function of energy (table 8.2) was compared to the data using the log-likelihood method as in section 8.3.6. The same systematic errors are included as in the $\gamma\gamma$ analysis combined with the error from the $\pi^0\gamma$ Monte Carlo statistics of 1.4%, giving a total systematic error of 2.8%. Maximizing $\log\mathcal{L}$ the 95% c.l. obtained on the branching ratio $B(Z \to \pi^0\gamma)$ is 2.1×10^{-4}. The signal which would be produced for this value of $B(Z \to \pi^0\gamma)$ is shown on fig. 11.1.

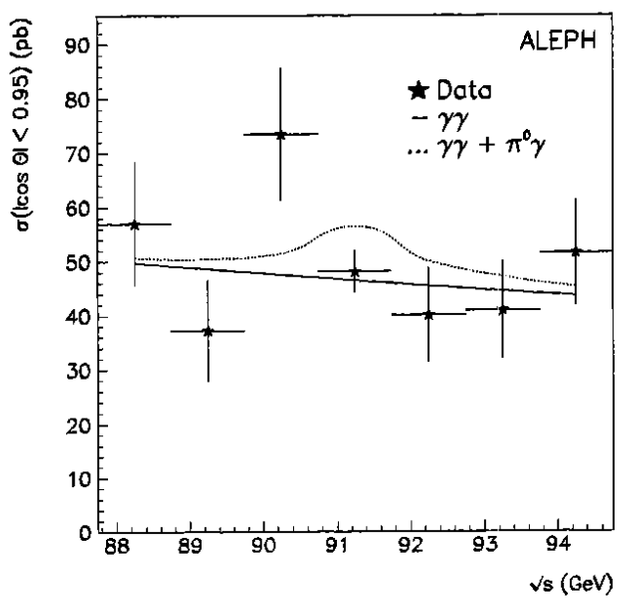

Figure 11.1: Cross-section for $e^+e^- \to \gamma\gamma$ for the region $|\cos\theta| < 0.95$ showing the 95% c.l. limit for $Z \to \pi^0\gamma$.

11.1.2 The decays $Z \to \eta\gamma$ and $Z \to \eta'\gamma$

Two search techniques are used for these channels, the first based on the neutral decay modes of the η (branching ratio 0.708) and the second based on final states containing a $\pi^+\pi^-$ pair together with neutrals for both the η (0.285) and η' (0.613).

The η decays into the neutral modes $\gamma\gamma$ and $\pi^0\pi^0\pi^0$ with branching ratios 0.39 and 0.32 respectively. Since its mass is $548.8\,\mathrm{MeV}/c^2$, the electromagnetic cluster produced by these decay products in the high granularity ALEPH electromagnetic calorimeter is measureably wider than the cluster produced by a single photon or by the two photons from a π^0, even at an energy of 45 GeV. The search for these decay modes is therefore for events with two back to back clusters, one of which is wider than that produced by a single photon at this energy.

The preselected event sample of 307 events was identical to that used for the $\gamma\gamma$ analysis (section 8.3.6) and the $\pi^0\gamma$ search (section 11.1.2). The search for η decays was performed using the estimator F_4, the fraction of the cluster energy in the highest four towers, and W, the second moment of the energy distribution projected onto the major axis of the cluster. Since the analysis uses the detailed shape of the cluster it is sensitive to defects in the calorimeter. An additional requirement was therefore made on the energy measurements from the pads and wires for the modules with energy deposits using the quantity $\Delta = (E_{pad} - E_{wire})/E_{wire}$. The distribution of Δ was studied on real Bhabha events and a cut made at $\pm 14\%$ (3σ) giving an efficiency of 96%. Distributions of F_4 *vs* W are shown in fig. 11.2 for Monte Carlo simulated events of the final states $\gamma\gamma$, $\pi^0\gamma$ and $\eta\gamma$ and for the data, excluding events where either cluster is in an overlap region or a crack. Since the resolutions on F_4 and and W are different in the endcaps and the barrel the cuts applied were different, being in the endcap $W > 2.86\,\mathrm{cm}$, $F_4 < 0.814$, and in the barrel $W > 2.84\,\mathrm{cm}$, $F_4 < 0.784$.

One event (A on fig. 11.2) passes all the cuts. One of the clusters in this event contains two merged peaks consistent with energy deposits by two photons of approximately 9 and 35 GeV. With this hypothesis the invariant mass of the parent of the photons is $828\,\mathrm{MeV}/c^2$, about 6σ above the η mass. However, this event is consistent with the process $e^+e^- \to \gamma\gamma\gamma$ for which a Monte Carlo study shows that 0.2 events are predicted to lie within the cuts of this analysis. Event B on fig. 11.2 fails the cut on F_4; its large value of W results from a spurious 2 GeV energy deposit in a middle storey at the edge of the cluster.

The detection efficiency for $Z \to \eta\gamma$ with the η decaying to neutral channels is 37.1%. The principal losses are from photon conversions (6% per photon) and geometrical cuts on $\cos\theta$, cracks and the overlap regions. The detection efficiency including branching ratios is therefore 26.3%.

The search for decay modes containing two charged pions opposite a high energy photon is made with the following cuts: *(i)* a photon with energy $E_\gamma > 0.85 E_{beam}$; *(ii)* two tracks of opposite charge with summed momentum vector at an angle greater than 170° to the photon; *(iii)* invariant mass of the pair, $m_\pm$, less than $1.0\,\mathrm{GeV}/c^2$; *(iv)* momentum sum of the pair, $p_\pm$, less than $0.85 E_{beam}$; *(v)* neither track in the event identified as a muon or an electron.

Thirty-seven events survive cuts *(i)* to *(iii)*. Particle identification allows these to be classified as 28 e^+e^- pairs, 3 $\mu^+\mu^-$ pairs, 5 $\pi^+\pi^-$ pairs and 1 $\tau^+\tau^-$ pair in which one τ has decayed to $\mu\nu_\tau$ and the other to $\rho\nu_\tau$. The distribution of $p_\pm/E_{beam}$ for these events is plotted in fig. 11.3 showing clearly that they are principally internal or external photon conversions. The Monte Carlo expectations for $Z \to \eta\gamma$ and $Z \to \eta'\gamma$ are shown in the same figure. Seven events pass cuts *(i)* to *(iv)*; in four both tracks are identified as electrons, in two one is identified as an electron, while the last is the $\tau^+\tau^-$ event described above. In three of the e^+e^- events one track is badly measured and in the other three one particle has emitted an energetic photon.

The Monte Carlo calculation gives a detection efficiency for $Z \to \eta\gamma$ decays containing a $\pi^+\pi^-$ pair of 45.4% with the above cuts. Thus the efficiency for $Z \to \eta\gamma$ with η producing a

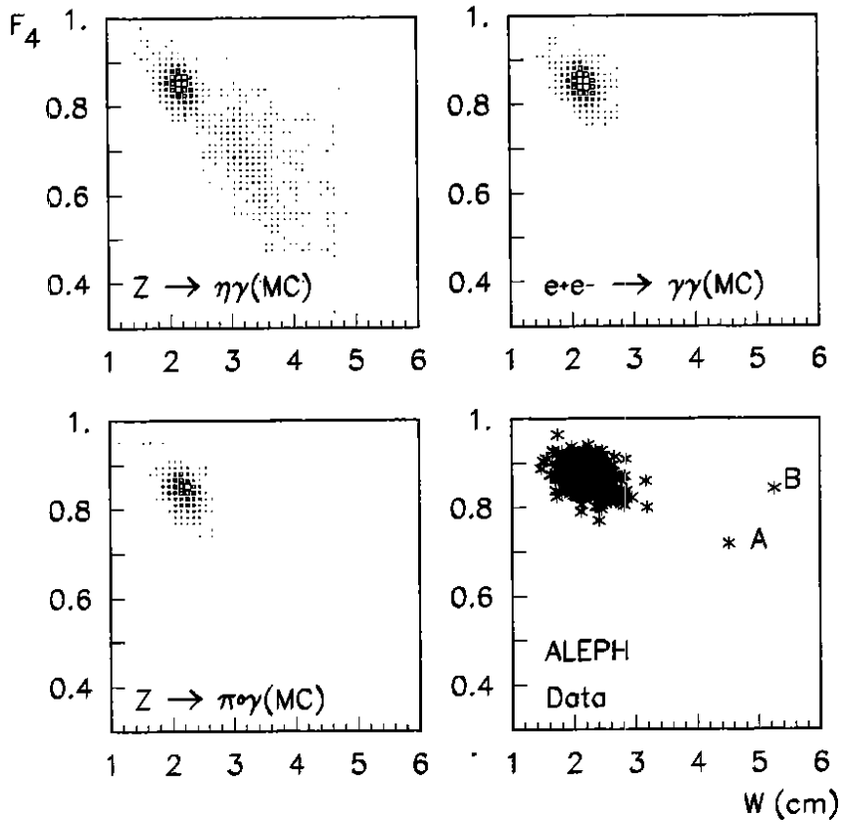

Figure 11.2: Distribution of clusters in the F_4 *vs* W plane for Monte Carlo events with final states $\eta\gamma$, $\gamma\gamma$ and $\pi^0\gamma$ and for the data.

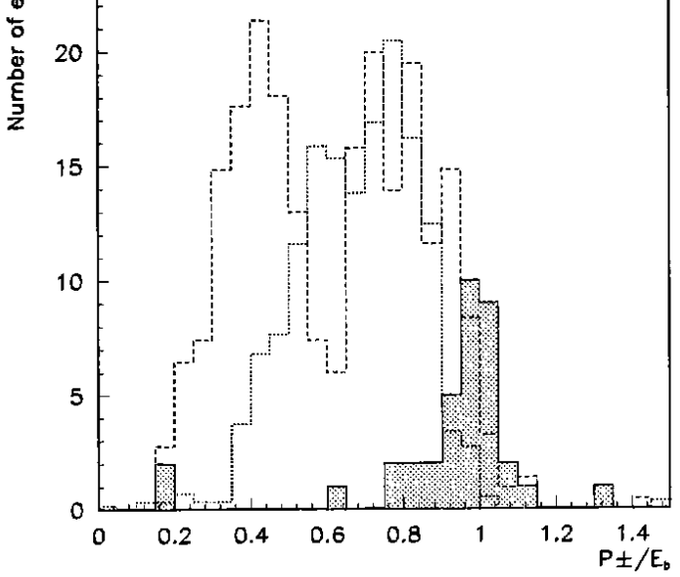

Figure 11.3: Momentum distribution of the charged pair (in units of E_{beam}) for $m_{\pm} < 1\,\mathrm{GeV}/c^2$. The hatched area shows events in the data, the dashed and dotted histograms are the η' and η Monte Carlo predictions respectively, with arbitrary normalization.

final state containing a $\pi^+\pi^-$ pair is 12.9%. Adding this to the 26.3% for the neutral channels gives a total efficiency of 39.2%. Since one event passes the neutral channel cuts the 95% c.l. is at 4.74 events giving a branching ratio limit of 5.1×10^{-5}.

The detection efficiency for $Z \rightarrow \eta'\gamma$ decays with a $\pi^+\pi^-$ pair is 41.6% giving a total efficiency of 28.0%. Since no events pass the cuts the branching ratio limit is 4.2×10^{-5}.

11.1.3 The decays $Z \rightarrow \pi W$ and $Z \rightarrow \rho W$

The signal for the decay $Z \rightarrow \pi W$ is a charged pion of approximately 10 GeV plus the decay products of the W. The W decays to $q\bar{q}'$ or $\ell\nu$ with branching ratios of about 70% and 30% respectively. However the relative advantage in branching ratio of the former channel is lost in the difficulty of extracting the signal in the presence of the very large hadronic Z decay background.

The signal when the W decays to an electron or a muon is an acoplanar lepton and pion, with the lepton energy between 30 and 50 GeV, and missing energy between 30 and 50 GeV. For the tau channel the visible lepton energy will be less on average and the missing energy will be correspondingly larger.

The search for acoplanar pairs has already been described in section 5.3.2 with no events passing the cuts. Since no particle identification was used in that search the result can be directly applied to this channel using only the detection efficiency. To simulate the decay, 1500 Monte Carlo events were produced at $\sqrt{s} = 91.2$ GeV with the LUND 7.3 generator using a Z decay angular distribution $\propto 1 + \cos^2\theta$. The calculated detection efficiency for $Z \rightarrow \pi W$ was 56% for the leptonic decays of the W giving, when a systematic error is included, a 95% c.l. limit on the branching ratio of 7.0×10^{-5}.

The decay $Z \rightarrow \rho W$ also produces an acoplanar pair of tracks. A Monte Carlo calculation showed that the detection efficiency for this decay is 48%, somewhat lower than for πW because of the sharing of the energy of the ρ between the charged and neutral pions. The branching ratio limit for this channel is 8.3×10^{-5}.

11.1.4 Summary

A summary of the 95% c.l. branching ratio limits for $Z \rightarrow P + V$ derived above is given in table 11.1.

Table 11.1: Z rare decay branching ratio limits in units of 10^{-5}.

Channel	Limit
$Z \rightarrow \pi^0\gamma$	21
$Z \rightarrow \eta\gamma$	5.1
$Z \rightarrow \eta'\gamma$	4.2
$Z \rightarrow \pi W$	7.0
$Z \rightarrow \rho W$	8.3

11.2 Lepton Flavour Violating Decays

Lepton flavour is conserved in the standard model. This is not the case for a number of models which incorporate physics beyond the standard model, and a direct search for lepton flavour violating decays of the Z complements limits extracted from low energy data [161]. The simplest such decays to search for are $Z \rightarrow e\mu$, $Z \rightarrow e\tau$ and $Z \rightarrow \mu\tau$ with two unlike back to back leptons with energy E_{beam}. Background arises from standard model leptonic final states and falls into two classes: *(i)* incorrectly reconstructed e^+e^- and $\mu^+\mu^-$ events and *(ii)* $\tau^+\tau^-$ events where one or both of the tau decays leptonically giving a charged track momentum close to the beam

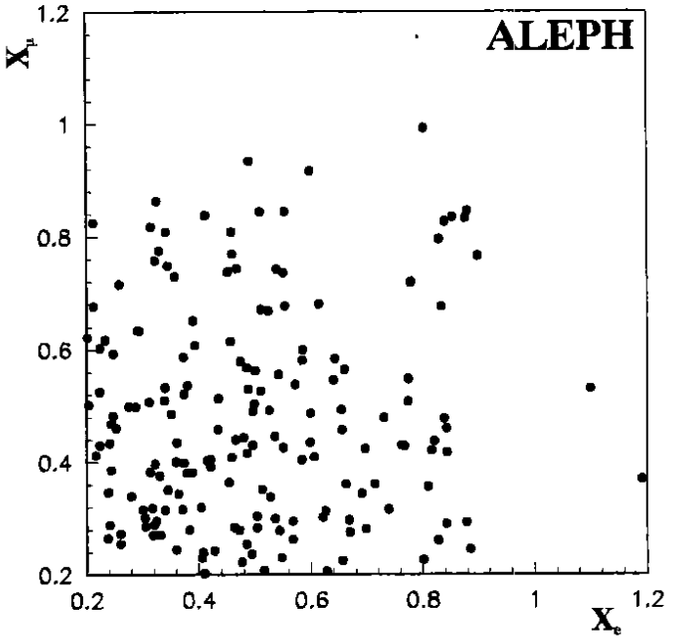

Figure 11.4: Normalized electron energy versus normalized muon momentum for eμ candidate events.

momentum. In this analysis the former background was reduced by cuts on the data while the latter was calculated from a Monte Carlo simulation.

Certain features of the analysis were common to all channels. Events were selected with two or four good tracks and a total charge of zero. In the two track topology the acollinearity of the tracks were required to be greater than 170°. In the four track topology one track was demanded in one hemisphere and three in the other with the same acollinearity condition on the isolated track and the sum of the momenta of the three recoil tracks. The invariant mass of the three tracks, considered as pions, was required to be less than 1.7 GeV/c^2. Track assignments to electron and muon hypotheses were made based on the estimators of sections 3.3.1 and 3.3.2. Electron energies and muon momenta are normalized relative to the beam energy and are referred to as X_e and X_μ respectively.

About 30,000 Monte Carlo events were generated to study backgrounds from the channels e^+e^- (using BABAMC [98,99]), $\mu^+\mu^-$ (using KORALZ [100]) and $\tau^+\tau^-$ (also using KORALZ). Modified versions of KORALZ were used to generate signal events.

11.2.1 $Z \rightarrow e\mu$

Events were selected with two oppositely charged tracks, one a muon candidate and the other an electron candidate. Fig. 11.4 shows the normalized electron energy *vs* the normalized muon momentum for the events selected. Signal events will populate the region where both ratios are close to 1.0. The average resolutions (σ), for electrons and muons with energy E_{beam} in the angular range of this search ($|\cos\theta| < 0.95$) are 4.2% and 4.6% respectively. No events lie within the region where the normalized quantities are greater than 0.85 giving a 95% c.l. limit on the signal of three events. In the sample of $\tau^+\tau^-$ Monte Carlo events none was found in the same region and no misidentified e^+e^- or $\mu^+\mu^-$ Monte Carlo events fell within the same cuts. The efficiency of the analysis as determined by the signal Monte Carlo is 46.5% and the branching ratio limit is 2.6×10^{-5}.

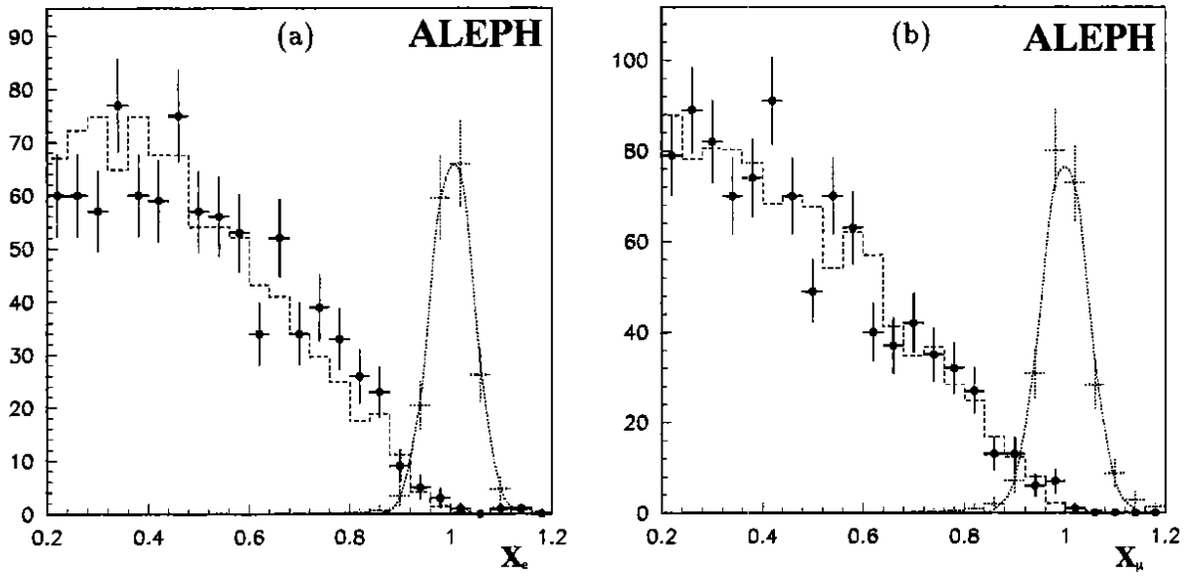

Figure 11.5: (a) Normalized electron energy for the $e\tau$ candidates and (b) normalized μ momentum for the $\mu\tau$ candidates. The expected signal shape is also shown on each plot.

11.2.2 $Z \rightarrow e\tau$

In the two track topology events were selected with one and only one electron candidate. In addition cuts were made as follows. Both tracks were required to be out of ECAL cracks and the overlap region of the ECAL barrel and endcap. The total energy measured on the ECAL wires for all modules had to be $< 0.8\sqrt{s}$ and the momentum of the track recoiling against the electron candidate had to be $< 0.85 p_{beam}$. These latter cuts were introduced to reject e^+e^- final state background where one of the electrons is not identified. The efficiency of these cuts, as calculated from the signal Monte Carlo, including the τ branching ratio, is 28.1%. The four track topology suffers less background contamination and the cuts are correspondingly less severe. The isolated track was required to be the only electron candidate in the event and to be away from ECAL cracks and the overlap region. The efficiency of these cuts, again calculated using the signal Monte Carlo, is 7.3%. The total efficiency for $Z \rightarrow e\tau$ is 35.4%. No e^+e^- or $\mu^+\mu^-$ Monte Carlo events satisfied the cuts. The sum of the normalized electron energy distributions from the two and four track samples is shown in fig. 11.5.

The predicted spectra from the τ pair background for this channel is shown in fig. 11.5(a) The expected signal is represented by a Gaussian distribution whose shape has been determined from e^+e^- events extracted from the data and is also shown on the same figure. A maximum likelihood fit to the data was made for the sum of the expected $\tau^+\tau^-$ background plus the signal Gaussian to give the 95% c.l. limit on the branching ratio. The fitted signal is 5.3 ± 3.1 events with zero background, and the 95% c.l. limit is 10.4 events. The corresponding branching ratio limit is 12×10^{-5}.

11.2.3 $Z \rightarrow \mu\tau$

In the two track topology one and only one of the charged tracks had to be a muon candidate. The momentum of the track recoiling against the muon candidate had to be $< 0.85 p_{beam}$. The track recoiling against the muon candidate had to pass through a region of HCAL (including the muon chambers) with at least ten active planes, have no plane fired in the last three active planes and fewer than four planes fired in the last ten active planes. The sum of the charged

track energy and the energy in neutral electromagnetic clusters was required to be less than $0.8\sqrt{s}$. The efficiency estimated from the signal Monte Carlo is 32%. The predicted background from $\mu^+\mu^-$ is 1.0 events.

The four track sample was selected as follows. The isolated track was required to be the only muon candidate in the event. The three recoiling tracks had to pass through a region of HCAL with at least ten active planes. Furthermore none of the three recoiling tracks was allowed to be an electron candidate. Again the efficiency of these cuts was calculated using the signal Monte Carlo and was found to be 6%. No background Monte Carlo events satisfied the cuts.

Thus the total efficiency for the $Z \to \mu\tau$ analysis is 38% and the expected background is 1.0 events. The sum of the normalized muon momentum distributions from the two and four track samples is shown in fig. 11.5(b). The same fitting procedure described above was used for the $\mu\tau$ channel. The fitted signal is 3.3 ± 3.6 events, consistent with the predicted background of 1.1 ± 0.5 events. The 95% c.l. limit on the signal is 9.6 events. The branching ratio limit for $Z \to \mu\tau$ is then 10×10^{-5}.

11.2.4 Summary

The results derived above are summarized in table 11.2 together with those derived from non-observation of certain μ and τ decays such as $\mu \to eee$, $\tau \to eee$ and $\tau \to \mu\mu\mu$. The corresponding predicted limit for each Z decay mode is given in the last column of the table. It can be seen that limits from LEP are becoming competitive for lepton flavour violation involving τs but the $Z \to e\mu$ channel is clearly beyond the reach of LEP. OPAL [170] and L3 [171] have also reported limits for these decays.

Channel	Eff. (%)	Fitted signal	95% c.l. limit	B.R. limit	Low energy limit
$Z \to e\mu$	46.5	–	3.0	2.6×10^{-5}	6×10^{-13}
$Z \to e\tau$	35.4	5.3 ± 3.1	10.4	12×10^{-5}	10×10^{-5}
$Z \to \mu\tau$	48.0	3.3 ± 3.6	9.6	10×10^{-5}	6×10^{-5}

Table 11.2: Summary of the derivation of lepton flavour violation limits. The low energy limits derived in ref. [161] have been updated from later CLEO limits [172] for $e\tau$ and $\mu\tau$.

12 Summary and Conclusions

In this report we have described the search for new particles and phenomena outside the standard model made by ALEPH in the first two years of LEP operation. No evidence has been found so far for such effects but signifiant improvements have been made to the mass limits for Higgs bosons, supersymmetric and composite particles, and leptoquarks.

Before LEP limits on the minimal standard model Higgs mass were very weak. For example, the Particle Data Group statement about the minimal standard model Higgs in April 1988 is "the only cast-iron constraint on the Higgs mass is $m_{H^0} > 14\,\mathrm{MeV}/c^2$. A combination of theoretical arguments and bounds from B, Υ and K decays probably excludes the range below $4\,\mathrm{GeV}/c^2$" [173]. This limit has now been extended to $48\,\mathrm{GeV}/c^2$ and further data should continue to improve the mass to which searches for the MSM Higgs are sensitive. Searches for charged and neutral Higgs particles in extended Higgs models have been made at lower energy e^+e^- machines and achieved limits of about $20\,\mathrm{GeV}/c^2$ for the charged Higgs mass, while in the

neutral Higgs sector limits of a few GeV/c^2 were quoted within the framework of the MSSM. The ALEPH limit on the $\mathrm{H}^{\pm}$ mass is now $41.7\,\mathrm{GeV}/c^2$, and neutral sector limits, generally valid in two-doublet models, translate into a lower mass limit on h of $41\,\mathrm{GeV}/c^2$ within the MSSM when one-loop radiative corrections are taken into account.

Many searches have a natural mass limit set by the available centre-of-mass energy but, compared to earlier machines, the presence of the Z resonance has allowed the kinematic limit to be quickly reached at LEP. Thus the masses of the supersymmetric partners of the charged leptons must exceed $45\,\mathrm{GeV}/c^2$ and chargino masses must exceed $47\,\mathrm{GeV}/c^2$ if the mass of the lightest supersymmetric particle is $\lesssim 40\,\mathrm{GeV}/c^2$. The neutralino sector was essentially unexplored before LEP; now upper limits of a few 10^{-5} have been presented in this report for the Z branching ratio into neutralinos, thus excluding a large fraction of the kinematically available parameter space of the MSSM.

The mass limits on excited charged leptons and excited quarks are $46\,\mathrm{GeV}/c^2$ and $45\,\mathrm{GeV}/c^2$ respectively and for an excited neutrino decaying by photon emission it is $47\,\mathrm{GeV}/c^2$. During the coming years, lower coupling ranges for excited fermions with a mass between $m_{\mathrm{Z}}/2$ and m_{Z} will be explored but the reach for these couplings only improves as the fourth root of the integrated luminosity. Leptoquarks having the most conservative cross-section are excluded up to a mass of $44\,\mathrm{GeV}/c^2$. A search for a new weakly interacting particle with unknown coupling to the Z has been unsuccessful, giving an upper limit on the branching ratio for $B(\mathrm{Z} \to \mathrm{X}^0\ell^+\ell^-)/B(\mathrm{Z} \to \ell^+\ell^-)$ of 7.2×10^{-4} for a mass up to $60\,\mathrm{GeV}/c^2$.

No unexpected decay modes of the Z boson have been found but this is an area which will gain increasing attention as sensitivity reaches branching ratios of 10^{-6}. The limits on lepton flavour violation from non-observation of the decays $\mathrm{Z} \to \mathrm{e}\tau$ and $\mathrm{Z} \to \mu\tau$ are close to the sensitivity of those from searches for τ decays violating lepton flavour.

13 Acknowledgements

ALEPH could not have been built or be operated without the efforts of a large number of engineers and technicians at CERN and at our laboratories outside CERN. We thank them for the way they have maintained the excellent performance of ALEPH. We thank also the LEP engineers and technicians for providing the source of our data so quickly after the start of LEP operations. Those of us from non-member states thank CERN for its hospitality.

References

[1] S. Komamiya, "Search for new particles in $\mathrm{e}^+\mathrm{e}^-$ annihilation", in *Proceedings of the 1985 International Symposium on Lepton and Photon Interactions at High Energies*, (M. Konuma and K. Takahashi, eds.), p612, (1989).

[2] M. Miyamoto, "Searches for new particles at TRISTAN", in *Proceedings of the XXVth Rencontres de Moriond*, p127, Editions Frontières, (1990).

[3] ALEPH Collab., D. Decamp *et al.*, *Phys. Lett. B* **236** (1990) 511.

[4] DELPHI Collab., P. Abreu *et al.*, *Phys. Lett. B* **242** (1990) 536.

[5] L3 Collab., B. Adeva *et al.*, *Phys. Lett. B* **251** (1990) 321.

[6] OPAL Collab., M. Akrawy *et al.*, *Phys. Lett. B* **236** (1990) 364.

[7] OPAL Collab., M. Akrawy *et al.*, *Phys. Lett. B* **240** (1990) 250.

[8] K. Sliwa, "A new limit on the mass of the top quark", in *Proceedings of the XXVth Rencontres de Moriond*, p459, Editions Frontières, (1990).

[9] CDF Collab., F. Abe *et al*, *Phys. Rev. Lett.* **64** (1990) 152.

[10] UA1 Collab., C. Albajar *et al*, *Phys. Lett. B* **253** (1991) 503.

[11] UA2 Collab., J. Alitti *et al*, *Z. Phys. C* **47** (1990) 11.

[12] CDF Collab., F. Abe *et al*, *Phys. Rev. D* **43** (1991) 2070.

[13] UA2 Collab., J. Alitti *et al*, *Phys. Lett. B* **241** (1990) 150.

[14] ALEPH Collab., D. Decamp *et al.*, "Improved measurements of electroweak parameters from Z decays into fermion pairs", preprint CERN-PPE/91-105, (1991).

[15] ALEPH Collab., D. Decamp *et al.*, *Nucl. Instr. Meth. A* **294** (1990) 121.

[16] W. Atwood *et al.*, *Nucl. Instr. Meth. A* **306** (1991) 446.

[17] ALEPH Collab., D. Decamp *et al.*, "Measurement of the absolute luminosity with the ALEPH detector", preprint CERN-PPE/91-129, (1991).

[18] ALEPH Collab., D. Decamp *et al.*, *Phys. Lett. B* **244** (1990) 551.

[19] ALEPH Collab., D. Decamp *et al.*, "Measurement of the forward-backward asymmetry in $Z \to b\bar{b}$ and $Z \to c\bar{c}$", preprint CERN-PPE/91-71, (1991).

[20] R. Brun *et al.*, "GEANT3", CERN DD/EE/84-1, (1987).

[21] G. Burgers, "The shape and size of the Z resonance", in *Polarization at LEP*, (G. Alexander *et al.*, ed.), CERN 88-06, (1988), 121. Program GAMMAZ courtesy of G. Burgers and W. Hollik.

[22] G. Burgers and W. Hollik, "Explicit formulae for one-loop weak corrections in the on-shell scheme", in *Polarization at LEP*, (G. Alexander *et al.*, ed.), CERN 88-06, (1988), 136.

[23] ALEPH Collab., D. Decamp *et al.*, *Phys. Lett. B* **257** (1991) 479.

[24] J. Bjorken, "Weak interaction theory and neutral currents", in *Proceedings of the 1976 SLAC Summer Institute on Particle Physics*, SLAC-198, (1976).

[25] ALEPH Collab., D. Decamp *et al.*, *Phys. Lett. B* **236** (1990) 233.

[26] ALEPH Collab., D. Decamp *et al.*, *Phys. Lett. B* **241** (1990) 141.

[27] ALEPH Collab., D. Decamp *et al.*, *Phys. Lett. B* **245** (1990) 289.

[28] ALEPH Collab., D. Decamp *et al.*, *Phys. Lett. B* **246** (1990) 306.

[29] ALEPH Collab., D. Decamp *et al.*, "Searches for the standard Higgs boson produced in the reaction $e^+e^- \to H^0Z^*$", preprint CERN-PPE/91-19, (1991).

[30] DELPHI Collab., P. Abreu *et al.*, *Nucl. Phys. B* **342** (1990) 1.

[31] DELPHI Collab., P. Abreu *et al.*, "A search for neutral Higgs particles in Z^0 decays", preprint CERN-PPE/91-132, (1991).

[32] DELPHI Collab., P. Abreu *et al.*, *Z. Phys. C* **51** (1991) 25.

[33] L3 Collab., B. Adeva *et al.*, *Phys. Lett. B* **248** (1990) 203.

[34] L3 Collab., B. Adeva *et al.*, *Phys. Lett. B* **252** (1990) 518.

[35] L3 Collab., B. Adeva *et al.*, *Phys. Lett. B* **257** (1991) 450.

[36] OPAL Collab., M. Akrawy *et al.*, *Phys. Lett. B* **236** (1990) 224.

[37] OPAL Collab., M. Akrawy *et al.*, *Z. Phys. C* **49** (1991) 1.

[38] OPAL Collab., M. Akrawy *et al.*, *Phys. Lett. B* **251** (1990) 211.

[39] OPAL Collab., M. Akrawy *et al.*, *Phys. Lett. B* **253** (1991) 511.

[40] OPAL Collab., M. Akrawy *et al.*, "Decay mode independent search for a light Higgs boson and new scalars", preprint CERN-PPE/91-116, (1991).

[41] T. Sjöstrand, *Comput. Phys. Commun.* **28** (1983) 229.

[42] F. Berends and R. Kleiss, *Nucl. Phys. B* **260** (1985) 32.

[43] M. Consoli and W. Hollik, "Electroweak radiative corrections for Z physics", in *Z Physics at LEP 1*, (G. Altarelli, R. Kleiss, and C. Verzegnassi, eds.), CERN 89-08, vol. 1, (1989), 7.

[44] D. Kennedy and B. Lynn, *Nucl. Phys. B* **322** (1989) 1.

[45] O. Nicrosini and L. Trentadue, *Phys. Lett. B* **196** (1987) 551.

[46] Z. Hioki, *Phys. Lett. B* **224** (1989) 417.

[47] R. Kleiss, *Phys. Lett. B* **180** (1986) 400.

[48] M. Bengtsson and T. Sjöstrand, *Phys. Lett. B* **185** (1987) 435.

[49] T. Sjöstrand and M. Bengtsson, *Comput. Phys. Commun.* **43** (1987) 367.

[50] M. Bengtsson and T. Sjöstrand, *Nucl. Phys. B* **289** (1987) 810.

[51] M. Drees and H. Hikasa, *Phys. Rev. D* **41** (1990) 1547.

[52] P. Janot, "Update and improvements of the ALEPH Higgs decay simulation, H0SDECAY", LAL preprint 89-45, (1989).

[53] J. Gunion, H. Haber, G. Kane, and S. Dawson, *The Higgs Hunter's Guide.* Addison Wesley, (1990).

[54] P. Franzini and P. Taxil *et al.*, "Higgs search", in *Z Physics at LEP 1*, (G. Altarelli, R. Kleiss, and C. Verzegnassi, eds.), CERN 89-08, vol. 2, (1989), 59.

[55] CELLO Collab., H.-J. Behrend *et al.*, *Phys. Lett. B* **193** (1987) 376.

[56] T. Sjöstrand *et al.*, "QCD generators", in *Z Physics at LEP 1*, (G. Altarelli, R. Kleiss, and C. Verzegnassi, eds.), CERN 89-08, vol. 3, (1989), 143.

[57] JADE Collab., S. Behtke *et al.*, *Phys. Lett. B* **213** (1988) 235.

[58] H. Nilles, *Phys. Rep. C* **110** (1984) 1.

[59] H. Haber and G. Kane, *Phys. Rep. C* **117** (1985) 75.

[60] R. Barbieri, *Riv. Nuovo Cimento* **11**, no. 4 (1988) 1.

[61] Y. Okada, M. Yamaguchi, and T. Yanagida, *Prog. Theor. Phys. Lett.* **85** (1991) 1.

[62] Y. Okada, M. Yamaguchi, and T. Yanagida, *Phys. Lett. B* **262** (1991) 54.

[63] J. Ellis, G. Ridolfi, and F. Zwirner, *Phys. Lett. B* **257** (1991) 83.

[64] J. Ellis, G. Ridolfi, and F. Zwirner, *Phys. Lett. B* **262** (1991) 477.

[65] H. Haber and R. Hempfling, *Phys. Rev. Lett.* **66** (1990) 1815.

[66] R. Barbieri, M. Frigeni, and M. Caravaglios, *Phys. Lett. B* **258** (1991) 167.

[67] R. Barbieri and M. Frigeni, *Phys. Lett. B* **258** (1991) 395.

[68] F. Zwirner (private communication).

[69] ALEPH Collab., D. Decamp *et al.*, *Phys. Lett. B* **241** (1990) 623.

[70] ALEPH Collab., D. Decamp *et al.*, *Phys. Lett. B* **237** (1990) 291.

[71] DELPHI Collab., P. Abreu *et al.*, *Phys. Lett. B* **245** (1990) 276.

[72] L3 Collab., B. Adeva *et al.*, *Phys. Lett. B* **252** (1990) 511.

[73] L3 Collab., B. Adeva *et al.*, *Phys. Lett. B* **251** (1990) 311.

[74] OPAL Collab., M. Akrawy *et al.*, *Phys. Lett. B* **242** (1990) 299.

[75] P. Fayet and S. Ferrara, *Phys. Rep. C* **32** (1977) 249.

[76] L. Maiani, "All you need to know about the Higgs boson", in *Ecole d'été de Physique des Particules*, IN2P3, Paris, (1980), 1.

[77] P. Fayet, *Unification of the Fundamental Particle Interactions*, p587. Plenum, (1980).

[78] J. Ellis *et al.*, *Nucl. Phys. B* **238** (1984) 453.

[79] L. Ibañez, *Phys. Lett. B* **137** (1984) 160.

[80] H. Baer *et al.*, "New particles", in *Physics at LEP*, (J. Ellis and R. Peccei, eds.), CERN 86-02, vol. 1, (1986), 297.

[81] M. Chen *et al.*, *Phys. Rep. C* **159** (1988) 203.

[82] R. Barbieri *et al.*, "Supersymmetry searches", in *Z Physics at LEP 1*, (G. Altarelli, R. Kleiss, and C. Verzegnassi, eds.), CERN 89-08, vol. 2, (1989), 121.

[83] H. Haber and D. Wyler, *Nucl. Phys. B* **323** (1989) 267.

[84] UA2 Collab., J. Alitti *et al*, *Phys. Lett. B* **235** (1990) 363.

[85] ALEPH Collab., D. Decamp *et al*, *Phys. Lett. B* **236** (1990) 86.

[86] ALEPH Collab., D. Decamp *et al*, *Phys. Lett. B* **244** (1990) 541.

[87] DELPHI Collab., P. Abreu *et al*, *Phys. Lett. B* **247** (1990) 157.

[88] L3 Collab., B. Adeva *et al*, *Phys. Lett. B* **233** (1989) 530.

[89] OPAL Collab., M. Akrawy *et al*, *Phys. Lett. B* **240** (1990) 261.

[90] OPAL Collab., M. Akrawy *et al*, *Phys. Lett. B* **248** (1990) 211.

[91] F. Boudjema and F. Renard, "Compositeness", in *Z Physics at LEP1*, (G. Altarelli, R. Kleiss, and C. Verzegnassi, eds.), CERN 89-08, vol. 2, (1989), 185.

[92] K. Hagiwara, S. Komamiya, and D. Zeppenfeld, *Z. Phys. C* **29** (1985) 115.

[93] F. Boudjema and A. Djouardi, *Phys. Lett. B* **240** (1990) 485.

[94] F. Renard, *Z. Phys. C* **14** (1982) 209.

[95] A. Courau and P. Kessler, *Phys. Rev. D* **33** (1986) 2024.

[96] DELCO Collab., G. Bonneaud *et al.*, *Phys. Lett. B* **177** (1986) 109.

[97] D. Karlen, *Nucl. Phys. B* **289** (1987) 23.

[98] M. Böhm, A. Denner, and W. Hollik, *Nucl. Phys. B* **304** (1988) 687.

[99] F. Berends, R. Kleiss, and W. Hollik, *Nucl. Phys. B* **304** (1988) 712.

[100] S. Jadach, B. Ward, and Z. Wąs, "The MC program KORALZ, version 3.8, for lepton or quark pair production at LEP/SLC energies", preprint CERN-TH.5994/91, (1991).

[101] M. Martinez, R. Miquel, and C. Mana, *Z. Phys. C* **46** (1990) 637.

[102] F. Berends and P. Daverveldt, *Nucl. Phys. B* **272** (1986) 131.

[103] ALEPH Collab., D. Decamp *et al.*, *Phys. Lett. B* **236** (1990) 501.

[104] DELPHI Collab., P. Abreu *et al.*, "Search for excited charged leptons onZ^0 decays", preprint CERN-PPE/91-100, (1991).

[105] L3 Collab., B. Adeva *et al.*, *Phys. Lett. B* **247** (1990) 177.

[106] L3 Collab., B. Adeva *et al.*, *Phys. Lett. B* **250** (1990) 205.

[107] OPAL Collab., M. Akrawy *et al.*, *Phys. Lett. B* **244** (1990) 135.

[108] A. Litke, "Experiments with electron-positron colliding beams", PhD thesis – Harvard University, (1970).

[109] F. Berends and R. Kleiss, *Nucl. Phys. B* **186** (1981) 22.

[110] DELPHI Collab., P. Abreu *et al.*, "The reaction $e^+e^- \to \gamma\gamma(\gamma)$ at Z^0 energies", preprint CERN-PPE/91-109, (1991).

[111] L3 Collab., B. Adeva *et al.*, *Phys. Lett. B* **250** (1990) 199.

[112] OPAL Collab., M. Akrawy *et al.*, *Phys. Lett. B* **257** (1991) 531.

[113] AMY Collab., S. Kim *et al.*, *Phys. Lett. B* **223** (1989) 476.

[114] TOPAZ Collab., I. Adachi *et al.*, *Phys. Lett. B* **200** (1988) 391.

[115] VENUS Collab., K. Abe *et al.*, *Z. Phys. C.* **45** (1989) 175.

[116] CELLO Collab., H.-J. Behrend *et al.*, *Phys. Lett. B* **123** (1983) 127.

[117] CELLO Collab., H.-J. Behrend *et al.*, *Phys. Lett. B* **168** (1986) 420.

[118] B. Narosa, *Phys. Rep. C* **148** (1987) 67.

[119] MARKJ Collab., B. Adeva *et al.*, *Phys. Lett. B* **152** (1985) 439.

[120] PLUTO Collab., Ch. Berger *et al.*, *Phys. Lett. B* **94** (1980) 87.

[121] TASSO Collab., M. Althoff *et al.*, *Z. Phys. C.* **26** (1984) 337.

[122] HRS Collab., M. Derrick *et al.*, *Phys. Lett. B* **166** (1986) 468.

[123] MAC Collab., E. Fernandez *et al.*, *Phys. Rev. D* **35** (1987) 1.

[124] R. Miquel, C. Mana, and M. Martinez, *Z. Phys. C* **48** (1990) 309.

[125] D. Karlen, "A study of low q^2 radiative Bhabha scattering", PhD thesis – SLAC Report 325, (1988).

[126] ALEPH Collab., D. Decamp *et al.*, *Phys. Lett. B* **250** (1990) 172.

[127] L3 Collab., B. Adeva *et al.*, *Phys. Lett. B* **252** (1990) 525.

[128] F. Renard, *Phys. Lett. B* **132** (1983) 449.

[129] F. Renard, *Nuovo Cim. A* **77** (1983) 1.

[130] ALEPH Collab., D. Decamp *et al.*, *Phys. Lett. B* **234** (1990) 209.

[131] ALEPH Collab., D. Decamp *et al.*, *Phys. Lett. B* **264** (1991) 476.

[132] OPAL Collab., M. Akrawy *et al.*, *Phys. Lett. B* **246** (1990) 285.

[133] OPAL Collab., M. Akrawy *et al.*, *Phys. Lett. B* **264** (1991) 219.

[134] CELLO Collab., H.-J. Behrend *et al.*, *Phys. Lett. B* **181** (1986) 178.

[135] F. Renard, *Nucl. Phys. B* **196** (1982) 93.

[136] M. Laursen *et al.*, *Phys. Rev. D* **23** (1981) 2795.

[137] R. Kleiss and W. Stirling, *Phys. Lett. B* **179** (1986) 159.

[138] J. Pati and A. Salam, *Phys. Rev. D* **10** (1974) 275.

[139] R. Mohapatra, G. Segrè, and L. Wolfenstein, *Phys. Lett. B* **145** (1984) 433.

[140] B. Schrempp and F. Schrempp, *Nucl. Phys. B* **231** (1984) 109.

[141] B. Schrempp and F. Schrempp, *Nucl. Phys. B* **242** (1984) 203.

[142] B. Schrempp and F. Schrempp, *Phys. Lett. B* **153** (1985) 101.

[143] S. Dimopoulos and L. Susskind, *Nucl. Phys. B* **155** (1979) 237.

[144] S. Dimopoulos, *Nucl. Phys. B* **168** (1980) 69.

[145] E. Eichten and K. Lane, *Phys. Lett. B* **90** (1984) 125.

[146] V. Angelopoulos *et al.*, *Nucl. Phys. B* **292** (1987) 59.

[147] D. Schaille and P. Zerwas, "Leptoquarks and diquarks in ee collisions up to 2 TeV", in *Proceedings of the Workshop on Physics at Future Accelerators*, CERN 87-07, (1988).

[148] N. Tracas and S. Vlassopoulos, *Phys. Lett. B* **220** (1989) 285.

[149] C. Heusch, "Looking for leptoquarks", in *Rencontre de Physique de la Vallée d'Aoste*, p399, Editions Frontières, (1989).

[150] J. Hewett and T. Rizzo, *Phys. Rev. D* **36** (1987) 3367.

[151] JADE Collab., W. Bartel *et al.*, *Z. Phys. C* **36** (1987) 15.

[152] AMY Collab., G. Kim *et al.*, *Phys. Lett. B* **240** (1990) 243.

[153] H. Grassmann, "Limits on leptoquarks from missing energy and from muon events at the $\overline{\mathrm{p}}\mathrm{p}$ collider", PhD thesis — RWTH Aachen, (1988).

[154] C. Peterson *et al.*, *Phys. Rev. D* **27** (1983) 105.

[155] DELPHI Collab., P. Abreu *et al.*, "Search for scalar leptoquarks from Z^0 decays", preprint CERN-PPE/91-138, (1991).

[156] L3 Collab., B. Adeva *et al*, *Phys. Lett. B* **261** (1991) 169.

[157] OPAL Collab., M. Akrawy *et al*, *Phys. Lett. B* **263** (1991) 123.

[158] UA2 Collab., J. Alitti *et al.*, "A search for scalar leptoquarks at the CERN $\overline{\mathrm{p}}\mathrm{p}$ collider", preprint CERN-PPE (to appear), (1991).

[159] R. Kleiss (private communication).

[160] ALEPH Collab., D. Decamp *et al.*, *Phys. Lett. B* **262** (1991) 139.

[161] E. Glover and J. van der Bij, "Rare Z decays", in *Z Physics at LEP1*, (G. Altarelli, R. Kleiss, and C. Verzegnassi, eds.), CERN 89-08, vol. 2, (1989), 1.

[162] L. Arnellos *et al.*, *Nucl. Phys. B* **196** (1982) 378.

[163] A. Manohar, *Phys. Lett. B* **244** (1990) 101.

[164] M. Jacob and T. Wu, *Phys. Lett. B* **232** (1989) 529.

[165] S. Ghosh and D. Chatterjee, *Mod. Phys. Lett. A* **5** (1989) 1493.

[166] G. West, *Mod. Phys. Lett. A* **5** (1990) 2281.

[167] D. Chatterjee and S. Ghosh, *Z. Phys. C* **50** (1991) 103.

[168] ALEPH Collab., D. Decamp *et al.*, *Phys. Lett. B* **241** (1990) 635.

[169] DELPHI Collab., P. Abreu *et al.*, "Search for non-standard Z decays in two-particle final states", preprint CERN-PPE/90-167, (1990).

[170] OPAL Collab., M. Akrawy *et al.*, *Phys. Lett. B* **254** (1991) 293.

[171] L3 Collab., B. Adeva *et al.*, "Search for lepton flavour violation in Z^0 decays", L3 preprint #34, (1991).

[172] CLEO Collab., T. Bowcock *et al.*, *Phys. Rev. D* **41** (1990) 805.

[173] Particle Data Group, *Phys. Lett. B* **204** (1988) 1.